TIME-REVERSED ACOUSTICS IN A RANDOMLY CHANGING MEDIUM

By

Daniel G. Alfaro Vigo

Research Supervisor: Prof. André Nachbin

INSTITUTO NACIONAL DE MATEMÁTICA PURA E APLICADA
(IMPA)
ESTRADA D. CASTORINA 110, JARDIM BOTÂNICO
RIO DE JANEIRO, BRASIL

MAY 2004

To my sons Daniel David and Vítor Augusto.

Contents

Abstract

In this work we study how random perturbations of an acoustic random medium affect the propagation of waves. By applying asymptotic analysis techniques for stochastic differential equations, we first characterized how the reflected pulses are correlated, with and without the medium perturbation. Furthermore, we focused on the effects of medium perturbations in time-reversal experiments. It is remarkable that the presence of perturbations does not destroy refocusing, but the statistical stabilization property (self-averaging) is lost. Actually, the refocused pulse depends on the media realization and is not deterministic as in the unperturbed case. We gave a complete description of the refocused pulse as a stochastic process, related to the solution of an Itô stochastic partial differential equation driven by a single standard one-dimensional Brownian motion. Moreover the conditions for a statistically stable refocusing appears in a simple way in this framework. Furthermore, under simplifying assumptions we obtained explicit formulas allowing for a deeper understanding of the coherent refocused pulse structure and laying a basis for a quantitative numerical validation of the present theory. For this validation a lagrangian code for the one-dimensional acoustic equation was developed and successfully tested. The numerical results showed an excellent agreement with the theory.

Resumo

Neste trabalho estudamos como perturbações aleatórias em um meio acústico afetam a propagação de ondas. Aplicando técnicas de análise assintótica de equações diferenciais estocásticas, primeiro caracterizamos como os pulsos refletidos estão correlacionados pelo meio com ou sem perturbações. Depois, nos concentramos no efeito das perturbações do meio em experimentos de reversão temporal. É notável que a presença das perturbações não elimina a refocalização do pulso, mas perde-se a estabilização estatística. Certamente, o pulso refocalizado vai depender da realização dos meios aleatórios envolvidos e não é determinístico como no caso não perturbado. Damos uma descrição completa do pulso refocalizado na forma de um processo estocástico, relacionado-o à solução de uma equação diferencial parcial estocástica de Itô associada a apenas um movimento Browniano uni-dimensional standard. Adicionalmente, as condições para uma refocalização estatísticamente estável aparecem numa forma muito simples. Além disso, sob hipóteses simplificadoras nós obtivemos fórmulas explícitas que permitem uma compreensão mais profunda da estrutura do pulso refocalizado coerente e estabelecemos as bases para a validação numérica da teoria apresentada. Para isto foi desenvolvido, um código lagrangeano para as equações da acústica uni-dimensional e testado com sucesso. Os resultados numéricos estão em excelente acordo com a teoria.

Acknowledgements

First of all, I would like to express my deepest gratitude to my advisor Prof. André Nachbin. I have appreciated his enthusiasm and dedication to guide me through my thesis research and to enrich my scientific life during these years of collaboration and friendship.

I thank the IMPA's staff for the unconditional support I have received, as well as for their contribution to my formation as applied mathematician, regarding this I am specially indebted to Professors Dan Marchesin, Jorge P. Zubelli and once again André Nachbin. It is noteworthy that the excellent atmosphere for doing high quality mathematical research, created here, and the great opportunity to work at the Laboratory of Fluid Dynamics were crucial to the successful completion of this project.

I am also grateful to Prof. Josselin Garnier (Université Paul Sabatier, France) for the initiated collaboration between us, that gave me a better perspective on my own results, and to Prof. George Papanicolaou (Stanford University, USA) whose comments, during a short discussion at IMPA, motivated a deeper interpretation of some issues of this work. And I thankful to Professors Paulo Ruffino (UNICAMP), Pedro P. Schirmer (USP), Enrique Pujals (IMPA) and Jorge P. Zubelli (IMPA), for taking part in the Examining Committee, and for their valuable opinions and comments that helped improve the initial manuscript.

I should also acknowledge the financial support of the Brazilian National Research Council (CNPq) through a Doctoral Fellowship.

Last, but not least, I thank my family for their love and support. Without their understanding and encouragement, I would not have seen this thesis through.

Rio de Janeiro, Brazil Daniel G. Alfaro Vigo
July 16, 2004

Chapter 1

Introduction

1.1 General remarks

Waves are everywhere around us. We experience some waves directly, for example, sound, light, water waves; and some other waves we feel indirectly — radio waves and microwaves for instance. A wave is any recognizable signal that is transferred from one part of a medium to another with a recognizable velocity of propagation. Moreover, with the signal is associated a moving spatial distribution of (some kind of) energy and wave propagation is one of the means by which this energy travels through the medium.

A random medium is a family of media together with a probability distribution which specifies the probabilities of the various members of the family. Thus the properties that characterize the propagation medium can be regarded as random functions of space, and the differential equations describing the wave propagation become partial differential equations with random coefficients [37, 38].

Keller [37] gives two main reasons for studying wave propagation through random media:

- The medium is not known precisely but we may know that it is a member of a known family of media.

- The medium has very complex properties, however we may know further that it is a member of a family with less complex or more tractable statistical properties.

However, this viewpoint encountered some criticism — for instance, in seismology and geophysics there is only one Earth and not a statistical ensemble of realizations. G. Papanicolaou [52] repudiates this objection by expressing: "What the stochastic processes model is uncertainty, lack of information and its consequences when only imperfect and sparse observations or measurements are available, and even desirable"

Actually, the development of the subject of waves in random media had to overcome some conceptual barriers. It is worth noticing that astrophysicists at the turn of the 20th century, studying light propagation through a turbulent atmosphere developed a new, phenomenological theory, the radiative transport theory instead of using Maxwell's equations for a fluctuating (random) medium. It was during the 1940s that the study of waves propagating through a random medium emerges as a subject of great interest stimulated by practical problems of radio wave propagation through the atmosphere and ionosphere, sound wave propagation in the ocean and the atmosphere, etc.. The papers by Keller [37, 38] in the 1960s had a great influence because they were the first ones written by a mathematician and established the conceptual foundations for separating heuristics from legitimate calculations. It was also at this time that the relation between radiative transport and stochastic wave equations was clarified. After that the interest on the subject continued to grow and influence in many areas of applications and technology until now (see an issue of the journal *Waves in Random Medium* for example).

1.2 Wave propagation in random medium

This work focuses on the propagation of acoustic waves in random media. We shall concentrate in the study of the scattered and time-reversal refocused signals associated with a pulse that propagates through a rapidly varying heterogeneous slab. More specifically, we analyze how these signals are affected by medium perturbations. Our study is based on a statistical approach, since a detailed description of the scattering of the wave by the heterogeneities would be prohibitively complex. Moreover, the detailed fine scale structure of the medium is not always known in applications such as geophysics and medicine.

In this framework the heterogeneous medium is modelled as having a smooth deterministic background, that incorporates the large-scale features, over which are superimposed random fluctuations for modelling a disordered micro-scale structure. Therefore, the acoustic model consists of a system of partial differential equations with random coefficients.

Waves propagating in a randomly heterogeneous medium are expected to change somewhat, because of the distortion of their travel paths, and to lose some of their coherent energy to small scale wave fluctuations. This can be confirmed by a perturbation expansion. However, when the random heterogeneities are strong the waves do not propagate very far. They become localized around the region where they are generated, and all their energy is eventually converted into random fluctuations. In two- or one-dimensional environments such as a layered media, however, waves are localized even when the random inhomogeneities are weak [3]. This is in contrast with the case where the inhomogeneities are not too anisotropic in which multiple scattering may lead to radiative transport of the wave energy in phase space [61].

We consider the case of a layered random medium, which is a useful model, for example, in the understanding of geophysical applications. Moreover, we address the case of plane waves normally incident upon the layered medium, which leads to a one-dimensional wave propagation model. This one-dimensional setup allows for a simple analytical formulation while maintains the main aspects of the general case. Furthermore, in the framework of separation of scales introduced by G. Papanicolaou and his collaborators, an asymptotic description of the quantities of interest is possible through the use of powerful tools from the asymptotic theory of stochastic differential equations and stochastic analysis.

There are two cases corresponding to the above mentioned separation of scales which are called the *strong* and *weak* medium fluctuations regimes [3, 67]. The first regime is characterized by the propagation of waves whose typical wavelengths are long compared to the size of the random fluctuations but short compared to the characteristic length scale of the large-scale features of the medium. Moreover, the inhomogeneities need not be weak. Although in this case the pulse strongly interacts with the heterogeneities, when it propagates over short distances it practically stays undistorted, travelling with the speed corresponding to the homogenized medium and does not generate much reflection. However, as the pulse propagates further the effect of the fine scale becomes more appreciable and it looses some of its coherent energy to small scale fluctuations which are, for example, transferred to the reflected wave.

In the second regime in addition to the weak magnitude of the inhomogeneities the propagating pulse has a typical wavelength of the same order of the size of the random heterogeneities but short compared to the characteristic length scale of the large-scale features of the medium. As a consequence, the propagating pulse has a strong interaction with the heterogeneities but for relatively short propagation distances it practically travels undistorted with the speed corresponding to the homogenized medium and effectively does not generate reflection. However, for long propagation distances the effect of the fine scale becomes appreciable and the pulse looses some of its coherent energy to small scale fluctuations which is almost transferred to the reflected wave.

We recall some fundamental features of wave propagation in layered random media analyzed in the above mentioned regimes using asymptotic techniques. First, we refer to the wave localization phenomenon mentioned above. In the frequency domain it means that the dominant behavior of the wave harmonics penetrating through the random medium must decay like $\exp(-\gamma d)$ as the penetration distance d goes to $+\infty$ and $l = 1/\gamma$ is the localization length (it is frequency dependent). Consequently, the transmission coefficient as a function of the penetration distance decays exponentially fast, i.e. there is no transmission through an infinitely long one-dimensional random medium. We refer to [63], see also [64, 65, 72]. Another important issue concerns the description of the transmitted wave front. This study was initiated by O'Doherty & Anstey [50] which based on physical grounds proposed a formula for the characterization of the propagated pulse. Further generalizations gave a mathematical account of their result that became known as the O'Doherty-Anstey theory. In short, it says that relative to a random arrival time the transmitted pulse is given as the convolution of the initial pulse with a **deterministic kernel** having a Gaussian shape. Moreover, as the pulse propagates further the width of the Gaussian kernel increases. This causes the attenuation and spreading effects of the propagating pulse observed in seismic data. Recall that since the acoustic equations constitute a hyperbolic system of PDEs, the energy is conserved, thus this is an *apparent attenuation* effect which reflects the fact that the pulse energy is transferred into incoherent small scale fluctuations. We refer to [3, 67] and the references therein.

1.3 Time reversal and refocusing

Time-reversal techniques have emerged as a new important and fascinating discipline within wave propagation. They are based on the use of a time reversal mirror (TRM), which is a device capable of receiving a signal in time, keeping it in memory and re-emitting it back into the medium in the reversed direction of time. In the context of ultrasounds, TRM have been developed and their effects have been studied experimentally by Mathias Fink and his team at the Laboratoire Ondes et Acoustique (ESPCI-Paris). We refer to [25, 26].

We distinguish between two kinds of experiments: Time Reversal in Reflection (TRR) and Time Reversal in Transmission (TRT). They are performed as follows: we let a pulse propagate in a random heterogeneous medium, the reflected (transmitted) signal is processed by a TRM and re-emitted back into the medium. This results in a back-propagated wave which is called a *time-reversed wave in reflection (transmission)*. The main effect is the *refocusing* of this time-reversed wave near the initial pulse location. Namely the noisy incoherent signal recompresses into a smooth coherent pulse. Moreover, despite the fact that the refocusing effect is analyzed within a statistical framework, the shape of the refocused pulse is independent of the realization of the medium, which is known as *statistical stabilization* (self-averaging). Furthermore, in some situations the randomness of the medium helps to improve refocusing 'beating' the diffraction limit [6, 14, 32]. Potential applications of this effect are numerous in imaging, wireless communication, medicine, geophysics, underwater acoustic, etc [12, 15, 20, 21, 34, 45, 70].

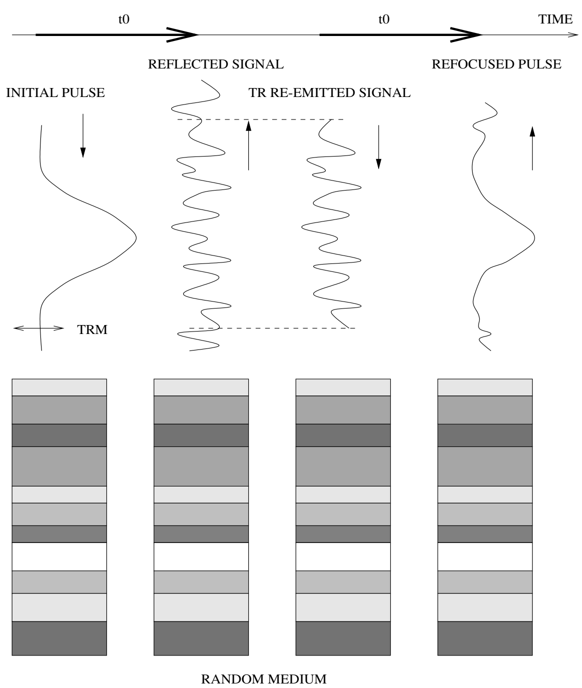

Figure 1.1: Schematic representation of a time reversal in reflection (TRR) experiment.

In figure 1.1 we schematically show time reversal in a reflection experiment. Here in the first two columns, we show the initial pulse and the reflected signal which is recorded at the TRM positioned at the interface during a time t_0 in length. The next columns present the signal to be re-emitted into the medium and the resulting back-propagated pulse after a time t_0. Note that this time-reversed pulse is centered at the same position of the initial pulse and resembles its waveform.

The first derivation of time reversal refocusing was given by Clouet & Fouque [19] for one-dimensional acoustics in the regime of strong fluctuations. The statistical stabilization of the refocused pulse was established and some applications of the time reversal method presented. For the regime of weak fluctuations a complete description of this phenomenon was given by K. Sølna in [66], some special cases were thoroughly studied and numerical experiments presented. In these two references the linear acoustic waves were treated, so it is worth mentioning the work by Fouque & Nachbin [31] where the analogy of the one-dimensional linear shallow water equations with the acoustic equations is used to briefly present the time-reversal theory in this context. The robustness of the theory in the nonlinear shallow water equations is numerically illustrated when the nonlinear term is small but not negligible. A further study of nonlinear shallow water waves was carried out by Fouque, Garnier & Nachbin in [29]. They pointed out the regularizing effect of a disordered topography and realized its impact in TRT experiments. In the context of dispersive water waves Fouque, Garnier & Nachbin [30] thoroughly analyzed TRR and TRT, they obtained the statistical stabilization property and a precise description of the combined effect of randomness and dispersion. The pulse stabilization and refocusing of solitary dispersive water waves in the presence of random depth are analyzed and numerically studied by Muñoz-Grajales & Nachbin in [47].

For three-dimensional linear acoustic waves the analysis of time reversal was carried out by J. Ndzié Ewodo for a layered medium, the case of TRR is presented in [48] and TRT in [49]. In both cases the refocused pulse is characterized and its statistical stabilization established. For the parabolic or paraxial regime the study was initiated by Blomgren, Papanicolaou & Zhao [14] who gave the first explanation of the super-resolution effect of the medium heterogeneities in time reversal experiments. The parabolic approximation was further revisited by G. Papanicolaou et al. in [5, 55, 56] where other related limiting regimes were also analyzed. The authors characterized the refocused pulse and thoroughly studied its statistical stabilization. For three-dimensional classical (acoustic, elastic and electromagnetic) waves a thorough analysis was performed by Bal & Ryzhik in [6, 7]. For the acoustic case see also the review by Fink & Prada [27].

The aim of this work is to analyze how medium changes affect the outcome of a time reversal experiment. This is an important issue to be understood since in practical applications the medium properties can be subjected to changes, as for example in underwater or aerial communication [20, 21]. Moreover, some experimental studies have shown which modifications arise in the refocused signal as the underlying medium changes [34, 71]. Therefore, we analyze time reversal experiments in a slightly different setting. Namely, we allow the time-reversed wave to propagate back into a medium different from the one upon which the initial pulse impinged. We will refer to this time reversal procedure as *generalized* and to the one where medium changes are not allowed as *standard*, in case it is not totally clear from the context. This generalized time reversal procedure leads to more realistic models and presents a wider range of applications than the standard one [71]. See figure 1.2 where it is schematically represented a generalized time reversal in reflection experiment.

Recently, this setting has been theoretically studied. In [2] Alfaro-Vigo et al. thoroughly analyzed TRR and TRT in a time-dependent medium that slowly evolves within a class having some fixed statistical characteristics, in the case of one-dimensional waves. The main result in [2] states that the pulse shape is described by a random function, implying that the statistical stabilization property is lost. The characterization of the coherent refocused pulse for two and three dimensions in the transport and diffusive regimes is presented by Bal & Verástegui in [9] based on the formal setting developed in [61] and additionally, their numerical experiments showed the statistical stabilization of the refocused pulse. In the parabolic or paraxial regime Bal & Ryzhik [8] rigorously studied the effect of a changing medium. They analyzed how the refocused pulse is affected and established its statistical stabilization.

In the present work we focus on the case where the medium changes are caused by

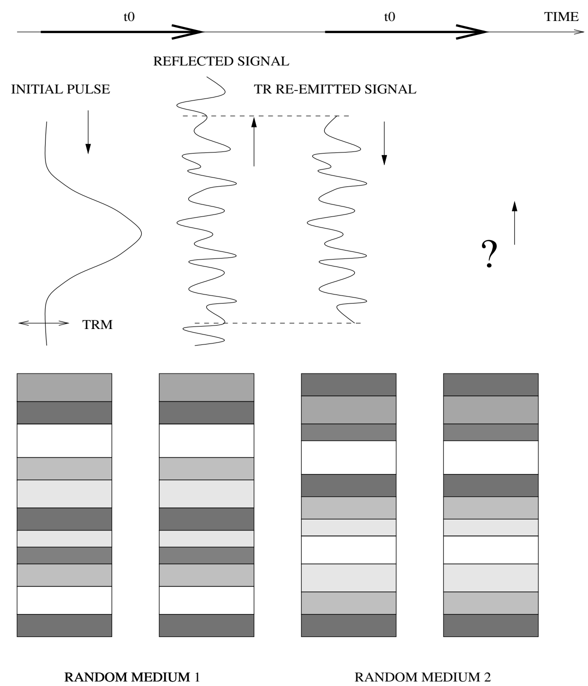

Figure 1.2: Schematic representation of a generalized time reversal in reflection (TRR) experiment. A natural question arises: will a coherent refocused pulse appear?

perturbations. More specifically, we consider the effect on the generalized TRR experiments by statistically independent medium perturbations which have the same order of magnitude as the random fluctuations. Our results are closely related to those in [2], but here we have additionally analyzed the weak fluctuations case. We established that the time-reversed pulse depends on the media realization and consequently the pulse shape is described by a random function, implying that the statistical stabilization property is lost. However, a coherent refocusing is still present. This is expected, since the unperturbed and perturbed media are still correlated and therefore some part of the energy transferred to small scale fluctuations, during the forward propagation, can still be recompressed into a coherent pulse after time-reversal. This general picture does not depend on the fact that the fluctuations are either strong or weak.

It is remarkable that in the generalized time reversal experiments the stabilization property is lost in the case of a layered random medium with strong or weak fluctuations ([2] and the present work) in contrast with the case of weak isotropic fluctuations in two or three dimensions [8, 9] where the statistically stable refocusing is not destroyed by the medium changes. As far as it is surprising, it is not paradoxical since wave propagation behaves totally different in both cases. In the first case the wave localization is the main feature and fluctuation phenomena dominate, while in the second the radiative transport characterizes the wave energy distribution and the wave energy spreads in a diffusive-like manner.

The theory we have developed gives a precise description for the class of stochastic processes that can be the outcome of a time reversal in reflection experiment under our modelling hypothesis. It is an asymptotic theory based on the separations of scales that we described before. These scales will be ordered as powers of a small dimensionless parameter ε. We give a rather complete account of the theory, as it applies to a uniform random half-space, obtaining analytical expressions that allow for a better understanding of the coherent refocused pulse. We derive equations for the statistics of the limiting refocused signal (as $\varepsilon \downarrow 0$) and establish its direct connection with the solution of an Itô stochastic partial differential equation driven by a single (standard) one-dimensional Brownian motion. Our main tool is the asymptotic analysis of stochastic differential equations, namely the probabilistic characterization of its solutions and their corresponding moments. See review [51] and appendix A for more references on the technology developed over the last three decades.

1.4 Outline

This thesis is organized as follows. In chapter 2 we introduce the acoustic wave equations (a linear 2×2 variable coefficient hyperbolic system) and describe the random medium model and the regimes of interest. After that some preliminary material is presented. Namely we consider: reflection coefficients, their associated (random)

Riccati equation, the integral representation of the reflected signal and its asymptotic statistical characterization. In the rest of this chapter we address the problem on how correlated are the reflected signals for the unperturbed and perturbed random media. In this analysis, we thoroughly study second order statistics of the corresponding reflection coefficients, by obtaining the corresponding Kolmogorov backward equations which lead to the associated W-equations. Moreover, we find explicit solutions to these diffusion equations under simplifying hypothesis that reveal their relationship with the localization phenomenon. It should be stressed that the second order statistics of the reflection coefficients play a fundamental role in the characterization of the coherent refocused pulse. Hence the material presented in this chapter is crucial for the subsequent study of time reversal. Moreover, the involved techniques concerning asymptotics of stochastic differential equations will constitute a fundamental tool in the analysis of time reversal.

In chapter 3 we perform an asymptotic analysis of generalized time reversal in reflection experiments. First, we characterize the coherent refocused pulse (i.e. the average of time-reversed reflections over media realizations) which is obtained by filtering the initial pulse (through a specific convolution) and by showing that some coherent energy can be recovered despite of medium perturbations. Moreover, by using the explicit formulas obtained in the previous chapter, we get an explicit expression for the coherent refocused pulse that allows for a better understanding of the effects of medium perturbations. Furthermore, we characterize the limiting refocused pulse as a random process. First, we use asymptotics for stochastic differential equations to characterize the limiting higher order moments of the refocused signal, through the associated Kolmogorov backward equations, in the same spirit as we did in chapter 2. Finally, applying the powerful techniques of Itô stochastic analysis the limiting signal is identified. It appears to be related to the large time asymptotic solution of an Itô stochastic partial differential equation driven by a single (standard) one-dimensional Brownian motion. Moreover, it is shown that simple statistical characteristics of the medium properties, and their perturbations, enter as coefficients in this stochastic differential equation.

It should be remarked that the description of the refocused pulse by asymptotics of the solution of an Itô stochastic partial differential equation emphasizes the randomness of the limiting refocused signal and the lack of statistical stabilization. However, for a special class of perturbations the corresponding stochastic differential equation becomes deterministic and one has the statistical stabilization of the refocused pulse.

In chapter 4, we describe the numerical experiments performed for validating the theory. First, we present the numerical schemes used and remark their relation with a set of discrete reflection-transmission cell problems and also a Goupillaud layered medium. Our code is capable of accurately computing the highly fluctuating reflected signals which have been multiply scattered by the sub-wavelength layers forming the microstructure. This code is a very useful tool for understanding the scope and robustness of the asymptotic theory. The numerical experiments show the main features of wave propagation in random media, e.g. the O'Doherty-Anstey approximation, the localization phenomenon and time reversal refocusing. Moreover, the numerical results corresponding to time reversal experiments present a remarkable agreement with the asymptotic theory developed in chapter 3.

In the appendices we have included some material to complement and help in the understanding of the main text. More specifically, in appendix A we formulate two theorems from the asymptotic theory of stochastic differential equations in the form in which they are applied in this work. The appendix B is devoted to the main computations leading to the expressions of the limiting joint correlation spectral density of the reflection coefficients, these explicit formulas are used throughout the work. In appendix C we briefly present an asymptotic result for the backward Itô stochastic parabolic differential equation which is related to the limiting refocused signal. And the appendix D is a short exposition of a useful discrete model of acoustic random media: a Goupillaud layered medium.

Chapter 2

Pulse reflection

2.1 Introduction

In this chapter we consider pulse reflection from an acoustic layered slab whose density and bulk modulus are locally stationary random functions, specially emphasizing the case of a layered half-space where the slab is infinitely large. By restricting our analysis to a plane-parallel pulse that is normally incident upon this slab from the adjoining homogeneous half-space, the model simplifies to the case of one-dimensional acoustic equations. The reflected signal generated at the interface has been extensively studied by asymptotic techniques in the regimes of weak and strong fluctuations mentioned above (see for example [3, 16, 17, 57]).

The aim of this chapter is to characterize how the reflected signals generated at the interface of the random half-space are correlated when the medium is subjected to perturbations. Our analysis will follow the general lines of the above mentioned references.

In section 2.2 we present some preliminary material, which conforms the basis for our further development [3, 16, 17]. Essentially, we present the one-dimensional acoustic model, the scaling corresponding to the regimes of strong and weak fluctuations, the integral representation of the signal scattered at the interface, and finally recall the asymptotic statistical behavior of this reflected signal (generated as in column 2 of figures 1.1 or 1.2).

In section 2.3 we introduce the joint reflection process which allow us to analyze the effect of media perturbation on the scattered signal, **reducing** this analysis to studying the joint reflection process' **correlation properties**. Namely, we formulate as our main problem to characterize the asymptotic behavior of the corresponding power spectral density (which is associated to the Fourier transform of the covariance). Section 2.4 is fully devoted to its solution and the regimes of strong and weak fluctuations are completely analyzed. For each case, we perform the characterization of the power spectral density corresponding to the joint reflection process. Moreover, we obtain their low frequency asymptotic, derive the corresponding W-equations for the moments and get some explicit solutions in a particular case. Additionally, for strong fluctuations we present its connection with localization. Finally, in section 2.5 some concluding remarks are given.

2.2 Preliminaries

2.2.1 One-dimensional acoustic waves

We consider propagation of linear acoustic waves in a heterogeneous time-independent medium. Let $\mathbf{v}(\mathbf{x},t)$, $p(\mathbf{x},t)$ be the velocity vector and pressure, respectively, with $\mathbf{x}\in\mathbf{R}^3$ representing the space variable and t the time. The linear conservation laws of momentum and mass are expressed by the equations:

$$\begin{cases} \varrho(\mathbf{x})\dfrac{\partial}{\partial t}\mathbf{v}(\mathbf{x},t)+\nabla p(\mathbf{x},t)=0 \\ \dfrac{1}{\kappa(\mathbf{x})}\dfrac{\partial}{\partial t}p(\mathbf{x},t)+\nabla\cdot\mathbf{v}(\mathbf{x},t)=0 \end{cases}$$

where $\varrho(\mathbf{x})$ and $\kappa(\mathbf{x})$ stand for the density and the bulk modulus respectively.

A model for a layered space is obtained by assuming that the medium properties only depend on the z-coordinate. Furthermore, by considering that a plane wave is normally incident to the layers, these equations become one-dimensional and are written as:

$$\begin{cases} \varrho(z)\dfrac{\partial}{\partial t}u(z,t) + \dfrac{\partial}{\partial z}p(z,t) = 0 \\ \dfrac{1}{\kappa(z)}\dfrac{\partial}{\partial t}p(z,t) + \dfrac{\partial}{\partial z}u(z,t) = 0 \end{cases} \tag{2.2.1}$$

where $u(z,t)$ is the z-component of the velocity vector $\mathbf{v}$.

Remark 2.2.1. Recall that according to homogenization theory the effective medium properties are characterized through the relations [11]

$$\varrho_{\text{eff}} = \mathbb{E}\{\varrho\} \quad \text{and} \quad \kappa_{\text{eff}}^{-1} = \mathbb{E}\{\kappa^{-1}\},$$

where $\mathbb{E}\{\cdot\}$ represents averaging with respect to the underlying probability measure.

We shall rewrite these equations in a dimensionless form. Let the average density and inverse bulk modulus vary in the length scale l_0 and have characteristic values $\bar{\varrho}_0$ and $\bar{\kappa}_0^{-1}$. Then the associated characteristic sound speed is $\bar{c}_0 = \sqrt{\bar{\kappa}_0/\bar{\varrho}_0}$. Re-scale the time and depth variables

$$z = l_0 z' \quad \text{and} \quad t = \frac{l_0}{\bar{c}_0}t',$$

and introduce the non-dimensional medium properties and wavefield magnitudes by the relations:

$$\varrho(z) = \bar{\varrho}_0\varrho'(z'), \qquad \kappa(z) = \bar{\kappa}_0\kappa'(z'), \tag{2.2.2}$$

$$u(z,t) = \bar{c}_0 u'(z',t'), \qquad p(z,t) = \bar{\kappa}_0 p'(z',t'). \tag{2.2.3}$$

After substitution in the equations above and dropping primes, we get a set of non-dimensional equations similar to (2.2.1) but with the corresponding average wavefield magnitudes of order $O(1)$.

Furthermore, we consider a layered random slab of length L surrounded by a homogeneous medium with matched interfaces:

$$\varrho(z) = \begin{cases} \varrho_0(z)\big(1+\eta^\varepsilon(z)\big), & \text{for } z \in [-L,0] \\ \varrho_0(0), & \text{for } z > 0 \\ \varrho_0(-L), & \text{for } z < -L \end{cases} \tag{2.2.4a}$$

$$\frac{1}{\kappa(z)} = \begin{cases} \frac{1}{\kappa_0(z)}\big(1+\nu^\varepsilon(z)\big), & \text{for } z \in [-L,0] \\ \frac{1}{\kappa_0(0)}, & \text{for } z > 0 \\ \frac{1}{\kappa_0(-L)}, & \text{for } z < -L \end{cases} \tag{2.2.4b}$$

where $\varrho_0(z)$ and $\kappa_0(z)$ are the nonrandom background density and bulk modulus, and $\eta^\varepsilon(z)$, $\nu^\varepsilon(z)$ are mean-zero, random functions with absolute values bounded by a deterministic constant C such that $C < 1$, and with correlation length l^ε. This representation of the random slab properties is consistent with the homogenization theory as we pointed out in remark 2.2.1. Therefore, the 'locally' homogenized medium properties for the slab are $\varrho_0(z)$ and $\kappa_0(z)$, and the corresponding sound speed and acoustic impedance are given by

$$c_0(z) = \sqrt{\frac{\kappa_0(z)}{\varrho_0(z)}} \quad \text{and} \quad \zeta_0(z) = \sqrt{\varrho_0(z)\kappa_0(z)}, \tag{2.2.5}$$

respectively.

We have introduced the small parameter $\varepsilon \ll 1$ that will be used for identifying regimes that are of interest to our analysis and to allow for an asymptotic treatment. The case where L is large (i.e. $L = +\infty$) corresponds to a layered random half-space. It is the case in which we shall be interested later on.

2.2.2 Scaling and medium fluctuations

When the background medium and the fluctuations vary on well-separated length scales, i.e. when $l^\varepsilon \ll 1$, we can think of the background as the macroscopic structure and the fluctuations as the random micro-structure of the medium.

The regimes in which the long term effect of the medium fluctuations is important appears when the pulse propagates over long distances compared to its typical wavelength and actively interacts with the random medium fluctuations.

Initially a downward travelling wave impinges upon the interface $z = 0$. For the incident pulse in time we consider

$$u_{\mathrm{inc}}(0,t) = -\frac{f(\frac{t}{\varepsilon})}{2\zeta_0^{1/2}(0)}, \qquad p_{\mathrm{inc}}(0,t) = \frac{\zeta_0^{1/2}(0)f(\frac{t}{\varepsilon})}{2} \tag{2.2.6}$$

where f is a smooth function with compact support contained in $[0,+\infty)$. Here the time scaling emphasizes that the typical wavelength of the propagating wave will be of $O(\varepsilon)$.

For the fluctuations we assume two different scaling. In the *strong fluctuations regime* we set:

$$\eta^\varepsilon(z) = \eta(z, \frac{z}{\varepsilon^2}) \quad \text{and} \quad \nu^\varepsilon(z) = \nu(z, \frac{z}{\varepsilon^2}), \tag{2.2.7}$$

and for the *weak fluctuations regime*:

$$\eta^\varepsilon(z) = \sqrt{\varepsilon}\eta(z, \frac{z}{\varepsilon}) \quad \text{and} \quad \nu^\varepsilon(z) = \sqrt{\varepsilon}\nu(z, \frac{z}{\varepsilon}), \tag{2.2.8}$$

where for each fixed z, $\eta(z,s)$ and $\nu(z,s)$ are mean zero stationary stochastic processes (for example: the components of a stationary ergodic Markov process or a process having strong mixing properties) with correlation length in s of $O(1)$ and with slowly varying statistics with respect to z. Consequently the 'microscopic' fluctuations' correlation length l^ε will be of $O(\varepsilon^2)$ and $O(\varepsilon)$ in the strong and weak fluctuations regimes, respectively.

Remark 2.2.2. This model of random fluctuations besides the micro-scale randomness effect takes into account its large scale statistical behavior [16]. A useful simplified model can be obtained by eliminating in (2.2.7) and (2.2.8) the dependence on the large-scale as follows:

$$\eta^\varepsilon(z) = \eta(\frac{z}{\varepsilon^2}), \quad \nu^\varepsilon(z) = \nu(\frac{z}{\varepsilon^2}),$$

and

$$\eta^\varepsilon(z) = \sqrt{\varepsilon}\eta(\frac{z}{\varepsilon}), \quad \nu^\varepsilon(z) = \sqrt{\varepsilon}\nu(\frac{z}{\varepsilon})$$

for the strong and weak fluctuations regimes, respectively. We will refer to it as a *statistically homogeneous random fluctuations* model.

2.2.3 Reflected signal

The mathematical setup and results of this section closely follows the works by Burridge et al. [16, 17] and the reviews [3, 28], so we will not enter into details.

First we recall the reflection problem for an incident pulse propagating in a random slab. By introducing the wave field decomposition into downward and upward travelling waves A, B defined as

$$\begin{cases} A(z,t) = -\zeta_0^{\frac{1}{2}}(z)u(z,t) + \zeta_0^{-\frac{1}{2}}(z)p(z,t) \\ B(z,t) = \zeta_0^{\frac{1}{2}}(z)u(z,t) + \zeta_0^{-\frac{1}{2}}(z)p(z,t), \end{cases} \tag{2.2.9}$$

for the reflected signal at the interface we have

$$u_{\mathrm{ref}}(0,t) = \frac{\zeta_0^{-1/2}(0)B(0,t)}{2} \quad \text{and} \quad p_{\mathrm{ref}}(0,t) = \frac{\zeta_0^{1/2}(0)B(0,t)}{2}.$$

In this variables the system is of the form:

$$\frac{1}{c_0}\begin{pmatrix} -(1+m^\varepsilon) & -n^\varepsilon \\ n^\varepsilon & 1+m^\varepsilon \end{pmatrix} \frac{\partial}{\partial t}\begin{pmatrix} A \\ B \end{pmatrix} + \frac{\partial}{\partial z}\begin{pmatrix} A \\ B \end{pmatrix} + \frac{\zeta_0'}{2\zeta_0}\begin{pmatrix} B \\ A \end{pmatrix} = \mathbf{0}$$

where

$$m^\varepsilon = \tfrac{1}{2}(\eta^\varepsilon + \nu^\varepsilon) \quad \text{and} \quad n^\varepsilon = \tfrac{1}{2}(\nu^\varepsilon - \eta^\varepsilon). \tag{2.2.10}$$

It should be noted that m^ε and n^ε are random functions so we have a system of linear partial differential equations with random coefficients; next it will be reduced to a system of ordinary differential equations with random coefficients for which 'Central Limit Theorems' are available in the literature.

In fact, by performing ε-scaled Fourier transforms

$$\begin{cases} \tilde{A}(z,\omega) = \varepsilon^{-1}\int \mathrm{e}^{\mathrm{i}\omega\frac{t}{\varepsilon}} A(z,t)\mathrm{d}t \\ \tilde{B}(z,\omega) = \varepsilon^{-1}\int \mathrm{e}^{\mathrm{i}\omega\frac{t}{\varepsilon}} B(z,t)\mathrm{d}t \end{cases} \tag{2.2.11}$$

and introducing a wave delay with respect to the travel time

$$\tau(z) = \int_z^0 \frac{\mathrm{d}s}{c_0(s)}, \tag{2.2.12}$$

through the relations

$$a(z,\omega) = \mathrm{e}^{-\mathrm{i}\omega\frac{\tau(z)}{\varepsilon}} \tilde{A}(z,\omega) \qquad b(z,\omega) = \mathrm{e}^{\mathrm{i}\omega\frac{\tau(z)}{\varepsilon}} \tilde{B}(z,\omega), \tag{2.2.13}$$

after some elementary transformations we get the linear ordinary differential equations for a, b:

$$\begin{aligned} \frac{\mathrm{d}}{\mathrm{d}z}\begin{pmatrix} a \\ b \end{pmatrix} &= \frac{\mathrm{i}\omega}{\varepsilon} c_0^{-1} \begin{pmatrix} -m^\varepsilon & -n^\varepsilon \mathrm{e}^{-2\mathrm{i}\omega\frac{\tau(z)}{\varepsilon}} \\ n^\varepsilon \mathrm{e}^{2\mathrm{i}\omega\frac{\tau(z)}{\varepsilon}} & m^\varepsilon \end{pmatrix} \begin{pmatrix} a \\ b \end{pmatrix} \\ &\quad - \frac{\zeta_0'}{2\zeta_0} \begin{pmatrix} 0 & \mathrm{e}^{-2\mathrm{i}\omega\frac{\tau(z)}{\varepsilon}} \\ \mathrm{e}^{2\mathrm{i}\omega\frac{\tau(z)}{\varepsilon}} & 0 \end{pmatrix} \begin{pmatrix} a \\ b \end{pmatrix} \\ &= Q^\varepsilon(z,\omega) \begin{pmatrix} a \\ b \end{pmatrix}. \end{aligned} \tag{2.2.14}$$

Based on the linearity of the solutions we take boundary conditions corresponding to the case where a downward normalized wave is incident at $z = 0$ and there is no upward travelling wave at $z = -L$ (see figure 2.1), that is:

$$a(0,\omega) = 1 \quad \text{and} \quad b(-L,\omega) = 0. \tag{2.2.15}$$

Using these equations for the associated quantities of interest we shall deduce random ordinary differential equations which can be analyzed in a probabilistic asymptotic fashion, as will be shown in the sequel.

Integral representation of the reflected signal

Define the transmission and reflection coefficients for the random slab as:

$$T_L^\varepsilon(\omega) = a(-L,\omega) \quad \text{and} \quad R_L^\varepsilon(\omega) = b(0,\omega), \tag{2.2.16}$$

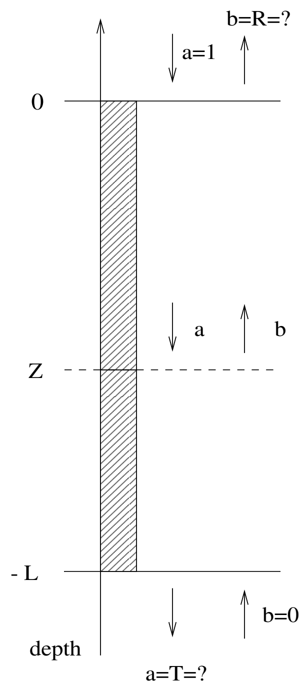

Figure 2.1: Definition of the reflection and transmission coefficients. The invariant embedding technique.

respectively (see fig. 2.1). Therefore, for the upward travelling wave field the following integral representation is valid:

$$B(0,t) = \frac{1}{2\pi} \int \mathrm{e}^{-\mathrm{i}\omega \frac{t}{\varepsilon}} \tilde{A}(0,\omega) R_L^{\varepsilon}(\omega) \mathrm{d}\omega. \qquad (2.2.17)$$

Note that $\tilde{A}(0,\omega)$ is the Fourier content of the down-travelling wave incident at the interface.

Reflection coefficient and the random Riccati equation

The computation of the reflection coefficient using (2.2.14) is rather complicated and involves the solution of a two-point boundary value problem. However, the application of propagator matrices leads to an initial value problem to determine the reflection coefficient which is more tractable situation. Next, we proceed to obtain this initial value problem: a random Riccati equation with a trivial initial condition.

Let $\mathbf{Y}_L(z,\omega)$ be the fundamental or propagator complex matrix corresponding to equation (2.2.14), so it satisfies the corresponding matrix equation with initial condition $\mathbf{Y}_L(-L,\omega) = \mathbf{I}_2$ (the 2×2 identity matrix). Since $Q^\varepsilon(z,\omega)$ belongs to the Lie algebra $\mathfrak{su}(1,1)$ then the equation defines a curve on the Lie group $\mathrm{SU}(1,1)$ [1] and consequently the propagator matrix has the form [62]

$$\mathbf{Y}_L(z,\omega) = \begin{pmatrix} \alpha(z,\omega) & \bar{\beta}(z,\omega) \\ \beta(z,\omega) & \bar{\alpha}(z,\omega) \end{pmatrix}$$

with

$$|\alpha|^2 - |\beta|^2 = 1. \tag{2.2.18}$$

Additionally, we have that $[\alpha(z,\omega),\ \beta(z,\omega)]^t$ is the solution of (2.2.14) with initial condition $[\alpha(-L,\omega),\ \beta(-L,\omega)]^t = [1,\ 0]^t$.

From the definition of the transmission and reflection coefficients for the random slab $[-L,0]$, by (2.2.16), we have:

$$\begin{pmatrix} \alpha(0,\omega) & \bar{\beta}(0,\omega) \\ \beta(0,\omega) & \bar{\alpha}(0,\omega) \end{pmatrix} \begin{pmatrix} T_L^\varepsilon \\ 0 \end{pmatrix} = \begin{pmatrix} 1 \\ R_L^\varepsilon \end{pmatrix},$$

implying that:

$$R_L^\varepsilon(\omega) = \frac{\beta(0,\omega)}{\alpha(0,\omega)} \quad \text{and} \quad T_L^\varepsilon(\omega) = \frac{1}{\alpha(0,\omega)}. \tag{2.2.19}$$

We can now extend this definition in an invariant embedding spirit [10]. Reformulating these relations in the slab section $[-L,z]$ with the right extremity varying (see fig. 2.1), one has the transmission and reflection coefficients

$$R_L^\varepsilon(z,\omega) = \frac{\beta(z,\omega)}{\alpha(z,\omega)} \quad \text{and} \quad T_L^\varepsilon(z,\omega) = \frac{1}{\alpha(z,\omega)}. \tag{2.2.20}$$

As a consequence of (2.2.18) we have a conservation of energy relation:

$$|R_L^\varepsilon(z,\omega)|^2 + |T_L^\varepsilon(z,\omega)|^2 = 1. \tag{2.2.21}$$

[1] The Lie group $\mathrm{SU}(1,1)$ consists of 2×2 complex matrices A such that $\det \mathrm{A} = 1$ and $\mathrm{AGA}^* = \mathrm{G}$ where $\mathrm{G} = \left(\begin{smallmatrix} 1 & 0 \\ 0 & -1 \end{smallmatrix}\right)$. His Lie algebra $\mathfrak{su}(1,1)$ is spanned by matrices of the form $\left(\begin{smallmatrix} \mathrm{i}a & \beta \\ \bar{\beta} & -\mathrm{i}a \end{smallmatrix}\right)$ with $a \in \mathbf{R}$, $\beta \in \mathbf{C}$.

Using (2.2.14), one obtains the following **random Riccati equation** for the reflection coefficient:

$$\begin{aligned}\frac{\mathrm{d}}{\mathrm{d}z}R_L^\varepsilon = \frac{\mathrm{i}\omega}{\varepsilon}c_0^{-1}(z)\big(n^\varepsilon(z)\mathrm{e}^{2\mathrm{i}\omega\frac{\tau(z)}{\varepsilon}} + 2m^\varepsilon(z)R_L^\varepsilon + n^\varepsilon(z)\mathrm{e}^{-2\mathrm{i}\omega\frac{\tau(z)}{\varepsilon}}(R_L^\varepsilon)^2\big)\\ - \frac{\zeta_0'(z)}{2\zeta_0(z)}\big(\mathrm{e}^{2\mathrm{i}\omega\frac{\tau(z)}{\varepsilon}} - \mathrm{e}^{-2\mathrm{i}\omega\frac{\tau(z)}{\varepsilon}}(R_L^\varepsilon)^2\big)\end{aligned} \tag{2.2.22}$$

with initial condition:

$$R_L^\varepsilon(-L,\omega) = 0.$$

Remark 2.2.3. This condition at $z = -L$ is for termination of the random slab by a matched uniform medium (see relations (2.2.4)). However, if the random medium is statistically homogeneous beyond $z = -L$ (i.e. $\varrho_0(z)$, $\kappa_0(z)$ are constant and the fluctuations statistics do not depend on z for $z < -L$) then we will have total reflection at $z = -L$ because the wave cannot penetrate the random medium to infinite depth [16].

Taking into account this remark, the case of a random half-space can be simplified analyzing (2.2.22) with a *totally reflecting termination* (i.e. $|T_L^\varepsilon(z)| = 0$), so that

$$R^\varepsilon(z,\omega) = \mathrm{e}^{-\mathrm{i}\phi^\varepsilon(z,\omega)}$$

with ϕ^ε real, which reduces the degrees of freedom to one. After substitution in (2.2.22) we get the **random ordinary differential equation**

$$\frac{\mathrm{d}}{\mathrm{d}z}\phi^\varepsilon = -2\frac{\omega}{\varepsilon}c_0^{-1}(z)\big(m^\varepsilon(z)+n^\varepsilon(z)\cos(\phi^\varepsilon+2\omega\frac{\tau(z)}{\varepsilon})\big)+\frac{\zeta_0'(z)}{\zeta_0(z)}\sin(\phi^\varepsilon+2\omega\frac{\tau(z)}{\varepsilon}) \tag{2.2.23}$$

and take ϕ^ε to be asymptotically stationary as $z \to -\infty$.

Lastly, we remark that the totally reflecting termination assumption can also be used to analyze reflection for times $t < \frac{L}{2c_0}$, since until this moment the wave does not feel the medium beyond $z = -L$.

2.2.4 Statistics of the reflected signal

First, we re-scale the amplitude of the incident pulse (2.2.6) to make its energy independent of ε by setting:

$$u_{\text{inc}}(0,t) = -\frac{\zeta_0^{-1/2}(0) f(\frac{t}{\varepsilon})}{2\varepsilon^{1/2}} \quad \text{and} \quad p_{\text{inc}}(0,t) = \frac{\zeta_0^{1/2}(0) f(\frac{t}{\varepsilon})}{2\varepsilon^{1/2}}, \tag{2.2.24}$$

which corresponds to make $A(0,t) = \varepsilon^{-1/2} f(\frac{t}{\varepsilon})$. Therefore the reflected signal reduces to:

$$B(0,t) = \frac{1}{2\pi\varepsilon^{1/2}} \int_{-\infty}^{+\infty} \mathrm{e}^{-\mathrm{i}\omega\frac{t}{\varepsilon}} \hat{f}(\omega) R_L^\varepsilon(0,\omega) \mathrm{d}\omega, \tag{2.2.25}$$

where $\hat{f}$ is the Fourier transform of f.

Characterizing this scattered signal appears to be a difficult task because it is not stationary, however (asymptotically) it is locally stationary and this allows for a great simplification of the analysis [3, 16, 17]. More exactly, observing the reflected signal in the same time scale of the incident pulse leads to considering the stochastic process

$$B_{t,f}^\varepsilon(s) = \frac{1}{2\pi\varepsilon^{1/2}} \int \mathrm{e}^{-\mathrm{i}\omega\frac{t+\varepsilon s}{\varepsilon}} \hat{f}(\omega) R_L^\varepsilon(0,\omega) \mathrm{d}\omega. \tag{2.2.26}$$

It has been shown [16, 57] that this stochastic signal converges in distribution to a stationary centered Gaussian process with covariance given by:

$$\begin{aligned} C_{t,f}(s) &= \lim_{\varepsilon \downarrow 0} \mathbb{E}\{B_{t,f}^\varepsilon(s) B_{t,f}^\varepsilon(0)\} \\ &= \frac{1}{2\pi} \int \mathrm{e}^{-\mathrm{i}\omega s} |f(\omega)|^2 \Lambda(t,\omega) \mathrm{d}\omega \end{aligned}$$

where

$$\Lambda(t,\omega) = \frac{1}{2\pi} \int \mathrm{e}^{\mathrm{i}ht} \lim_{\varepsilon \downarrow 0} \mathbb{E}\{R_L^\varepsilon(0,\omega + \tfrac{\varepsilon}{2}h) \overline{R_L^\varepsilon}(0,\omega - \tfrac{\varepsilon}{2}h)\} \mathrm{d}h. \tag{2.2.27}$$

Moreover, an asymptotic analysis of the Riccati equation for the reflection coefficient (2.2.22) allows for a characterization of the normalized power spectral density $\Lambda(t,\omega)$ [3, 16, 57]. For simplicity, we recall the case of a uniform random half-space with random fluctuations only of the density where explicit formula have been found. Without lost of generality we can set $c_0 = 1$. Moreover, we have $\nu^\varepsilon = 0$ and

$\eta^\varepsilon(z) = \eta(\frac{z}{\varepsilon^2})$ for strong and $\eta^\varepsilon(z) = \sqrt{\varepsilon}\eta(\frac{z}{\varepsilon})$ for weak fluctuations, respectively. The unscaled fluctuation $\eta(\cdot)$ coming from a stationary ergodic Markov process. In the strong medium fluctuations case we have that:

$$\Lambda(t,\omega) = \frac{\gamma_\eta \omega^2}{(1+\gamma_\eta\omega^2 t)^2}, \tag{2.2.28}$$

where $\gamma_\eta = \frac{1}{4}\int_0^\infty \mathbb{E}\{\eta(0)\eta(s)\}\mathrm{d}s$. And for weak medium fluctuations we get:

$$\Lambda(t,\omega) = \frac{\gamma_\eta^c(\omega)\omega^2}{(1+\gamma_\eta^c(\omega)\omega^2 t)^2}, \tag{2.2.29}$$

where $\gamma_\eta^c(\omega) = \frac{1}{4}\int_0^\infty \mathbb{E}\{\eta(0)\eta(s)\cos(2\omega s)\}\mathrm{d}s$.

2.3 Joint reflection process

In this section we address the problem about the effects of medium perturbations on the reflected signal. More specifically, we consider two random media with the same underlying background and such that the random fluctuations of one medium are obtained by a noisy perturbation of fluctuations corresponding to the other. The perturbation is considered to be statistically independent from the original unperturbed random medium. Physically this assumption represents the case where the perturbation is caused by a factor independent of those generated the unperturbed fluctuations or by a random medium that changed in time.

Let us introduce two random media with properties $(\varrho_1(z), \kappa_1(z))$, $(\varrho_2(z), \kappa_2(z))$, for which fluctuations $(\eta_1^\varepsilon(z), \nu_1^\varepsilon(z))$, $(\eta_2^\varepsilon(z), \nu_2^\varepsilon(z))$ are related to the macroscopic properties by expressions analogous to (2.2.4), respectively. We assume that for fixed z the corresponding unscaled fluctuations $(\eta_j(z,\cdot), \nu_j(z,\cdot))$, $j = 1, 2$, are mean zero components of a stationary ergodic Markov process $\mathbf{q}(z,\cdot)$ whose state space is a compact subset of $\mathbf{R}^d$, $d \geq 4$.

The hypothesis of statistical independence of the perturbations are formulated in terms of the combined fluctuations $m_j = \frac{1}{2}(\nu_j + \eta_j)$ and $n_j = \frac{1}{2}(\nu_j - \eta_j)$, $j = 1, 2$ as follows:

$$m_1 = m \qquad\qquad n_1 = n \tag{2.3.1a}$$

$$m_2 = m + \delta m \qquad\qquad n_2 = n + \delta n, \tag{2.3.1b}$$

and

$$\mathbb{E}\{n(z, s_1)\delta n(z, s_2)\} = 0 \tag{2.3.1c}$$

$$\mathbb{E}\{m(z, s_1)\delta m(z, s_2)\} = 0 \tag{2.3.1d}$$

for fixed z and $s_1, s_2 \geq 0$.

For each random medium there is a corresponding stochastic reflection process:

$$B_{t,f}^{j,\varepsilon}(s) = \frac{1}{2\pi\varepsilon^{1/2}} \int \mathrm{e}^{-\mathrm{i}\omega\frac{t+\varepsilon s}{\varepsilon}} \hat{f}(\omega) R_{L,j}^{\varepsilon}(0,\omega) d\omega, \tag{2.3.2}$$

where $j = 1, 2$ labels the medium and $R_{L,j}^{\varepsilon}(0,\omega)$ is the corresponding reflection coefficient.

If the two media are statistically independent then asymptotically the reflected signals are independent, centered, stationary Gaussian processes. However, we are interested in the situation where the media are statistically correlated. Therefore, we shall analyze the *joint reflection process*:

$$(\mathbf{B}_{t,f}^{\varepsilon}(s), s \in \mathbf{R}) = (B_{t,f}^{1,\varepsilon}(s), B_{t,f}^{2,\varepsilon}(s))_{s\in\mathbf{R}}.$$

To characterize the statistical behavior of the joint reflection process we shall perform an asymptotic analysis as ε goes to zero. Since each component is stationary and has a mean zero limit, the joint reflection process is asymptotically stationary and centered. Further, we will focus on the characterization of the covariance matrix and (matrix valued) spectral density of this limit process.

After a straightforward calculation, for the covariance matrix of the limit process we have:

$$\begin{aligned}\mathbf{C}_{t,f}(s) &= \lim_{\varepsilon\downarrow 0} \mathbb{E}\{\mathbf{B}_{t,f}^{\varepsilon}(s) \otimes \mathbf{B}_{t,f}^{\varepsilon}(0)\} \\ &= \frac{1}{2\pi} \int \mathrm{e}^{-\mathrm{i}\omega s} |\hat{f}(\omega)|^2 \mathbf{\Lambda}(t,\omega) \mathrm{d}\omega\end{aligned} \tag{2.3.3}$$

where the matrix $\mathbf{\Lambda}(t,\omega)$ has entries:

$$\Lambda_{jk}(t,\omega) = \frac{1}{2\pi}\int \mathrm{e}^{-iht} u_{jk}(\omega,h)\mathrm{d}h \quad j,k=1,2, \tag{2.3.4}$$

with

$$u_{jk}(\omega,h) = \lim_{\varepsilon\downarrow 0}\mathbb{E}\{R^{\varepsilon}_{L,j}(0,\omega+\tfrac{\varepsilon}{2}h)\overline{R^{\varepsilon}_{L,k}}(0,\omega-\tfrac{\varepsilon}{2}h)\}, \tag{2.3.5}$$

the limiting joint correlation of the reflection coefficients at the interface $z=0$ for two nearby frequencies. From this, we have that the matrix valued power spectral density of the limit process is given by $|\hat{f}(\omega)|^2\mathbf{\Lambda}(t,\omega)$.

Remark 2.3.1. The existence of the limit in (2.3.5) will be established in the next section for $L\to+\infty$, as a first step toward the characterization of the power spectral density. However, its inverse Fourier transform (2.3.4) exists just in a generalized sense, i.e. by smoothing this formal expression with a test function and changing the order of integration [16, 57]. Nevertheless, we proceed by directly using this formal expression for the characterization of the power spectral density. We remark that these results obtained in a formal way can be rigourously justified using the method of generalized reflection functional, introduced in [16] and thoroughly applied in [57], associated with the joint reflection process.

2.4 Characterization of the power spectral density

We should note that the diagonal entries of the normalized power spectral density matrix $\mathbf{\Lambda}(t,\omega)$ corresponds to the normalized power spectral densities of the reflection processes for each individual random medium. These are well-known as we have remarked in the previous section. Therefore, we shall concentrate on the calculation of the off-diagonal entries $\Lambda_{12}(t,\omega)=\overline{\Lambda}_{21}(t,\omega)$.

We first apply the asymptotic theory of stochastic differential equations in order to obtain a characterization of $u_{12}(\omega,h)$. In order to do so we consider the embedding of the slab in a medium with a totally reflecting termination or a totally reflecting half-space. Thus, the reflection coefficients are expressed as:

$$R_j(z,\omega) = \mathrm{e}^{-\mathrm{i}\phi_j^\varepsilon(z,\omega)}, \tag{2.4.1}$$

with ϕ_j^ε real, $j = 1, 2$. Define

$$\psi_{1,2}^\varepsilon(z,\omega,h) = \phi_{1,2}^\varepsilon(z,\omega \pm \varepsilon\frac{h}{2}), \tag{2.4.2}$$

then $u_{12}(\omega,h) = \lim_{\varepsilon\downarrow 0} \mathbb{E}\{\mathrm{e}^{\mathrm{i}(\psi_2^\varepsilon(0,\omega,h)-\psi_1^\varepsilon(0,\omega,h))}\}$

Now we analyze these objects in the two regimes mentioned earlier: strong and weak fluctuations.

2.4.1 Strong medium fluctuations

Asymptotics for the joint correlation

In this case from equation (2.2.23)

$$\frac{\mathrm{d}}{\mathrm{d}z}\phi_j^\varepsilon = -2\frac{\omega}{\varepsilon}c_0^{-1}\left(m_j^\varepsilon + n_j^\varepsilon\cos(\phi_j^\varepsilon + 2\omega\frac{\tau}{\varepsilon})\right) + \frac{\zeta_0'}{\zeta_0}\sin(\phi_j^\varepsilon + 2\omega\frac{\tau}{\varepsilon})$$

and using the corresponding scaling in the half-space $z \le 0$

$$m_j^\varepsilon(z) = m_j(z,\frac{z}{\varepsilon^2}) \quad \text{and} \quad n_j^\varepsilon(z) = n_j(z,\frac{z}{\varepsilon^2})$$

for $\boldsymbol{\psi}^\varepsilon = [\psi_1^\varepsilon, \psi_2^\varepsilon]^t$, we have after some elementary transformations the random ordinary differential equation

$$\frac{\mathrm{d}}{\mathrm{d}z}\boldsymbol{\psi}^\varepsilon = \varepsilon^{-1}\mathbf{F}(z,\boldsymbol{\psi}^\varepsilon,\mathbf{q}(z,\frac{z}{\varepsilon^2}),\frac{\tau(z)}{\varepsilon}) + \mathbf{G}(z,\boldsymbol{\psi}^\varepsilon,\mathbf{q}(z,\frac{z}{\varepsilon^2}),\frac{\tau(z)}{\varepsilon}). \tag{2.4.3}$$

Here $\mathbf{F} = [F_1, F_2]^t$ and $\mathbf{G} = [G_1, G_2]^t$ are defined by

$$F_j(z,\boldsymbol{\psi},\mathbf{q}(z,s),\mu) = \\ -\frac{2\omega}{c_0(z)}\Big(m_j(z,s) + n_j(z,s)\cos\big(\psi_j + 2\omega\mu + (-1)^{j-1}h\tau(z)\big)\Big), \tag{2.4.4}$$

and

$$G_j(z, \boldsymbol{\psi}, \mathbf{q}(z,s), \mu) = \\ (-1)^j \frac{h}{c_0(z)} \Big(m_j(z,s) + n_j(z,s) \cos\big(\psi_j + 2\omega\mu + (-1)^{j-1} h\tau(z)\big)\Big) \\ + \frac{\zeta_0'(z)}{\zeta_0(z)} \sin\big(\psi_j + 2\omega\mu + (-1)^{j-1} h\tau(z)\big). \quad (2.4.5)$$

Note that the random ordinary differential equation above becomes singular as ε goes to zero, however the fact that $\mathbf{F}$ is centered (i.e. $\mathbb{E}\{\mathbf{F}\} = 0$) and the proper scaling on the z variable gives a consistent limiting behavior. Namely, according to the diffusion-approximation theorem A.1 (see appendix A and also the references therein), as ε goes to zero, $\boldsymbol{\psi}^\varepsilon$ converges in distribution to a diffusion process $\boldsymbol{\psi}$ with infinitesimal generator given by:

$$\mathcal{L}_z V = \int_0^{+\infty} \big\langle \mathbb{E}\{\mathbf{F}(z, \boldsymbol{\psi}, \mathbf{q}(z,0), \mu) \cdot \nabla_{\boldsymbol{\psi}} [\mathbf{F}(z, \boldsymbol{\psi}, \mathbf{q}(z,r), \mu) \cdot \nabla_{\boldsymbol{\psi}} V]\}\big\rangle_\mu \mathrm{d}r \\ + \big\langle \mathbb{E}\{\mathbf{G}(z, \boldsymbol{\psi}, \mathbf{q}(z,0), \mu) \cdot \nabla_{\boldsymbol{\psi}} V\}\big\rangle_\mu \quad (2.4.6)$$

where $\mathbb{E}\{\cdot\}$ represents expectation with respect to the stationary process $\mathbf{q}(z, \cdot)$ and $\langle \cdot \rangle_\mu = \lim_{\mu_0 \to +\infty} \frac{1}{\mu_0} \int_0^{\mu_0} \cdot \mathrm{d}\mu$ is the average with respect to the fast phase $\mu = \frac{\tau(z)}{\varepsilon}$. Therefore $u_{12}(\omega, h) = \mathbb{E}\{\exp[\mathrm{i}(\psi_2(0) - \psi_1(0))]\}$ can be computed solving the corresponding Kolmogorov backward equation

$$\begin{cases} (\dfrac{\partial}{\partial z} + \mathcal{L}_z) V = 0, & z < 0 \\ V|_{z=0} = \mathrm{e}^{\mathrm{i}(\psi_2 - \psi_1)} \end{cases}$$

and determining the limit

$$u_{12}(\omega, h) = \lim_{z \to -\infty} V(z, \boldsymbol{\psi}, \omega, h).$$

As we will see later on this limit actually exists and is independent of $\boldsymbol{\psi}$, if we assume that the media behave statistically homogeneous as $z \to -\infty$.

Now we calculate the infinitesimal generator corresponding to our problem of interest. After some elementary computations we arrive to the expression:

$$\begin{aligned}\mathcal{L}_z V = \frac{4\omega^2}{c_0(z)}\Big\{&\big(\gamma_m(z) + \tfrac{1}{2}\gamma_n(z)\big)\big(\partial_{\psi_1} + \partial_{\psi_2}\big)^2 \\ &+ \gamma_n(z)\big(\cos\big(\psi_1 - \psi_2 + 2h\tau(z)\big) - 1\big)\partial^2_{\psi_1\psi_2} + \big(\gamma_{\delta m}(z) + \tfrac{1}{2}\gamma_{\delta n}(z)\big)\partial^2_{\psi_2}\Big\}V \end{aligned} \tag{2.4.7}$$

where we have set

$$\gamma_g(z) = \frac{1}{c_0(z)}\int_0^\infty \mathbb{E}\{g(z,0)g(z,r)\}\,\mathrm{d}r$$

for $g = m, n, \delta m, \delta n$.

The infinitesimal generator structure allows for some simplifications. Introduce $\tilde{\gamma}_{m,n}(z) = \gamma_{\delta m}(z) + \frac{1}{2}\gamma_{\delta n}(z)$ and the new variables $\psi = \psi_2 - \psi_1$, $\tilde{\psi} = (\psi_1 + \psi_2)/2$. Note that after this change of variables the generator coefficients do not depend on the spatial variable $\tilde{\psi}$. Consequently, we have that ψ is Markovian by itself and through restricting to functions that depend only on this spatial variable ψ we obtain the corresponding generator:

$$\tilde{\mathcal{L}}_z V = \frac{4\omega^2}{c_0(z)}\big\{\gamma_n(z)\big(1 - \cos\big(\psi - 2h\tau(z)\big)\big) + \tilde{\gamma}_{m,n}(z)\big\}\partial^2_\psi V. \tag{2.4.8}$$

Moreover, for calculating $u_{12}(\omega, h)$ now we have to solve the associated Kolmogorov backward equation

$$\begin{cases} (\dfrac{\partial}{\partial z} + \tilde{\mathcal{L}}_z)V = 0, & z < 0 \\ V|_{z=0} = \mathrm{e}^{\mathrm{i}\psi} \end{cases}$$

and determine the limit

$$u_{12}(\omega, h) = \lim_{z\to-\infty} V(z, \psi, \omega, h).$$

Furthermore, the change of variables $z' = z$, $\psi' = \psi - 2h\tau(z)$ leads to the equation (after dropping primes)

$$\begin{cases} (\dfrac{\partial}{\partial z} + \mathcal{L}^0)V = 0, & \text{for } z < 0 \\ V|_{z=0} = \mathrm{e}^{\mathrm{i}\psi} \end{cases} \tag{2.4.9}$$

where

$$\mathcal{L}^0 V = \frac{2h}{c_0(z)}\partial_\psi V + \frac{4\omega^2}{c_0(z)}\big\{\gamma_n(z)(1-\cos\psi) + \tilde{\gamma}_{m,n}(z)\big\}\partial_\psi^2 V. \tag{2.4.10}$$

Since $\tau(0) = 0$ then

$$u_{12}(\omega, h) = \lim_{z\to-\infty} V(z,\psi,\omega,h). \tag{2.4.11}$$

Remark 2.4.1. It should be noted that since ψ is Markovian, the further description of the quantities of interest to us becomes simpler because only a one-dimensional diffusion process is involved. This is a remarkable simplification since according to the diffusion aproximation theorem A.1 one should expect a description involving a two-dimensional diffusion process.

Remark 2.4.2. We have to note that the limit (2.4.11) exists and is independent of ψ if $c_0(z)$, $\gamma_n(z)$ and $\tilde{\gamma}_{m,n}(z)$ satisfy appropriate conditions. This follows, for instance, if $c_0^{-1}(z)$, $\frac{\gamma_n(z)}{c_0(z)}$ and $\frac{\tilde{\gamma}_{m,n}(z)}{c_0(z)}$ are bounded and $\frac{\tilde{\gamma}_{m,n}(z)}{c_0(z)} \geq \beta_0 > 0$ for $-\infty < z \leq 0$, applying the results in [35]. An interesting situation appears whem asymptotically the medium background is uniform, and the fluctuations and perturbations are statistically homogeneous at infinite depth ($z \to -\infty$), in the sense that their 'local' autocorrelations do not depend on depth, which is in complete agreement with the totally reflecting termination assumption. If additionally $\lim_{z\to-\infty} c_0(z) > 0$, $\lim_{z\to-\infty}\tilde{\gamma}_{m,n}(z) > 0$ then the previous conditions hold for z sufficiently deep ($z < z_0 \leq 0$), and the existence and independence of ψ of the limit (2.4.11) follows. In this case, the Markov process associated with the generator given by (2.4.10) is asymptotically stationary, with an ergodic limiting process (see Appendix B) so it is expected that its asymptotic behavior does not depend on the initial state.

Remark 2.4.3. We have to note that if we set $\delta m = \delta n = 0$, this is equivalent to considering just the first random medium, namely the unperturbed random medium. Then the equations above take the appropriate form for the computation of $u_{11}(\omega, h)$. More exactly, we have to solve (2.4.9) with the generator given by

$$\mathcal{L}^0 V = \frac{2h}{c_0(z)}\partial_\psi V + \frac{4\omega^2\gamma_n(z)}{c_0(z)}(1-\cos\psi)\partial_\psi^2 V,$$

and let $u_{11}(\omega, h) = \lim_{z\to-\infty} V(z,\psi,\omega,h)$, in complete agreement with [16]. Furthermore, if above we replace γ_n by $\gamma_{n_2} = \gamma_n + \gamma_{\delta n}$ these become equations for obtaining $u_{22}(\omega, h)$.

Once $u_{12}(\omega, h)$ is obtained, $\Lambda_{12}(\omega, t)$ can be determined by applying the inverse Fourier transform. However, as we noticed above it exists only in a generalized sense, so we formulate a system of equations that allows a more direct representation. More specifically we write a system of transport equations, the so-called *W-equations*, whose solution is related to $\Lambda_{12}(\omega, t)$ in a simple way. The W-equations to be obtained are slight modifications of those corresponding to the 'unperturbed' case given in [3, 16, 57].

We proceed by solving equation (2.4.9) using Fourier series in ψ:

$$V(z,\psi,\omega,h) = \sum_{N=-\infty}^{\infty} V^N \mathrm{e}^{\mathrm{i}N\psi}. \tag{2.4.12}$$

Substituting into (2.4.9) we obtain an infinite-dimensional system of linear equations for the coefficients V^N:

$$\begin{aligned}\frac{\partial V^N}{\partial z} + \frac{2\mathrm{i}hN}{c_0(z)}V^N + \frac{2\omega^2\gamma_n(z)}{c_0(z)}\{(N+1)^2V^{N+1} - 2N^2V^N + (N-1)^2V^{N-1}\}& \\ - \frac{4\omega^2}{c_0(z)}\tilde{\gamma}_{m,n}(z)N^2V^N = 0,&\end{aligned} \tag{2.4.13}$$

for $z < 0$, with the final conditions

$$V^N|_{z=0} = \delta_{N,1}, \tag{2.4.14}$$

where $\delta_{M,S}$ represents the Kronecker delta. Note that the equations corresponding to $N < 0$ decouple from the rest of the system. Moreover, because of the linearity together with the final conditions we obtain that $V^N \equiv 0$, for $N < 0$. Furthermore, since u_{12} not depend on ψ we get that

$$\begin{aligned}&\lim_{z\to-\infty} V^0(z,\omega,h) = u_{12}(\omega,h),\\ &\lim_{z\to-\infty} V^N(z,\omega,h) = 0, \qquad\qquad \text{for } N > 0.\end{aligned}$$

After introducing the inverse Fourier transform

$$U^N(z,\omega,t) = \frac{1}{2\pi}\int_{-\infty}^{+\infty} \mathrm{e}^{-\mathrm{i}ht} V^N \mathrm{d}h, \qquad \text{for } N \geq 0, \tag{2.4.15}$$

and the travel time $\tau(z)$ with respect to the background medium (2.2.12) as a new coordinate, we obtain the new system:

$$\begin{aligned}\frac{\partial U^N}{\partial \tau} + 2N\frac{\partial U^N}{\partial t} &= 2\omega^2\gamma_n(\tau)\big\{(N+1)^2U^{N+1} - 2N^2U^N + (N-1)^2U^{N-1}\big\} \\ &\quad - 4\omega^2\tilde{\gamma}_{m,n}(\tau)N^2U^N\end{aligned} \tag{2.4.16}$$

for $\tau > 0$, $N \geq 0$, with the initial conditions

$$U^N|_{\tau=0} = \delta_{N,1}\delta(t) \tag{2.4.17}$$

where $\delta(t)$ stands for the Dirac δ-function. Finally, we have that

$$\Lambda_{12}(t,\omega) = \lim_{\tau\to+\infty} U^0(\tau,t,\omega)$$

and as a consequence of the hyperbolicity of the equations

$$\Lambda_{12}(t,\omega) = U^0(\frac{t}{2},t,\omega). \tag{2.4.18}$$

Remark 2.4.4. Note that in accordance with remark 2.4.3 for obtaining $\Lambda_{11}(t,\omega)$ we have the equations

$$\frac{\partial U^N}{\partial \tau} + 2N\frac{\partial U^N}{\partial t} = 2\omega^2\gamma_n(\tau)\big\{(N+1)^2U^{N+1} - 2N^2U^N + (N-1)^2U^{N-1}\big\} \tag{2.4.19}$$

with initial conditions (2.4.17), and the representation $\Lambda_{11}(t,\omega) = U^0(\frac{t}{2},t,\omega)$ which is in full agreement with [16]. Furthermore, substituting γ_n by $\gamma_{n_2} = \gamma_n + \gamma_{\delta n}$ we arrive to the equations for computing $\Lambda_{22}(t,\omega)$.

Remark 2.4.5. It should be noted that for solving these equations we have to get rid of two fundamental difficulties since it is an infinite-dimensional system with distribution-valued initial data. This second difficulty can be overcome representing the solutions as distribution derivatives in t of smooth solutions since the coefficients are independent of t (see [3]).

The problem concerning infinite-dimension is much more difficult to deal with. However, since our main interest is in determining $U^0(\tau,t,\omega)$ one can partially overcome this problem by performing an asymptotic analysis.

Low frequency asymptotic

Let us expand U^N as a power series in ω^2:

$$U^N(\tau,t,\omega) = U^{N,0}(\tau,t) + \omega^2 U^{N,1}(\tau,t) + \ldots.$$

Substitution in the equations above yields

$$\frac{\partial U^{N,0}}{\partial \tau} + 2N\frac{\partial U^{N,0}}{\partial t} = 0,$$

and

$$\begin{aligned}\frac{\partial U^{N,k}}{\partial \tau} + 2N\frac{\partial U^{N,k}}{\partial t} &= 2\gamma_n(\tau)\big\{(N+1)^2 U^{N+1,k-1} - 2N^2 U^{N,k-1} \\ &\quad + (N-1)^2 U^{N-1,k-1}\big\} - 4\tilde{\gamma}_{m,n}(\tau) N^2 U^{N,k-1},\end{aligned}$$

for $k \geq 1$, with initial conditions

$$U^{N,k}|_{\tau=0} = \delta_{N,1}\delta_{k,0}\delta(t), \quad \text{for } k \geq 0.$$

Noting that

$$U^0(\tau,t,\omega) = 2\omega^2 \int_0^\tau \gamma_n(\tau')U^1(\tau',t,\omega)\mathrm{d}\tau',$$

and solving the equations above one gets the asymptotic result

$$\Lambda_{12}(t,\omega) \approx \omega^2\gamma_n(\frac{t}{2})\big\{1 - 4\omega^2\int_0^{\frac{t}{2}} \big(\gamma_n(\tau') + \tilde{\gamma}_{m,n}(\tau')\big)\mathrm{d}\tau'\big\}, \tag{2.4.20}$$

for $|\omega|$ small. Surprisingly in this approximation the effect of the medium perturbation is not present in the lower order term. The asymptotics coincide with that for the 'unperturbed' case. Moreover as one should expect, the dependence on perturbation appears in a cumulative way through integrals along the domain of influence.

Remark 2.4.6. It should be noted that using remark 2.4.3 one easily gets the asymptotics for the diagonal entries. More exactly we have

$$\Lambda_{11}(t,\omega) \approx \omega^2\gamma_n(\frac{t}{2})\big\{1 - 4\omega^2\int_0^{\frac{t}{2}} \gamma_n(\tau')\mathrm{d}\tau'\big\}$$

$$\Lambda_{22}(t,\omega) \approx \omega^2\big(\gamma_n(\frac{t}{2}) + \gamma_{\delta n}(\frac{t}{2})\big)\big\{1 - 4\omega^2\int_0^{\frac{t}{2}} \big(\gamma_n(\tau') + \gamma_{\delta n}(\tau')\big)\mathrm{d}\tau'\big\}$$

for $|\omega|$ small.

Further, we will obtain another system of transport equations for determining $\Lambda_{12}(t,\omega)$ that has some advantages in comparison with the previous formulation.

System of W-equations

We recall that the W-equations constitute a hierarchy of transport equations for the moments of the reflection coefficient [3].

Let us introduce the bilinear form:

$$\langle W(\tau), U(\tau)\rangle = \int \mathrm{d}t \sum_{N\geq 0} W^N(\tau,t)U^N(\tau,t). \tag{2.4.21}$$

Then the adjoint system corresponding to equations (2.4.16) with respect to this form can be written as:

$$\begin{aligned}\frac{\partial W^N}{\partial \tau} + 2N\frac{\partial W^N}{\partial t} + 2\omega^2 N^2\big\{\gamma_n(\tau)(W^{N+1} - 2W^N + W^{N-1})\\ - 2\tilde{\gamma}_{m,n}(\tau)W^N\big\} = 0,\end{aligned} \tag{2.4.22}$$

for $\tau > 0$, $N \geq 0$.

One can easily verify that (2.4.21) is a conserved quantity, that is

$$\frac{\partial}{\partial \tau}\langle W(\tau), U(\tau)\rangle = 0.$$

Now, using the final conditions

$$W^N|_{\tau=\tau_0} = \delta_{N,N_0}\delta(t-t_0),$$

we have that

$$U^{N_0}(\tau_0, t_0, \omega) = W^1(0,0,\omega)$$

where U^N is the solution of the transport equations (2.4.16)-(2.4.17).

Introducing the change of variable $t' \to t_0 - t$ and re-writing equations (2.4.22) we obtain the W-equations:

$$\begin{aligned}\frac{\partial W^N}{\partial \tau} - 2N\frac{\partial W^N}{\partial t'} + 2\omega^2 N^2\big\{\gamma_n(\tau)(W^{N+1} - 2W^N + W^{N-1})\\ - 2\tilde{\gamma}_{m,n}(\tau)W^N\big\} = 0,\end{aligned} \tag{2.4.23}$$

for $\tau > 0$, $N \geq 0$. And with the terminal conditions

$$W^N|_{\tau=\tau_0} = \delta_{N,N_0}\delta(t'), \tag{2.4.24}$$

one has that

$$U^{N_0}(\tau_0, t_0, \omega) = W^1(0, t_0, \omega).$$

So the solutions U^N of the initial value problem for the transport equations (2.4.16)-(2.4.17) and the W-equations (2.4.23) with terminal conditions (2.4.24) are closely related.

It should be noted that the W-equations have a form simpler than those obtained before (cf. (2.4.16)). This is very useful for obtaining a probabilistic representation of their solutions [4].

Finally, setting $N_0 = 0$, $\tau_0 = \frac{t}{2}$ and $t_0 = t$ we get the representation

$$\Lambda_{12}(t, \omega) = W^1(0, t, \omega)$$

where W^N solve the W-equations (2.4.23) with the terminal conditions

$$W^N|_{\tau=\frac{t}{2}} = \delta_{N,0}\delta(t'). \tag{2.4.25}$$

We have to note that one needs distribution-valued solutions of the W-system. The interpretation in the spirit of remark 2.4.5 is satisfactory for our purpose, however a completely rigorous treatment can be gained by using the method of generalized reflection functional [16, 57].

Remark 2.4.7. It should be noted that the observations in remark 2.4.3 pointed out the corresponding modifications for the computation of the diagonal entries of the normalized spectral density. More exactly, we have that $\Lambda_{11}(t, \omega) = W^1(0, t, \omega)$ where W^N solve the 'unperturbed' W-equations

$$\frac{\partial W^N}{\partial \tau} - 2N\frac{\partial W^N}{\partial t'} + 2\omega^2 N^2 \{\gamma_n(\tau)(W^{N+1} - 2W^N + W^{N-1}) = 0$$

with terminal conditions (2.4.25). Moreover, substituting γ_n by $\gamma_{n_2} = \gamma_n + \gamma_{\delta n}$ we arrive to the equations for computing $\Lambda_{22}(t, \omega)$.

Uniform random medium case

In this case we have a medium with a uniform background, consequently $c_0(z) =$ const. Moreover, since the fluctuations are statistically homogeneous it follows that $\gamma_n(z) =$ const, $\gamma_{\delta n}(z) =$ const, $\gamma_{\delta m}(z) =$ const. Therefore the generator (2.4.6) is independent of z and consequently the limit diffusion process is 'time homogeneous.

Under this simplifications it is possible to obtain an explicit expression for the joint correlation $\Lambda_{12}(t,\omega)$. After a lengthy but straightforward calculation, that involves the computation of the invariant probability density corresponding to the limiting diffusion process and some Fourier transforms, we obtain ((B.4) from the appendix B, see details therein)

$$\Lambda_{12}(t,\omega) = \gamma_n\omega^2 \frac{1-\tanh^2(2\sqrt{\alpha(1+\alpha)}\gamma_n\omega^2 t)}{\left(1+\frac{1+2\alpha}{2\sqrt{\alpha(1+\alpha)}}\tanh(2\sqrt{\alpha(1+\alpha)}\gamma_n\omega^2 t)\right)^2} \tag{2.4.26}$$

where $\alpha = \frac{1}{2}\tilde{\gamma}_{m,n}/\gamma_n$ measures the perturbation intensity. Recall that from the results in [3, 16] we also have

$$\Lambda_{11}(t,\omega) = \frac{\gamma_n\omega^2}{\left(1+\gamma_n\omega^2 t\right)^2}$$
$$\Lambda_{22}(t,\omega) = \frac{(\gamma_n+\gamma_{\delta n})\omega^2}{\left(1+(\gamma_n+\gamma_{\delta n})\omega^2 t\right)^2}.$$

As expected, when $\alpha \to 0$ we get that

$$\Lambda_{12}(t,\omega) = \Lambda_{11}(t,\omega) + O(\alpha), \tag{2.4.27}$$

uniformly for ω bounded. This is a nice consistency check for the calculations above.

Furthermore, we make an interpretation of the result obtained and its relation to localization (for details on wave localization see [64, 65, 72]). Let us introduce a representation of the normalized joint correlation spectral density in terms of relevant non-dimensional parameters. Recall that $l(\omega) = \frac{c_0}{\gamma_n\omega^2}$ is the frequency dependent localization length in the limit $\varepsilon \to 0$ for the unperturbed random medium, for the perturbed medium one has the localization length $\tilde{l}(\omega) = \frac{c_0}{(\gamma_n+\gamma_{\delta n})\omega^2} = \frac{l(\omega)}{1+\beta}$ where we introduce the dimensionless parameter $\beta = \frac{\gamma_{\delta n}}{\gamma_n}$ that statistically measures the perturbation intensity of the fluctuation n. Let t be a fixed time and introduce the cutoff frequency $\omega_c = (\gamma_n t)^{-1/2}$ and the scaled frequency $\chi = \frac{\omega}{\omega_c}$. The cutoff frequency ω_c represents the frequency at which the localization length $l(\omega)$ of the unperturbed medium equals the mean travelled distance $c_0 t$. Hence we can re-write the entries of the normalized matrix valued joint correlation spectral density in terms of dimensionless parameters as

$$\Lambda_{11}(t,\omega) = \frac{1}{t}\mu_{11}(\chi), \quad \Lambda_{22}(t,\omega) = \frac{1}{t}\mu_{22}(\chi,\beta) \quad \text{and} \quad \Lambda_{12}(t,\omega) = \frac{1}{t}\mu_{12}(\chi,\alpha)$$

where

$$\mu_{11}(\chi) = \frac{\chi^2}{\left(1+\chi^2\right)^2} \tag{2.4.28}$$

$$\mu_{22}(\chi,\beta) = \frac{(1+\beta)\chi^2}{\left(1+(1+\beta)\chi^2\right)^2} = \mu_{11}(\chi\sqrt{1+\beta}) \tag{2.4.29}$$

$$\mu_{12}(\chi,\alpha) = \chi^2 \frac{1-\tanh^2(2\sqrt{\alpha(1+\alpha)}\chi^2)}{\left(1+\frac{1+2\alpha}{2\sqrt{\alpha(1+\alpha)}}\tanh(2\sqrt{\alpha(1+\alpha)}\chi^2)\right)^2}, \tag{2.4.30}$$

which shows the universality of the normalized matrix valued joint correlation spectral density as a function of the scaled frequency χ and the perturbation intensity parameters α and β. Note that the dimensionless parameters are constrained by the inequalities $4\alpha \geq \beta \geq 0$.

A measure of how well are correlated the reflected signals corresponding to the unperturbed and perturbed random media in the frequency domain is given by the coherency spectrum [59, 74]. As a function of the scaled frequency the coherency spectrum is written as

$$\rho(\chi,\alpha,\beta) = \frac{\mu_{12}(\chi,\alpha)}{\sqrt{\mu_{11}(\chi)\mu_{22}(\chi,\beta)}}. \tag{2.4.31}$$

In figures 2.2 and 2.3 we show some graphics for the coherency spectrum $\rho(\chi,\alpha,\beta)$ for different values of α and β. Actually, we only show the extreme cases $\beta = 0$ and $\beta = 4\alpha$, so the coherency spectrum becomes a function only of χ and α. The maximum value of the coherency spectrum is $\frac{1}{\sqrt{1+\beta}}$ which is attained at $\chi = 0$ and consequently, low frequency modes are the more correlated. Moreover as χ increases the coherency spectrum approaches zero exponentially fast. However, since the power spectral of both reflected signals vanishes for $\chi = 0$, the low frequency modes do not have a significant correlation strength.

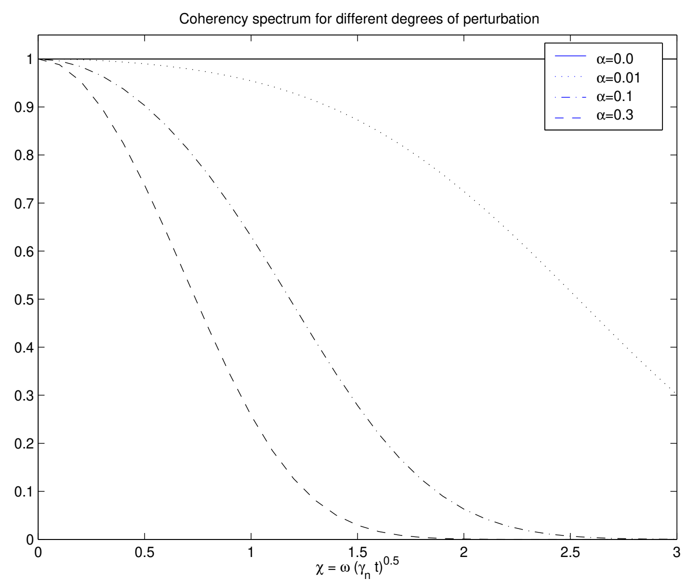

Figure 2.2: Coherency spectrum as a function of the scaled frequency $\chi = \omega\sqrt{\gamma_n t}$ for different values of the perturbation intensity α in the case where $\beta = 0$.

An appropriate measure of the correlation strength is given by the normalized joint correlation spectral density $\mu_{12}(\chi, \alpha)$. In figure 2.4 we show the graphics of $\mu_{12}(\chi, \alpha)$ as a function of the scaled frequency for different values of the perturbation intensity α. We can see that $\mu_{12}(\chi, \alpha)$ has peaks with value $\mu_{12}^*(\alpha)$ at $\chi = \pm\chi^*(\alpha)$ where $\chi^*(\alpha)$ is the positive solution of the equation:

$$4\sqrt{\alpha(1+\alpha)}\chi^2 = \tanh(2\sqrt{\alpha(1+\alpha)}\chi^2 + 2\ln(\sqrt{1+\alpha} + \sqrt{\alpha})). \qquad (2.4.32)$$

In figures 2.5 and 2.6 we show the graphics of $\chi^*(\alpha)$ and $\mu_{12}^*(\alpha)$, respectively.

From this, one identifies $\omega^* = \omega_c\chi^*(\alpha) \leq \omega_c$ as the frequency for which the two signals have the most strong correlation, i.e. a carrier frequency of the spectral

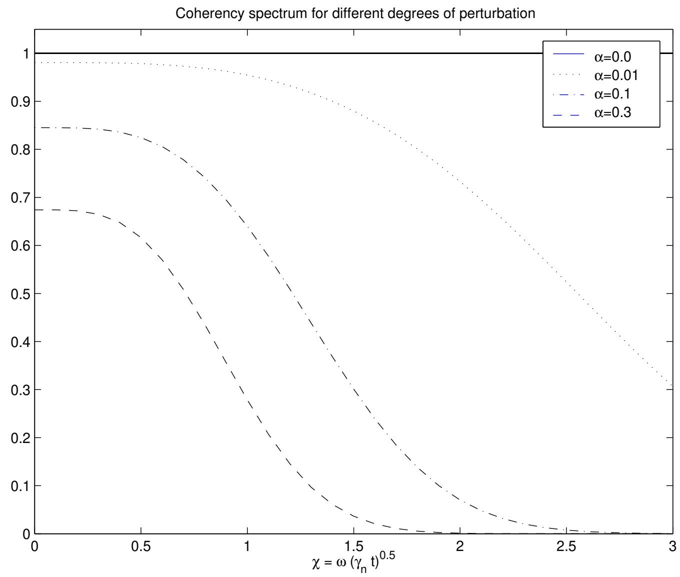

Figure 2.3: Coherency spectrum as a function of the scaled frequency $\chi = \omega\sqrt{\gamma_n t}$ for different values of the perturbation intensity α in the case where $\beta = 4\alpha$.

content of the reflected signal less affected by the medium perturbations. Moreover $\frac{1}{t}\mu_{12}^*(\alpha)$ represents an expected upper bound of the correlation strength for the given perturbation intensity at fixed t. Note that the peak value $\mu_{12}^*(\alpha)$ and the frequency $\omega^*(\alpha)$ decrease as the perturbation intensity α increases. This is expected, since increasing the perturbation intensity implies a decrease in the media correlation and consequently in the reflected signals correlation strength. Concerning the carrier frequency ω^*, first note that for $\alpha = 0$ it coincides with ω_c whose associated mode is mainly affected by single scattering during the travelled distance $c_0 t$ [65, 64], now if α increases one needs to get information mainly from single scattering (in order to maintain a high correlation strength) without probing too much the perturbed medium, this is achieved with modes associated to a frequency ω whose localization length satisfies $l(\omega) > l(\omega_c) = c_0 t$ which implies $\omega < \omega_c$. The same heuristic reasoning when $\alpha > 0$ gives that ω^* should decrease as a function of α.

In the time domain the interpretation is as follows: on measuring $t\Lambda_{12}(t, \omega)$ at a

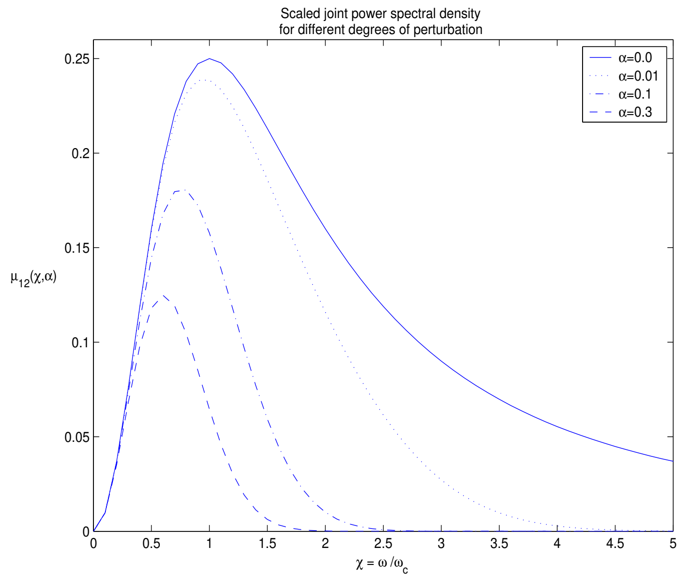

Figure 2.4: Normalized joint correlation spectral density for different values of the perturbation intensity.

certain frequency window centered at $\bar{\omega}$ one should observe a peak at some time $\bar{t}$ corresponding to $\chi = \chi^*(\alpha)$ that is $\bar{t} = \chi^{*2}(\alpha)\frac{l(\bar{\omega})}{c_0}$. Moreover, for times long compared to $\bar{t}$ the normalized joint correlation spectral density exhibits the exponential decay: $\Lambda_{12}(t, \bar{\omega}) \sim \exp\{-(4\frac{c_0}{l(\bar{\omega})}\sqrt{\alpha(1+\alpha)}\,)t\}$.

2.4.2 Weak medium fluctuations

In this situation, the results are obtained in a similar way to those in the previous section and we will not present all the details, just outlining the main differences.

Asymptotics for the joint correlation

In this case from equation (2.2.23) we have

$$\frac{\mathrm{d}}{\mathrm{d}z}\phi_j^\varepsilon = -2\frac{\omega}{\varepsilon}c_0^{-1}\big(m_j^\varepsilon + n_j^\varepsilon\cos(\phi_j^\varepsilon + 2\omega\frac{\tau}{\varepsilon})\big) + \frac{\zeta_0'}{\zeta_0}\sin(\phi_j^\varepsilon + 2\omega\frac{\tau}{\varepsilon})$$

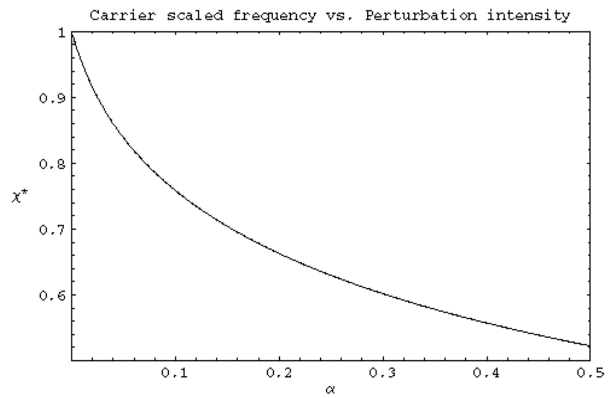

Figure 2.5: Scaled peak frequency χ^* vs. the perturbation intensity.

and using the corresponding scaling in the half-space $z \leq 0$:

$$m_j^\varepsilon(z) = \sqrt{\varepsilon} m_j(z, \frac{z}{\varepsilon}) \quad \text{and} \quad n_j^\varepsilon(z) = \sqrt{\varepsilon} n_j(z, \frac{z}{\varepsilon}).$$

For $\boldsymbol{\psi}^\varepsilon = [\psi_1^\varepsilon, \psi_2^\varepsilon]^t$ we have a random ordinary differential equation that after grouping terms of the same order in $\varepsilon^{1/2}$ takes the form

$$\frac{\mathrm{d}}{\mathrm{d}z}\boldsymbol{\psi}^\varepsilon = \varepsilon^{-1/2}\mathbf{F}(z, \boldsymbol{\psi}^\varepsilon, \mathbf{q}(z, \frac{z}{\varepsilon}), \frac{\tau(z)}{\varepsilon}) + \mathbf{G}(z, \boldsymbol{\psi}^\varepsilon, \mathbf{q}(z, \frac{z}{\varepsilon}), \frac{\tau(z)}{\varepsilon}) + \text{h.o.t.}, \qquad (2.4.33)$$

where h.o.t. stands for higher order terms and $\mathbf{F}$, $\mathbf{G}$ are defined below

$$F_j(z, \boldsymbol{\psi}, \mathbf{q}(z,s), \mu) = \\ \frac{2\omega}{c_0(z)}\Big(m_j(z,s) + n_j(z,s)\cos\big(\psi_j + 2\omega\mu + (-1)^{j-1}h\tau(z)\big)\Big), \qquad (2.4.34)$$

and

$$G_j(z, \boldsymbol{\psi}, \mathbf{q}(z,s), \mu) = \frac{\zeta_0'(z)}{2\zeta_0(z)}\sin\big(\psi_j + 2\omega\mu + (-1)^{j-1}h\tau(z)\big). \qquad (2.4.35)$$

The equation (2.4.33) is singular as ε goes to zero, moreover $\mathbf{F}$ is centered (i.e. $\mathbb{E}\{\mathbf{F}\} = 0$) and the 'time' ($z$ variable) in the driven stochastic process is consistently

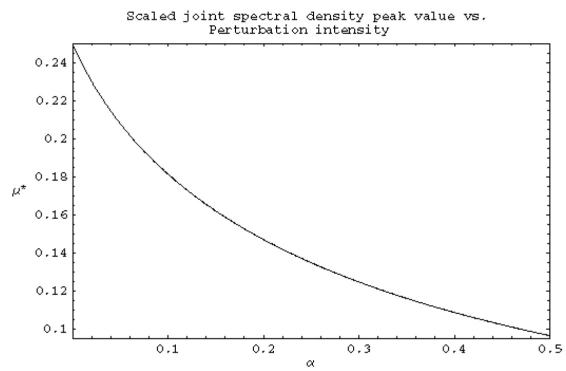

Figure 2.6: Scaled joint correlation spectral density peak value μ_{12}^* vs. the perturbation intensity.

scaled, so as before a diffusion-approximation takes place (see theorem A.2 in appendix A). More exactly, we have that as ε goes to zero, $\boldsymbol{\psi}^\varepsilon$ converges in distribution to a diffusion process $\boldsymbol{\psi}$ with infinitesimal generator:

$$\mathcal{L}_z V = \int_0^{+\infty} \left\langle \mathbb{E}\{\mathbf{F}(z, \boldsymbol{\psi}, \mathbf{q}(z,0), \mu) \cdot \nabla_{\boldsymbol{\psi}} [\mathbf{F}(z, \boldsymbol{\psi}, \mathbf{q}(z,r), \mu + \frac{r}{c_0(z)}) \cdot \nabla_{\boldsymbol{\psi}} V]\} \right\rangle_\mu \mathrm{d}r \\ + \left\langle \mathbb{E}\{\mathbf{G}(z, \boldsymbol{\psi}, \mathbf{q}(z,0), \mu) \cdot \nabla_{\boldsymbol{\psi}} V\} \right\rangle_\mu . \quad (2.4.36)$$

Remark 2.4.8. A fundamental difference (as compared with the strong fluctuations case) is that the fast phase averaging is coupled with the variable r that performs integration of the driven random process effect. This is a consequence of the fact that the deterministic phase of the oscillatory terms and the 'time' of the driven process vary in the same scale, resulting in a stronger interaction of the random fluctuations and the fast phase oscillations.

Following the steps presented at the previous section, after some elementary computation we arrive to the following Kolmogorov backward equation:

$$\begin{cases} (\frac{\partial}{\partial z} + \tilde{\mathcal{L}}^0)V = 0, & \text{for } z < 0 \\ V|_{z=0} = \mathrm{e}^{\mathrm{i}\psi} \end{cases} \tag{2.4.37}$$

where

$$\tilde{\mathcal{L}}^0 V = \frac{2\tilde{h}(z,\omega,h)}{c_0(z)}\partial_\psi V + \frac{4\omega^2}{c_0(z)}\big\{\gamma_n^c(z,\omega)(1-\cos\psi) + \breve{\gamma}_{m,n}(z,\omega)\big\}\partial_\psi^2 V, \tag{2.4.38}$$

and

$$u_{12}(\omega,h) = \lim_{z\to-\infty} V(z,\psi,\omega,h). \tag{2.4.39}$$

Above we have set

$$\gamma_g^c(z,\omega) = \frac{1}{c_0(z)}\int_0^\infty \mathbb{E}\{g(z,0)g(z,r)\}\cos(\frac{2\omega r}{c_0(z)})\,\mathrm{d}r$$
$$\gamma_g^s(z,\omega) = \frac{1}{c_0(z)}\int_0^\infty \mathbb{E}\{g(z,0)g(z,r)\}\sin(\frac{2\omega r}{c_0(z)})\,\mathrm{d}r$$

which characterize the frequency content of the 'local' correlation function of $g(z,\cdot)$ for $g = m, n, \delta m, \delta n$, and introduce

$$\breve{\gamma}_{m,n}(z,\omega) = \gamma_{\delta m}(z) + \tfrac{1}{2}\gamma_{\delta n}^c(z,\omega), \tag{2.4.40a}$$
$$\tilde{h}(z,\omega,h) = h - \omega^2\gamma_{\delta n}^s(z,\omega). \tag{2.4.40b}$$

Remark 2.4.9. It should be noted that the generators (2.4.10) and (2.4.38) corresponding to the strong and weak fluctuations case, respectively, have similar structures. However, the coefficients of the generator (2.4.38) above have a stronger dependence on the frequency ω (cf. (2.4.40a)). This represents a fundamental difference whose consequences will be discussed later on.

The limit (2.4.39) exists and is independent of ψ under suitable conditions, analogous to those discussed in remark 2.4.2. We have again a very interesting situation when asymptotically the medium background is uniform, and the fluctuations and perturbations are statistically homogeneous at infinite depth.

Remark 2.4.10. We have to note that proceeding as in the previous section one can obtain the equations for the computation of $u_{11}(\omega,h)$. More exactly, we have to solve (2.4.37) with the generator given by

$$\mathcal{L}^0 V = \frac{2h}{c_0(z)}\partial_\psi V + \frac{4\omega^2\gamma_n^c(z,\omega)}{c_0(z)}(1-\cos\psi)\partial_\psi^2 V,$$

and let $u_{11}(\omega,h) = \lim_{z\to-\infty} V(z,\psi,\omega,h)$, in complete agreement with [3]. Furthermore, if above we replace γ_n^c by $\gamma_{n_2}^c = \gamma_n^c + \gamma_{\delta n}^c$ these become equations for obtaining $u_{22}(\omega,h)$.

For the coefficients in the Fourier series decomposition of $V(z,\psi,\omega,h)$ we get the equations:

$$\frac{\partial V^N}{\partial z} + \frac{2\mathrm{i}\tilde{h}N}{c_0(z)}V^N + \frac{2\omega^2\gamma_n^c(z,\omega)}{c_0(z)}\{(N+1)^2V^{N+1} - 2N^2V^N + (N-1)^2V^{N-1}\} \\ - \frac{4\omega^2}{c_0(z)}\breve{\gamma}_{m,n}(z,\omega)N^2V^N = 0 \quad (2.4.41)$$

for $N \geq 0$ and $z < 0$, with the initial conditions

$$V^N|_{z=0} = \delta_{N,1}.$$

Then we have that $u_{12}(\omega,h) = \lim_{z\to-\infty} V^0(z,\omega,h)$. Using the inverse Fourier transform (2.4.15) and replacing depth by travel time we obtain the new system

$$\frac{\partial U^N}{\partial \tau} + 2N\frac{\partial U^N}{\partial t} = 2\omega^2\gamma_n^c(\tau,\omega)\big\{(N+1)^2U^{N+1} - 2N^2U^N + (N-1)^2U^{N-1}\big\} \\ - 2\omega^2(2N^2\breve{\gamma}_{m,n}(\tau,\omega) + \mathrm{i}N\gamma_{\delta n}^s(\tau,\omega))U^N \quad (2.4.42)$$

for $\tau > 0$, $N \geq 0$, with the initial conditions

$$U^N|_{\tau=0} = \delta_{N,1}\delta(t). \quad (2.4.43)$$

Finally, we have that $\Lambda_{12}(t,\omega) = \lim_{\tau\to+\infty} U^0(\tau,t,\omega)$ and as a consequence of hyperbolicity

$$\Lambda_{12}(t,\omega) = U^0(\tfrac{t}{2},t,\omega). \quad (2.4.44)$$

Remark 2.4.11. It should be noted that for the calculation of $\Lambda_{11}(t,\omega)$ we have the equations

$$\frac{\partial U^N}{\partial \tau} + 2N\frac{\partial U^N}{\partial t} = 2\omega^2\gamma_n^c(\tau,\omega)\big\{(N+1)^2U^{N+1} - 2N^2U^N + (N-1)^2U^{N-1}\big\} \quad (2.4.45)$$

with initial conditions (2.4.43), and the representation $\Lambda_{11}(t,\omega) = U^0(\frac{t}{2},t,\omega)$ which is in full agreement with [3]. Furthermore, substituting γ_n^c by $\gamma_{n_2}^c = \gamma_n^c + \gamma_{\delta n}^c$ we arrive to the equations for computing $\Lambda_{22}(t,\omega)$.

Remark 2.4.12. We have to draw attention to the differences between the equations (2.4.16) and (2.4.42) for the strong and weak fluctuations regimes, respectively. Note that they have a similar structure, however besides a more complicated dependence of (2.4.42) on the frequency ω there appears a new term containing an imaginary coefficient caused by the additional drift in the generator (2.4.38) (cf. (2.4.40b)). This new term eventually leads to a complex valued joint correlation density.

Low frequency asymptotic

In a similar way as we did in the previous section, one can (formally) obtain an asymptotic expression for $|\omega|$ small. In fact after some elementary calculations one gets that:

$$\Lambda_{12}(t,\omega) \approx \omega^2\big\{\gamma_n(\frac{t}{2})\big(1 - 4\omega^2\int_0^{\frac{t}{2}}\big(\gamma_n(\tau') + \tilde{\gamma}_{m,n}(\tau')\big)\mathrm{d}\tau'\big) - \omega^2\gamma_n^{(2)}(\frac{t}{2})\big\}, \quad (2.4.46)$$

for $|\omega|$ small, where we have set that

$$\gamma_n^{(2)}(\tau) = \frac{2}{c_0^3(\tau)}\int_0^\infty s^2\mathbb{E}\{n(z,s)n(z,0)\}\mathrm{d}s.$$

Note that, compared with the strong fluctuations case, a new term of order ω^4 appears but the effect of the additional drift is not present yet.

Remark 2.4.13. As we did before, one can easily get asymptotics for the diagonal entries. More exactly we have

$$\Lambda_{11}(t,\omega) \approx \omega^2\big\{\gamma_n(\frac{t}{2})\big(1-4\omega^2\int_0^{\frac{t}{2}}\gamma_n(\tau')\mathrm{d}\tau'\big)-\omega^2\gamma_n^{(2)}(\frac{t}{2})\big\}$$

$$\Lambda_{22}(t,\omega) \approx \omega^2\big\{\big(\gamma_n(\frac{t}{2})+\gamma_{\delta n}(\frac{t}{2})\big)\big(1-4\omega^2\int_0^{\frac{t}{2}}\big(\gamma_n(\tau')+\gamma_{\delta n}(\tau')\big)\mathrm{d}\tau'\big) \\ -\omega^2\big(\gamma_n^{(2)}(\frac{t}{2})+\gamma_{\delta n}^{(2)}(\frac{t}{2})\big)\big\},$$

for $|\omega|$ small.

System of W-equations

The corresponding adjoint system for equations (2.4.42) takes the form

$$\begin{aligned}\frac{\partial W^N}{\partial \tau}+2N\frac{\partial W^N}{\partial t}&+2\omega^2N^2\gamma_n^c(\tau,\omega)(W^{N+1}-2W^N+W^{N-1})\\ &-2\omega^2(2N^2\breve{\gamma}_{m,n}(\tau,\omega)-\mathrm{i}N\gamma_{\delta n}^s(\tau,\omega))W^N=0,\end{aligned} \tag{2.4.47}$$

for $\tau>0,\ N\geq 0$.

The same transformations as in the previous section lead to the W-equations

$$\begin{aligned}\frac{\partial W^N}{\partial \tau}-2N\frac{\partial W^N}{\partial t'}&+2\omega^2N^2\gamma_n^c(\tau,\omega)(W^{N+1}-2W^N+W^{N-1})\\ &+2\omega^2(2N^2\breve{\gamma}_{m,n}(\tau,\omega)-\mathrm{i}N\gamma_{\delta n}^s(\tau,\omega))W^N=0.\end{aligned} \tag{2.4.48}$$

Considering the terminal conditions

$$W^N|_{\tau=\frac{t}{2}}=\delta_{N,0}\delta(t'),$$

we have that

$$\Lambda_{12}(t,\omega)=W^1(0,t,\omega).$$

Remark 2.4.14. Note that performing a simple modification we get the W-equations for the diagonal entries of the normalized spectral density. More exactly, we have that $\Lambda_{11}(t,\omega)=W^1(0,t,\omega)$ where W^N solve the 'unperturbed' W-equations

$$\frac{\partial W^N}{\partial \tau}-2N\frac{\partial W^N}{\partial t'}+2\omega^2N^2\gamma_n^c(\tau,\omega)(W^{N+1}-2W^N+W^{N-1})=0,$$

with the same terminal conditions as above. Moreover, substituting γ_n^c by $\gamma_{n_2}^c=\gamma_n^c+\gamma_{\delta n}^c$ we arrive to the equations for computing $\Lambda_{22}(t,\omega)$.

Uniform random medium case

In this case we have that $c_0(z) = c_0 = \text{const}$, and the fluctuations statistics do not depend on depth, so that $\gamma_n^c(z,\omega) = \gamma_n^c(\omega)$, $\gamma_{\delta n}^s(z,\omega) = \gamma_{\delta n}^s(\omega)$ and $\breve{\gamma}_{m,n}(z,\omega) = \breve{\gamma}_{m,n}(\omega)$ are functions of the frequency ω only.

Using the formulas obtained in the strong fluctuations case we get the joint correlation spectral density:

$$\Lambda_{12}(t,\omega) = \omega^2\gamma_n^c(\omega)\exp\{-\mathrm{i}\omega^2\gamma_{\delta n}^s(\omega)t\} \times \frac{1-\tanh^2(2\sqrt{\tilde{\alpha}(\omega)(1+\tilde{\alpha}(\omega))}\omega^2\gamma_n^c(\omega)t)}{\big(1+\frac{1+2\tilde{\alpha}(\omega)}{2\sqrt{\tilde{\alpha}(\omega)(1+\tilde{\alpha}(\omega))}}\tanh(2\sqrt{\tilde{\alpha}(\omega)(1+\tilde{\alpha}(\omega))}\omega^2\gamma_n^c(\omega)t)\big)^2} \quad (2.4.49)$$

where $\tilde{\alpha}(\omega) = \frac{1}{2}\breve{\gamma}_{m,n}(\omega)/\gamma_n^c(\omega)$ measures the perturbation intensity for each frequency. Note that the joint correlation spectral density is complex-valued.

It is apparent that now the parameters involved are complicated functions of the frequency ω, that appears through the frequency content of the autocorrelation function of the fluctuations and their perturbations. This might lead to a cumbersome analysis in the frequency domain. For simplicity, we shall perform this analysis for a special case of autocorrelation functions without entering into much details.

We begin with the case where the perturbation $\delta n(\cdot) = 0$ almost surely, then the complex phase in equation (2.4.49) has no effect and the situation is similar to the case of strong fluctuations as will be explained below. However, the relation with the localization length remains a bit complicated due to the strong dependence on ω.

Let us assume that

$$\mathbb{E}\{n(s)n(0)\} = \alpha_0 \mathrm{e}^{-2\frac{\omega_0}{c_0}s}. \quad (2.4.50)$$

Then we have that

$$\gamma_n^c(\omega) = \gamma_n\big(1+(\frac{\omega}{\omega_0})^2\big)^{-1} \quad \text{and} \quad \tilde{\alpha}(\omega) = \alpha\big(1+(\frac{\omega}{\omega_0})^2\big),$$

where $\alpha = \tilde{\alpha}(0) = \frac{\gamma_{\delta m}}{2\gamma_n}$ is the perturbation intensity at frequency $\omega = 0$, which coincides with the perturbation intensity for the strong fluctuations case. By introducing the scaled frequency $\chi = \frac{\omega}{\omega_0}$ and the dimensionless parameter $\theta = \gamma_n \omega_0^2 t$, we can re-write the joint correlation spectral density as

$$\Lambda_{12}(t,\omega) = \frac{1}{t}\mu_{12}(\chi,\alpha,\theta)$$

where

$$\mu_{12}(\chi,\alpha,\theta) = \Big(\frac{\theta\chi^2}{1+\chi^2}\Big)\frac{1-\tanh^2\big(2\theta\chi^2\sqrt{\alpha\frac{1+\alpha(1+\chi^2)}{1+\chi^2}}\big)}{\Big(1+\frac{1+2\alpha(1+\chi^2)}{2\sqrt{\alpha(1+\chi^2)(1+\alpha(1+\chi^2))}}\tanh\big(2\theta\chi^2\sqrt{\alpha\frac{1+\alpha(1+\chi^2)}{1+\chi^2}}\big)\Big)^2}.$$

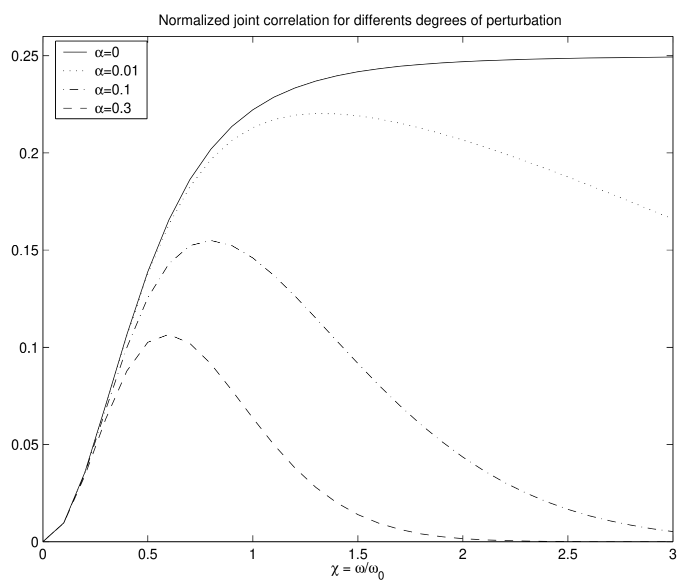

Figure 2.7: Normalized joint correlation spectral density for different values of the perturbation intensity α in the case where $\theta = 1$.

As was pointed out in the analysis of the strong fluctuation case, the correlation strength in the frequency domain is dictated by the normalized joint correlation spectral density $\mu_{12}(\chi,\alpha,\theta)$. Their graphics as functions of the scaled frequency χ for different values of the parameter α and θ fixed are shown in figures 2.7 and 2.8. Their qualitative behavior is very similar to the graphics corresponding to strong fluctuations. They have peaks at frequencies $\chi = \pm\chi^*(\alpha,\theta)$ with value

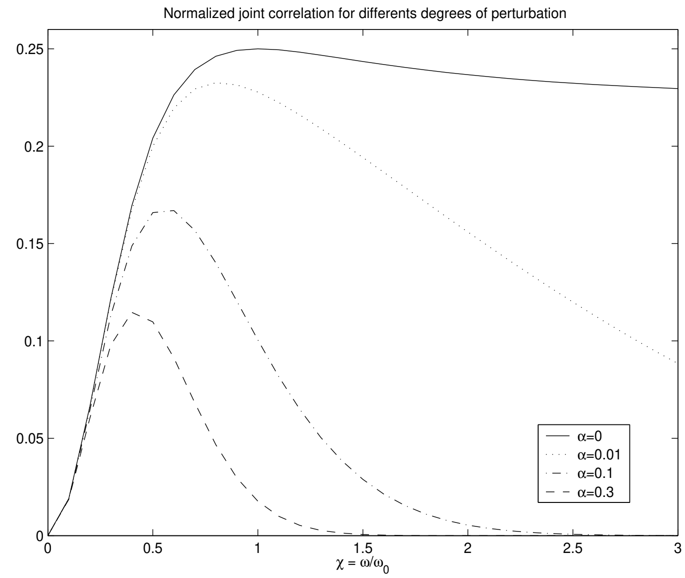

Figure 2.8: Normalized joint correlation spectral density for different values of the dimensionless parameter α in the case where $\theta = 2$.

$\mu_{12}^*(\alpha,\theta) = \mu_{12}(\chi^*(\alpha,\theta),\alpha,\theta)$. If the time t is fixed then the parameter θ is also fixed and the peak frequencies and value become functions of the perturbation intensity α only. Moreover, (with θ fixed) we have that $\omega^* = \omega_0\chi^*(\alpha,\theta)$ is the frequency at which the two signals have the most strong correlation and $\frac{1}{t}\mu_{12}^*(\alpha,\theta)$ represents an expected upper bound for the correlation strength.

Suppose now that $\delta n(\cdot)$ has an exponential correlation function. The joint correlation spectral density is complex-valued thus the behavior of the correlation strength in the frequency domain for the reflected signals is dictated by the absolute value of the normalized joint correlation [59, 74]. Moreover, since $\tilde{\alpha}(\omega)$ behaves in a qualitatively similar way as in the previously analyzed case we arrive to alike conclusions. The analysis can be carried out along the same lines as before but the details are more involved. Furthermore, from (2.4.49) now we have that the phase spectrum $-\gamma_{\delta n}^s(\omega)\omega^2 t$ is responsible for a time delay between the two reflected signals carried by the frequency ω. This delay is measured through the derivative of the phase spectrum with respect to the frequency [59].

Remark 2.4.15. It should be stressed that the presented analysis aimed at indicating the main similarities and differences between the strong and weak fluctuations regimes, without entering into an exhaustive study of the latter.

2.5 Conclusions

In this chapter, we have analyzed how perturbations of a random layered slab affect the signal reflected at the interface, which is generated when a pulse travelling from the homogeneous section impinges upon the interface. The basic assumptions are a separation of scales of variation of the random medium and the statistical independence of the perturbations. Namely, over a slowly varying smooth deterministic medium incorporating the large-scale features are superimposed rapidly varying random fluctuations determining a micro-scale structure. Furthermore, we consider that the perturbation only affects this micro-scale structure by generating random variations statistically independent of the unperturbed microstructure. We have analyzed the cases where the fluctuations are respectively, strong $O(1)$ and weak $O(\sqrt{\varepsilon})$, where ε represents the ratio between the microscopic and macroscopic scales. In these cases the pulse is long, or short, respectively. In both cases we obtain the appropriate relations for asymptotically characterizing the correlation of the reflected signals corresponding to the unperturbed and perturbed random media. The main ingredients are the introduction of a correctly scaled two-dimensional joint reflection random process and their characterization in terms of the corresponding reflection coefficients associated with the solution of a random Riccati equation. This allows for a description of their joint correlation spectral density through the solution of a random differential equation that can be treated applying the asymptotic analysis of stochastic differential equations.

Finally, the limiting correlation spectral density of the joint reflection process is related to the solution of an infinite-dimensional system of transport equations (W-equations). When comparing these W-equations with the equations corresponding to the unperturbed situation, there appear some extra terms which are responsible for a different asymptotic behavior. The main differences can be clearly seen in the case of a uniform random medium, where some explicit formulas were obtained. In the regime of strong fluctuations, this case was thoroughly analyzed. Our analysis reveals that the joint correlation spectral density is related to the localization length of the unperturbed medium and a statistical measure of the perturbations intensity. Moreover, as the perturbation intensity increases the strength of the correlation decreases and the carrier modes are shifted to low frequencies. Furthermore, as time goes on the correlation strength exponentially decays.

The results obtained will be useful in next chapter, where we analyze time-reversal in reflection. In fact, the time-reversed refocused pulse is closely related to the second order statistics of the reflection coefficients whose asymptotic analysis played a fundamental role during the characterization of the limiting joint correlation performed in this chapter. Moreover, the complete characterization of the refocused pulse shall also require the analysis of higher order moments, which will be achieved by the same technique presented in this chapter.

Chapter 3

Refocusing of time-reversed reflections

3.1 Introduction

In this chapter we shall deal with pulse refocusing in generalized time reversal experiments (see figure 1.2). We concentrate on the case where the medium changes are caused by an independent perturbative factor leading to the appearance of noisy perturbations in the random fluctuations. A thorough analysis of generalized time reversal in a closely related situation was performed by Alfaro-Vigo et al. [2].

As before the context is one-dimensional waves propagating in an acoustic random medium in the regimes of strong and weak medium fluctuations. For simplicity we mainly consider the case of a random half-space with a totally reflecting termination. This is a model general enough for explaining the main features observed on the outcome of the experiments. We will generalize the results obtained in [19, 66] where standard time reversal experiments were analyzed.

The presence of perturbations does not kill the coherent refocusing, but its quality (measured by the recovered coherent energy) is reduced as the perturbation intensity increases. Moreover, in contrast with the standard case, now the statistical stabilization property is lost: the refocused signal is random in general. It is worth noting that the refocused pulse shape depends on a single one-dimensional standard Brownian motion and some statistical parameters of the involved media. More exactly, the limiting refocused signal is related to the large time asymptotic solution of an Itô stochastic partial differential equation driven by a single one-dimensional standard Brownian motion whose coefficients are related to the statistics of the media fluctuations.

This chapter is organized as follows: in section 3.2 we obtain an integral representation for the time-reversed reflected pulse. Section 3.3 is devoted to the characterization of the coherent refocused signal. Furthermore, we establish the refocusing property and use the results of the previous chapter to obtain explicit formulas that will be useful later on during the numerical tests. In section 3.4 we obtain the main results of this work. We carry out the characterization of the asymptotic refocused pulse as a continuous random process and also discuss its statistical stabilization. And in the final section 3.5 we summarize the results obtained in this chapter.

3.2 Time-reversed reflections

We begin with a precise mathematical description of the time-reversed pulse obtained in a generalized time reversal (in reflection) experiment. Our analysis corresponds to a random half-space in the regimes of strong and weak medium fluctuations, discussed in the previous chapter.

The impinging acoustic pulse considered is a time signal incident at the interface of the random half-space, given by:

$$u_{\mathrm{inc}}(0,t) = -\frac{\zeta_0^{-1/2}(0) f(\frac{t}{\varepsilon})}{2}, \qquad p_{\mathrm{inc}}(0,t) = \frac{\zeta_0^{1/2}(0) f(\frac{t}{\varepsilon})}{2}. \tag{3.2.1}$$

We assume for simplicity that $f \in \mathcal{S}(\mathbf{R})$ with support contained in $\mathbf{R}_+ = [0, +\infty)$, where $\mathcal{S}(\mathbf{R})$ represents the Schwartz space of rapidly decaying functions. The scaling ensures that the characteristic wavelength is $O(\varepsilon)$. Therefore the reflected acoustic signal at the interface is represented as

$$u_{\mathrm{ref}}(0,t) = \frac{\zeta_0^{-1/2}(0)B_0(t)}{2}, \qquad p_{\mathrm{ref}}(0,t) = \frac{\zeta_0^{1/2}(0)B_0(t)}{2}.$$

with

$$B_0(t) = \frac{1}{2\pi}\int e^{-i\omega\frac{t}{\varepsilon}}\hat{f}(\omega)R^{\varepsilon}_{L,1}(0,\omega)d\omega,$$

where $\hat{f}$ and $R^{\varepsilon}_{L,1}(0,\omega)$, represent the Fourier transform of f and the reflection coefficient at the interface of the 'unperturbed' medium for frequency ω, respectively. This representation comes from (2.2.17) after using (3.2.1) and (2.2.11) as was explained in section 2.2.3 of the previous chapter.

After recording these signals up to time t_0, they are processed at the time reversal mirror (TRM). We introduce the cutoff function $G_{t_0}(\cdot)$ supported on the interval $[0,t_0]$ or rapidly decaying outside it, for representing the signal amplification and distortion caused by the TRM,. This step is completed by time-reversing the processed signal. As a consequence we obtain a new signal that is given by

$$u^{\mathrm{TR}}_{\mathrm{inc}}(0,t) = -\frac{\zeta_0^{-1/2}(0)A_0^{\mathrm{TR}}(t)}{2}, \qquad p^{\mathrm{TR}}_{\mathrm{inc}}(0,t) = \frac{\zeta_0^{1/2}(0)A_0^{\mathrm{TR}}(t)}{2} \tag{3.2.2}$$

with

$$A_0^{\mathrm{TR}}(t) = G_{t_0}(t_0 - t)B_0(t_0 - t). \tag{3.2.3}$$

This is the new initial pulse that will be re-emitted into the perturbed random medium by the TRM.

Finally, the reflected signal at the interface, due to the time-reversed data, is observed in a ε-scaled time window centered at t_1. In other words, during the observation we use a local a time scale in correspondence with the incident pulse time span. After using the integral representation (2.2.17), we have the following expression for the reflected signal

$$u^{\mathrm{TR}}_{\mathrm{ref}}(0,t_1+\varepsilon s) = \frac{\zeta_0^{-1/2}(0)B^{\varepsilon,\mathrm{TR}}_{t_0,t_1}(s)}{2}, \qquad p^{\mathrm{TR}}_{\mathrm{ref}}(0,t_1+\varepsilon s) = \frac{\zeta_0^{1/2}(0)B^{\varepsilon,\mathrm{TR}}_{t_0,t_1}(s)}{2},$$

with

$$B^{\varepsilon,\mathrm{TR}}_{t_0,t_1}(s) = \frac{1}{2\pi}\int e^{-i\omega(\frac{t_1+\varepsilon s}{\varepsilon})}\widetilde{A_0^{\mathrm{TR}}}(\omega)R^{\varepsilon}_{L,2}(0,\omega)d\omega,$$

where $\tilde{(\cdot)}$ stands for the scaled Fourier transform defined by (2.2.11) and $R^{\varepsilon}_{L,2}(0,\omega)$ is the reflection coefficient at the interface for the perturbed medium (at frequency ω). By using (3.2.3) and making some transformations we get

$$B^{\varepsilon,\mathrm{TR}}_{t_0,t_1}(s) = \frac{1}{(2\pi)^2}\iint \mathrm{e}^{\mathrm{i}\omega(\frac{t_1-t_0}{\varepsilon})}\mathrm{e}^{-\mathrm{i}\frac{h}{2}(t_1-t_0+\varepsilon s)}\mathrm{e}^{\mathrm{i}\omega s}\hat{f}(\omega+\tfrac{\varepsilon}{2}h)\overline{\hat{G}_{t_0}}(h)$$
$$R^{\varepsilon}_{L,1}(0,\omega+\tfrac{\varepsilon}{2}h)\overline{R^{\varepsilon}_{L,2}}(0,\omega-\tfrac{\varepsilon}{2}h)\mathrm{d}\omega\mathrm{d}h. \quad (3.2.4)$$

Remark 3.2.1. This representation of the time-reversed reflection is based on a TRM capable of processing the signal corresponding to the upward travelling wave. The TRM produces a time-reversed signal which is re-emitted into the medium as a downward travelling wave. The TRM generates time-reversed signals for the pressure and velocity acoustic field, by inverting the velocity direction when the new acoustic wave is re-emitted.

Remark 3.2.2. It should be noted that for obtaining the representation of the time-reversed reflection resulting from a standard time reversal experiment (i.e. when the medium is not perturbed) in equation (3.2.4) one has to substitute $R^{\varepsilon}_{L,2}$ by $R^{\varepsilon}_{L,1}$. This is in agreement with the results presented in [19, 28] and [66].

Very important information on the time-reversed acoustic field is gained by analyzing the asymptotic behavior of $B^{\varepsilon,\mathrm{TR}}_{t_0,t_1}$ as ε approaches zero. First, we address the problem of characterizing the coherent time-reversed reflection and its refocusing.

3.3 Coherent time-reversed reflection

The coherent time-reversed pulse is obtained by taking expectation over the media realizations, i.e. an ensemble average. The media are considered to have either strong or weak fluctuations as defined in (2.2.7) and (2.2.8) respectively. The random media perturbations satisfy the statistical independence assumption given by (2.3.1). We show the refocusing of the time-reversed reflections in the limit $\varepsilon \downarrow 0$. Moreover, refocusing takes place in time.

Let us introduce the limiting average time-reversed reflection as

$$\langle B^{\mathrm{TR}}_{t_0,t_1}\rangle(s) = \lim_{\varepsilon\downarrow 0} \mathbb{E}\{B^{\mathrm{TR},\varepsilon}_{t_0,t_1}(s)\},$$

where $\mathbb{E}\{\cdot\}$ stands for the expectation over realizations of the media. Actually, the expectation is taken with respect to the probability distribution induced by the random media fluctuations.

The time-reversal refocusing property in its simple form can be stated as follows:

Proposition 3.3.1. *Let $\hat{G}_{t_0} \in L^1(\mathbf{R})$. Then for the limiting average time-reversed reflection, we have that:*

$$\langle B^{\mathrm{TR}}_{t_0,t_1}\rangle(s) = \begin{cases} \big(\langle K^{\mathrm{TR}}_{t_0}\rangle(\cdot) \star f(-\cdot)\big)(s), & \text{if } t_1 = t_0 \\ 0, & \text{if } t_1 \neq t_0 \end{cases} \tag{3.3.1}$$

where

$$\begin{aligned} \widehat{\langle K^{\mathrm{TR}}_{t_0}\rangle}(\omega) &= \frac{1}{2\pi}\int u_{12}(\omega,h)\overline{\hat{G}_{t_0}}(h)\mathrm{d}h \\ &= \big(\Lambda_{12}(\omega,\cdot) \star G_{t_0}(-\cdot)\big)(0). \end{aligned} \tag{3.3.2}$$

Here $\star$, $\hat{\cdot}$ stand for convolution and Fourier transform in t, respectively. Furthermore, $u_{12}(\omega,h)$, $\Lambda_{12}(\omega,t)$ are defined through relations (2.3.5) *and* (2.3.4)*, they represent the limiting joint correlation of the reflection coefficients at nearby frequencies and their normalized joint correlation spectral density, respectively.*

Proof. Recall that from the results of the previous chapter the joint correlation $\mathbb{E}\{R^{\varepsilon}_{L,1}(0,\omega+\frac{\varepsilon}{2}h)\overline{R^{\varepsilon}_{L,2}}(0,\omega-\frac{\varepsilon}{2}h)\}$ is uniformly bounded by 1 and has a limit as $\varepsilon \downarrow 0$. Furthermore, we have that

$$\mathbb{E}\{\iint |\hat{f}(\omega+\tfrac{\varepsilon}{2}h)||\overline{\hat{G}_{t_0}}(h)||R^{\varepsilon}_{L,1}(0,\omega+\tfrac{\varepsilon}{2}h)\overline{R^{\varepsilon}_{L,2}}(0,\omega-\tfrac{\varepsilon}{2}h)|\mathrm{d}\omega\mathrm{d}h\} \leq \|\hat{f}\|_1\|\hat{G}_{t_0}\|_1$$

where $\|\cdot\|_1$ represents the usual norm on the space $L^1(\mathbf{R})$. Therefore, by the Riemann-Lebesgue Theorem we get that $\langle B^{\mathrm{TR}}_{t_0,t_1}\rangle(s) = 0$ for $t_1 \neq t_0$.

Let us now analyze the case where $t_1 = t_0$. We have that

$$\mathbb{E}\{B^{\varepsilon,\mathrm{TR}}_{t_0,t_0}(s)\} = \frac{1}{(2\pi)^2}\iint \mathrm{e}^{\mathrm{i}(\omega-\frac{\varepsilon}{2}h)s}\hat{f}(\omega+\tfrac{\varepsilon}{2}h)\overline{\hat{G}_{t_0}}(h) \\ \mathbb{E}\{R^{\varepsilon}_{L,1}(0,\omega+\tfrac{\varepsilon}{2}h)\overline{R^{\varepsilon}_{L,2}}(0,\omega-\tfrac{\varepsilon}{2}h)\}\mathrm{d}\omega\mathrm{d}h$$

and using the Dominated Convergence Theorem, we get after some manipulations that

$$\begin{aligned}\langle B^{\mathrm{TR}}_{t_0,t_0}\rangle(s) &= \frac{1}{(2\pi)^2}\iint \mathrm{e}^{\mathrm{i}\omega s}\hat{f}(\omega)\overline{\hat{G}_{t_0}}(h)u_{12}(\omega,h)\mathrm{d}\omega\mathrm{d}h \\ &= \frac{1}{2\pi}\int \mathrm{e}^{\mathrm{i}\omega s}\hat{f}(\omega)\widehat{\langle K^{\mathrm{TR}}_{t_0}\rangle}(\omega)\mathrm{d}\omega \\ &= \big(\langle K^{\mathrm{TR}}_{t_0}\rangle(\cdot)\star f(-\cdot)\big)(s).\end{aligned} \tag{3.3.3}$$

□

Taking into account this result in what follows our analysis will be concentrated in the case $t_0 = t_1$, so we introduce the simplified notations $B^{\varepsilon,\mathrm{TR}}_{t_0}$ and $\langle B^{\mathrm{TR}}_{t_0}\rangle$ in place of $B^{\varepsilon,\mathrm{TR}}_{t_0,t_0}$ and $\langle B^{\mathrm{TR}}_{t_0,t_0}\rangle$, respectively. Therefore, we recast equation (3.2.4) as:

$$B^{\varepsilon,\mathrm{TR}}_{t_0}(s) = \frac{1}{(2\pi)^2}\iint \mathrm{e}^{\mathrm{i}(\omega-\frac{\varepsilon}{2}h)s}\hat{f}(\omega+\tfrac{\varepsilon}{2}h)\overline{\hat{G}_{t_0}}(h) \\ R^{\varepsilon}_{L,1}(0,\omega+\tfrac{\varepsilon}{2}h)\overline{R^{\varepsilon}_{L,2}}(0,\omega-\tfrac{\varepsilon}{2}h)\mathrm{d}\omega\mathrm{d}h \tag{3.3.4}$$

and for the coherent time-reversed reflection

$$\begin{aligned}\langle B^{\mathrm{TR}}_{t_0}\rangle(s) &= \frac{1}{2\pi}\int \mathrm{e}^{\mathrm{i}\omega s}\hat{f}(\omega)\widehat{\langle K^{\mathrm{TR}}_{t_0}\rangle}(\omega)\mathrm{d}\omega \\ &= \big(\langle K^{\mathrm{TR}}_{t_0}\rangle(\cdot)\star f(-\cdot)\big)(s).\end{aligned} \tag{3.3.5}$$

We refer to $\langle K^{\mathrm{TR}}_{t_0}\rangle$ as the *time-reversal in reflection (averaging) convolution kernel*. Next, we analyze some special cases to get more information about its behavior.

3.3.1 Uniform random medium case

For this case, when $L \to +\infty$ we have an analytical expression for $\Lambda_{12}(t,\omega)$ presented in chapter 2, and therefore we can perform explicit calculations for the coherent refocused pulse. This result will be used later during the numerical validation of the presented theory.

We take as cutoff function $G_{t_0} = \mathbf{1}_{[0,t_0]}$, the indicator function of the interval $[0, t_0]$; in this case the TRM does not amplify neither distort the input signal. Although this cutoff function does not satisfy the conditions of the theorem above, we will see that its application to this case is in complete agreement with the numerical experiments' results.

Strong medium fluctuations

Using (3.3.2) and applying (2.4.26) we get:

$$\begin{aligned}\widehat{\langle K^{\mathrm{TR}}_{t_0}\rangle}(\omega) &= \int_0^{t_0} \Lambda_{12}(t,\omega)\mathrm{d}t \\ &= \frac{\tanh(2\sqrt{\alpha(1+\alpha)}\gamma_n\omega^2 t_0)}{2\sqrt{\alpha(1+\alpha)} + (1+2\alpha)\tanh(2\sqrt{\alpha(1+\alpha)}\gamma_n\omega^2 t_0)}\end{aligned} \tag{3.3.6}$$

where the corresponding asymptotics as $\alpha \to 0$ is given by

$$\widehat{\langle K^{\mathrm{TR}}_{t_0}\rangle}(\omega) = \frac{\gamma_n\omega^2 t_0}{1+\gamma_n\omega^2 t_0} + O(\alpha) \tag{3.3.7}$$

as predicted by the 'unperturbed' medium theory of Clouet & Fouque [19, 28].

In figure 3.1 we show the graphics of the convolution kernel's Fourier transform $\widehat{\langle K^{\mathrm{TR}}_{t_0}\rangle}$ for different values of the perturbation intensity α as a function of the scaled frequency $\chi = \omega\sqrt{\gamma_n t_0}$. From the figure, one sees that the convolution kernel filters the low frequencies while the high frequencies are scaled by a factor less than 1. The solid graphic corresponds to the kernel for standard time reversal.

More specifically, we have the following asymptotic behavior of the convolution kernel:

$$\widehat{\langle K^{\mathrm{TR}}_{t_0}\rangle}(\omega) \approx \begin{cases} \gamma_n\omega^2 t_0[1-(\gamma_n+\tilde{\gamma}_{m,n})\omega^2 t_0] & \text{for } |\omega| \text{ small}, \\ M^{\mathrm{TR}}_{\alpha} = \frac{1}{(\sqrt{\alpha}+\sqrt{1+\alpha})^2} & \text{for } |\omega| \text{ large}. \end{cases}$$

Therefore the limiting time-reversed coherent reflection is obtained by a high-pass filtering procedure. Moreover, when the recording step lasts an infinitely large amount

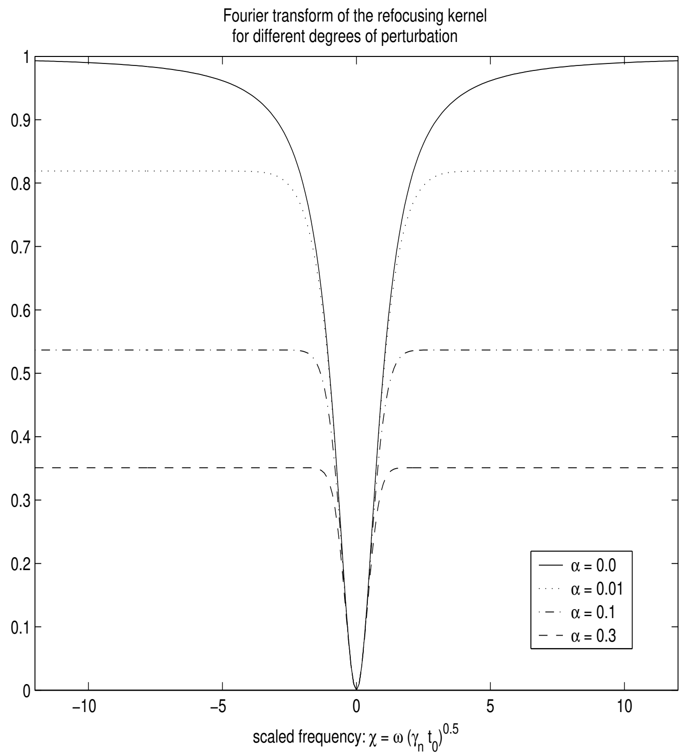

Figure 3.1: The Fourier transform of the convolution kernel $\widehat{\langle K_{t_0}^{\mathrm{TR}} \rangle}$ as a function of the scaled frequency $\chi = \omega\sqrt{\gamma_n t_0}$ for different values of the perturbation intensity.

of time (i.e. when $t_0 \to +\infty$) we get the following asymptotic behavior for the convolution kernel:

$$\langle K_{\infty}^{\mathrm{TR}} \rangle(t) = M_{\alpha}^{\mathrm{TR}} \delta(t). \tag{3.3.8}$$

Using (3.3.5) for the time-reversed average reflection we have

$$\langle B_{\infty}^{\mathrm{TR}} \rangle(s) = \frac{1}{2\pi} \int \mathrm{e}^{\mathrm{i}\omega s} M_{\alpha}^{\mathrm{TR}} \hat{f}(\omega) \mathrm{d}\omega = M_{\alpha}^{\mathrm{TR}} f(-s),$$

that corresponds to reversing time and scaling by M_{α}^{TR} the initial pulse. Note that $M_{\alpha}^{\mathrm{TR}} < 1$, if $\alpha > 0$, consequently some energy remains incoherent and cannot be recompressed. More specifically, we have the following assertion.

Proposition 3.3.2. *For the time-reversed coherent reflection the following estimates hold*

$$\|\langle B_{t_0}^{\mathrm{TR}}\rangle(\cdot) - M_\alpha^{\mathrm{TR}} f(-\cdot)\|_\infty \leq \frac{c_\alpha \|\hat{f}\|_\infty}{\sqrt{\gamma_n t_0}}$$
$$\|\langle B_{t_0}^{\mathrm{TR}}\rangle\|_2 \leq M_\alpha^{\mathrm{TR}} \|f\|_2$$

where $\|\cdot\|_2$, $\|\cdot\|_\infty$ *represents the usual norms on* $L^2(\mathbf{R})$ *and* $L^\infty(\mathbf{R})$ *respectively, and* $c_\alpha > 0$ *is a constant that only depends on* α.

Proof. The first estimate is obtained using the representation (3.3.5) and noting that

$$|\widehat{\langle K_{t_0}^{\mathrm{TR}}\rangle}(\omega) - M_\alpha^{\mathrm{TR}}| = M_\alpha^{\mathrm{TR}} g_\alpha(\omega^2 \gamma_n t_0)$$

with $\|g_\alpha\|_1 < \infty$.

For the second one, first note that since $0 \leq \tanh(2\sqrt{\alpha(1+\alpha)}\gamma_n \omega^2 t_0) \leq 1$. Then

$$(\sqrt{\alpha} + \sqrt{1+\alpha})^2 \tanh(2\sqrt{\alpha(1+\alpha)}\gamma_n \omega^2 t_0) \leq 2\sqrt{\alpha(1+\alpha)} + (1+2\alpha)\tanh(2\sqrt{\alpha(1+\alpha)}\gamma_n \omega^2 t_0)$$

which yields

$$\|\widehat{\langle K_{t_0}^{\mathrm{TR}}\rangle}\|_\infty \leq M_\alpha^{\mathrm{TR}}.$$

And now the inequality easily follows from Parseval identity. □

Remark 3.3.1. It should be noted that the proposition is also valid in the case $\alpha = 0$, i.e. for standard time reversal experiments. The proof is simpler and follows the same lines. Furthermore, since $M_0^{\mathrm{TR}} = 1$ then when $t_0 \to +\infty$ the original pulse shape is completely recovered after time reversal. It is remarkable that as in this case we have statistical stabilization, the waveform reconstruction can be achieved without the need of averaging.

Weak medium fluctuations

Recall that

$$\Lambda_{12}(t,\omega) = \omega^2\gamma_n^c(\omega)\exp\{-\mathrm{i}\omega^2\gamma_{\delta n}^s(\omega)t\} \\ \times \frac{1-\tanh^2(2\sqrt{\tilde\alpha(\omega)(1+\tilde\alpha(\omega))}\omega^2\gamma_n^c(\omega)t)}{\left(1+\frac{1+2\tilde\alpha(\omega)}{2\sqrt{\tilde\alpha(\omega)(1+\tilde\alpha(\omega))}}\tanh(2\sqrt{\tilde\alpha(\omega)(1+\tilde\alpha(\omega))}\omega^2\gamma_n^c(\omega)t)\right)^2}. \quad (3.3.9)$$

Note that the presence of a complex phase prevents the explicit calculation of

$$\widehat{\langle K_{t_0}^{\mathrm{TR}}\rangle} = \int_0^{t_0}\Lambda_{12}(t,\omega)\mathrm{d}t. \quad (3.3.10)$$

Let us first analyze the case where $\delta n(\cdot) = 0$ almost surely (cf. (2.3.1)). Then one gets

$$\widehat{\langle K_{t_0}^{\mathrm{TR}}\rangle}(\omega) = \frac{\tanh(2\tilde\beta(\omega)\omega^2 t_0)}{2\sqrt{\tilde\alpha(\omega)(1+\tilde\alpha(\omega))}+(1+2\tilde\alpha(\omega))\tanh(2\tilde\beta(\omega)\omega^2 t_0)} \quad (3.3.11)$$

where $\tilde\beta(\omega) = \gamma_n^c(\omega)\sqrt{\tilde\alpha(\omega)(1+\tilde\alpha(\omega))}$ and now the perturbation intensity reads as $\tilde\alpha(\omega) = \frac{\gamma_{\delta m}}{2\gamma_n^c(\omega)}$. The convolution kernel has the following asymptotic behavior:

$$\widehat{\langle K_{t_0}^{\mathrm{TR}}\rangle}(\omega) \approx \begin{cases} \gamma_n\omega^2 t_0[1-(\gamma_n+\gamma_{\delta m})\omega^2 t_0] - \omega^4\gamma_n^{(2)}t_0 & \text{for } |\omega| \text{ small,} \\ M^{\mathrm{TR}}(\omega) = \frac{1}{(\sqrt{\tilde\alpha(\omega)}+\sqrt{1+\tilde\alpha(\omega)})^2} & \text{for } |\omega| \text{ large.} \end{cases}$$

Here again the low frequencies are filtered but the behavior at high frequencies strongly depends on the function $M^{\mathrm{TR}}(\omega)$. Furthermore, if the correlation function of the fluctuation $n(\cdot)$ is in $L^1(\mathbf{R}^+)$ (i.e. $\int_0^\infty |\mathbb{E}\{n(s)n(0)\}|\mathrm{d}s < \infty$) then by the Riemann-Lebesgue Theorem we get that $|M^{\mathrm{TR}}(\omega)| \to 0$ as $|\omega|$ goes to infinity. Consequently the high frequencies are also filtered. This is a remarkable difference with the strong fluctuations regime.

Furthermore, if we perform a total record of the reflected signal (i.e. when $t_0 \to +\infty$) then we get the following asymptotics for the convolution kernel:

$$\widehat{\langle K_{\infty}^{\mathrm{TR}}\rangle}(\omega) = \left(\sqrt{\tilde\alpha(\omega)}+\sqrt{1+\tilde\alpha(\omega)}\right)^{-2}, \quad (3.3.12)$$

and therefore the time-reversed average reflection corresponds to

$$\langle B_\infty^{\mathrm{TR}}\rangle(s) = \big(\langle K_\infty^{\mathrm{TR}}\rangle(\cdot) \star f(-\cdot)\big)(s).$$

As an example, let us consider the case where the fluctuation $n(\cdot)$ has an exponential autocorrelation function:

$$\mathbb{E}\{n(s)n(0)\} = \alpha_0 \mathrm{e}^{-2\frac{\omega_0}{c_0}s}.$$

Introducing the scaled frequency $\chi = \frac{\omega}{\omega_0}$, the dimensionless parameter $\theta_0 = \gamma_n\omega^2 t_0$ and recalling that the perturbation intensity in the low frequency limit is now given as $\tilde{\alpha}(0) = \alpha = \frac{\gamma_{\delta m}}{2\gamma_n}$ the convolution kernel is given by

$$\widehat{\langle K_{t_0}^{\mathrm{TR}}\rangle}(\chi,\theta_0,\alpha) = \frac{\frac{1}{1+\chi^2}\tanh\Big(2\theta_0\chi^2\sqrt{\alpha\frac{1+\alpha(1+\chi^2)}{1+\chi^2}}\Big)}{2\sqrt{\alpha\frac{1+\alpha(1+\chi^2)}{1+\chi^2}} + \big(2\alpha + \frac{1}{1+\chi^2}\big)\tanh\Big(2\theta_0\chi^2\sqrt{\alpha\frac{1+\alpha(1+\chi^2)}{1+\chi^2}}\Big)}.$$

Next, we show some graphics corresponding to this example. In figures 3.2 and 3.3 we present the graphics of the convolution kernel as a function of χ for different values of the perturbation intensity α, when $\theta_0 = 1$, 5 respectively. These are medium-band filters as predicted above.

In figure 3.4 we show the limiting convolution kernel as $t_0 \to +\infty$ for different values of the perturbation intensity α. These are high frequency filters with optimal value at the frequency $\omega = 0$.

For the general case define

$$M^{\mathrm{TR}}(\omega) = \int_0^\infty \Lambda_{12}(t,\omega)\mathrm{d}t,$$

with $\Lambda_{12}(t,\omega)$ given by (3.3.9), and $\langle K_\infty^{\mathrm{TR}}\rangle(t)$ by its Fourier transform as

$$\widehat{\langle K_\infty^{\mathrm{TR}}\rangle}(\omega) = M^{\mathrm{TR}}(\omega). \tag{3.3.13}$$

This kernel dictates the asymptotic behavior of the convolution kernel $\langle K_{t_0}^{\mathrm{TR}}\rangle$ when the recording takes an infinitely large time ($t_0 \to +\infty$).

More precisely, we have the following assertion.

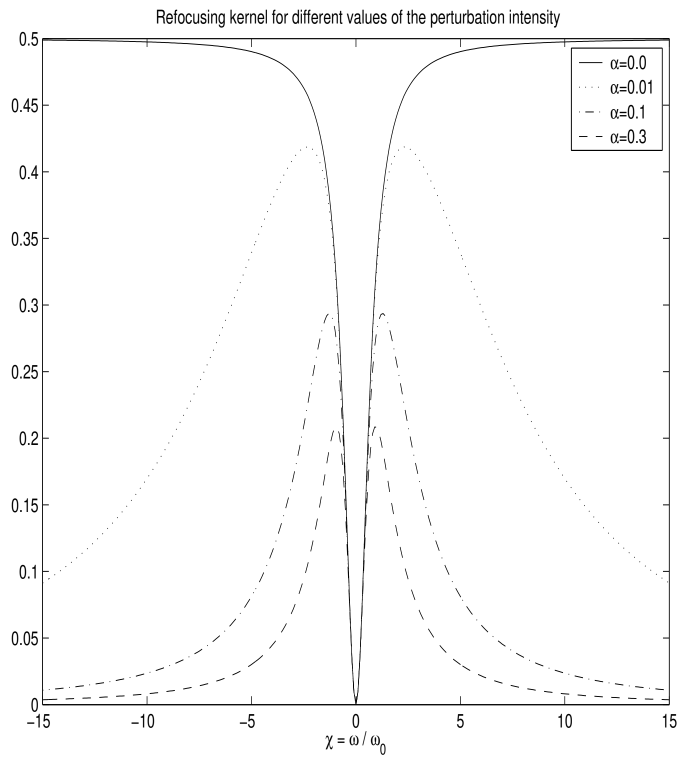

Figure 3.2: The Fourier transform of the convolution kernel $\widehat{\langle K_{t_0}^{\mathrm{TR}}\rangle}$ as a function of the scaled frequency $\chi = \frac{\omega}{\omega_0}$ for different values of the perturbation intensity α in the case where $\theta_0 = 1$.

Proposition 3.3.3. *Suppose that* $\gamma_{\delta m} \neq 0$. *Then for the time-reversed coherent reflection the following estimates hold*

$$\|\langle B_{t_0}^{\mathrm{TR}}\rangle(\cdot) - \langle K_{\infty}^{\mathrm{TR}}\rangle(\cdot) \star f(-\cdot)\|_{\infty} \leq \frac{c_1 \|\hat{f}\|_{\infty}}{\sqrt{t_0}},$$
$$\|\langle B_{t_0}^{\mathrm{TR}}\rangle\|_2 \leq \sup_{\omega \in \mathbf{R}} \left(\sqrt{\tilde{\alpha}(\omega)} + \sqrt{1+\tilde{\alpha}(\omega)}\right)^{-2} \|f\|_2$$

where the constant $c_1 > 0$ *only depends on the random media statistical properties.*

Proof. The proof is very similar to that of Proposition 3.3.2. The first estimate is

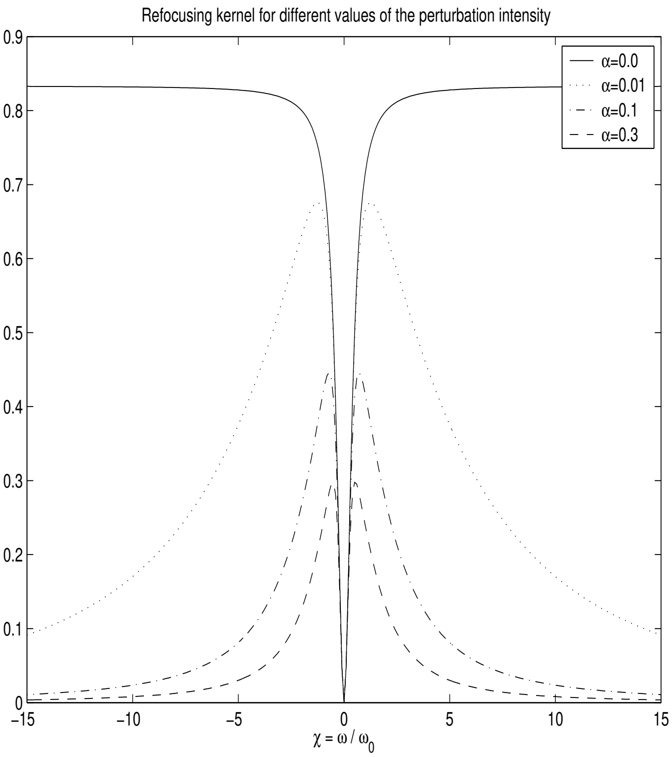

Figure 3.3: The Fourier transform of the convolution kernel $\widehat{\langle K_{t_0}^{\mathrm{TR}}\rangle}$ as a function of the scaled frequency $\chi = \frac{\omega}{\omega_0}$ for different values of the perturbation intensity α in the case where $\theta_0 = 5$.

obtained applying the following inequalities

$$\begin{aligned}
|\widehat{\langle K_{t_0}^{\mathrm{TR}}\rangle}(\omega) - M^{\mathrm{TR}}(\omega)| &\leq \int_{t_0}^{\infty} |\Lambda_{12}(\omega,t)| \mathrm{d}t \\
&\leq \Big(\tfrac{1}{\sqrt{\tilde{\alpha}(\omega)}+\sqrt{1+\tilde{\alpha}(\omega)}}\Big)^2 \Big(\frac{1-\tanh(2\tilde{\beta}(\omega)\omega^2 t_0)}{1+\tanh(2\tilde{\beta}(\omega)\omega^2 t_0)}\Big) \\
&\leq \mathrm{e}^{-4\tilde{\beta}(\omega)\omega^2 t_0} \\
&\leq \mathrm{e}^{-2\gamma_{\delta m}\omega^2 t_0},
\end{aligned}$$

where we have used that $0 < \gamma_{\delta m} < 2\tilde{\beta}(\omega)$.

And the second one, easily follows from Parseval identity, noting that:

$$|\widehat{\langle K_{t_0}^{\mathrm{TR}}\rangle}(\omega)| \leq \big(\sqrt{\tilde{\alpha}(\omega)} + \sqrt{1+\tilde{\alpha}(\omega)}\big)^{-2}.$$

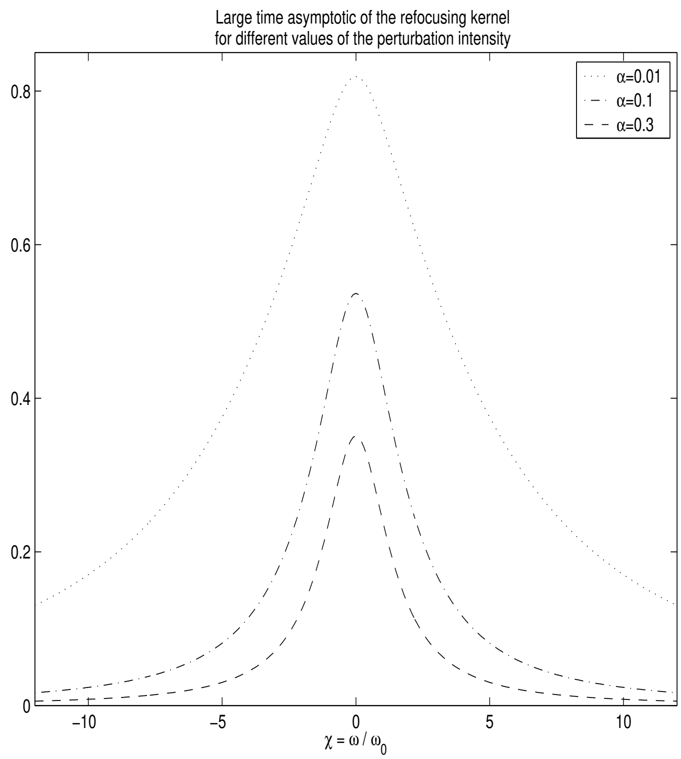

Figure 3.4: The Fourier transform of the convolution kernel $\widehat{\langle K_\infty^{\mathrm{TR}} \rangle}$ as a function of the scaled frequency $\chi = \frac{\omega}{\omega_0}$ for different values of the perturbation intensity α. Note that $\chi = 0$ is a discontinuity point where the functions take value 0.

$\square$

Remark 3.3.2. We have to notice that the estimate for the recompressed energy presented in the proposition above is a constant which only depends on the random fluctuations' statistics. Therefore this constant is a statistical characteristic of the loss of coherence due to medium perturbations.

3.4 Asymptotics of the refocused pulse

In this section we present the main results of this work. It is concerned with the probabilistic description of the asymptotic time-reversed reflected pulse (3.2.2) for ε

small, in the case of a random half-space with a totally reflecting termination. The regimes of strong and weak medium fluctuations can be handled in a similar way so we shall analyze both cases at once without entering into much details in this regard.

We begin by studying the time-reversed refocused reflection. More specifically, we will characterize the weak limit of the stochastic process $(B_{t_0}^{\varepsilon,\mathrm{TR}}(\sigma), \sigma \in \mathbf{R})$ as ε goes to zero.

By a simple application of the Dominated Convergence Theorem, one can get that $B_{t_0}^{\varepsilon,\mathrm{TR}}(\cdot)$ is almost surely continuous and therefore we introduce the family of continuous random functions: $\{B_{t_0}^{\varepsilon,\mathrm{TR}}(\sigma),\ \sigma \in \mathbf{R}\}_{0<\varepsilon<1}$, it is a family of stochastic processes with paths in $C(\mathbf{R})$ (the Fréchet space of continuous real-valued functions f on $\mathbf{R}$ with semi-norms $\{\sup_{|s|\leq T} |f(s)|\}_{T>0}$). The characterization of the weak limit of this family of random processes as ε goes to zero is the main goal of this section. We proceed by using a standard scheme, first we establish the tightness of the family and then identify the limit (see for example [13, 36]). This last step will be carried out by performing an asymptotic analysis of the moments corresponding to the finite-dimensional distributions.

3.4.1 Tightness

We first prove the tightness of this family of random functions.

Remark 3.4.1. Recall that $C(\mathbf{R})$ is endowed with the structure of a complete separable metric space and then tightness is equivalent to relative compactness [13, 36]. Therefore, for any sequence $\varepsilon_n \downarrow 0$ as $n \to \infty$ there exists a subsequence $\varepsilon_{n'} \downarrow 0$ such that $B_{t_0}^{\varepsilon_{n'},\mathrm{TR}}(\sigma)$ weakly converges as $n' \to \infty$. Moreover, we will prove that this limit does not depend on the chosen sequences, so its uniqueness will follow.

Lemma 3.4.1. *The family of stochastic processes $\{B_{t_0}^{\varepsilon,\mathrm{TR}}(\sigma),\ \sigma \in \mathbf{R}\}_{0<\varepsilon<1}$ with paths in $C(\mathbf{R})$ is tight.*

Proof. From the representation (3.3.4) and according to [13], it is enough to observe that the following uniform bounds are satisfied by the processes:

$$|B_{t_0}^{\varepsilon,\mathrm{TR}}(\sigma)| \leq C = (2\pi)^{-2}\|\hat{f}\|_1\|\hat{G}_{t_0}\|_1, \tag{3.4.1}$$

and their modulus of continuity:

$$\begin{aligned} M^\varepsilon(\delta) &= \sup_{|\sigma_2-\sigma_1|\leq\delta} |B_{t_0}^{\varepsilon,\mathrm{TR}}(\sigma_2) - B_{t_0}^{\varepsilon,\mathrm{TR}}(\sigma_1)| \\ &\leq \frac{1}{(2\pi)^2}\iint \sup_{|\sigma_2-\sigma_1|\leq\delta} |1-\mathrm{e}^{\mathrm{i}\omega(\sigma_2-\sigma_1)}||\hat{f}(\omega+\varepsilon h)||\hat{G}_{t_0}(h)|\mathrm{d}\omega\mathrm{d}h. \end{aligned}$$

So that by the Dominated Convergence Theorem $M^\varepsilon(\delta) \to 0$ as $\delta \to 0$, therefore for each $\gamma > 0$ and $\eta > 0$ there is a $\delta > 0$ such that $\mathbb{P}\{M^\varepsilon(\delta) \geq \gamma\} \leq \eta$, which implies tightness. $\square$

Remark 3.4.2. Note that concerning the reflection coefficients this proof uses only their boundedness. Consequently the lemma is valid in the general case of a random slab.

3.4.2 Finite-dimensional probability distributions

Moments of the finite-dimensional distributions

We note that for characterizing the corresponding finite-dimensional limit distribution it is enough to know all the associated moments. In fact, from (3.4.1) one easily obtains that for any reals $\sigma_1 < \cdots < \sigma_l$ and integers $p_1, \ldots, p_l$:

$$\mathbb{E}\{\big(B_{t_0}^{\varepsilon,\mathrm{TR}}(\sigma_1)\big)^{p_1}\cdots\big(B_{t_0}^{\varepsilon,\mathrm{TR}}(\sigma_l)\big)^{p_l}\} \leq C^M$$

where $M = p_1 + \cdots + p_l$. Consequently the finite-dimensional limit probability distributions are determined by their moments. Moreover, since:

$$\begin{aligned} &\mathbb{E}\{\big(B_{t_0}^{\varepsilon,\mathrm{TR}}(\sigma_1)\big)^{p_1}\cdots\big(B_{t_0}^{\varepsilon,\mathrm{TR}}(\sigma_l)\big)^{p_l}\} = \\ &\quad\frac{1}{(2\pi)^{2M}}\int\cdots\int \mathbb{E}\{\prod_{\substack{j=1,l\\k=1,p_j}} R_1^\varepsilon(0,\omega_{jk}+\tfrac{\varepsilon}{2}h_{jk})\overline{R_2^\varepsilon}(0,\omega_{jk}-\tfrac{\varepsilon}{2}h_{jk})\} \\ &\qquad\prod_{\substack{j=1,l\\k=1,p_j}} \mathrm{e}^{\mathrm{i}(\omega_{jk}-\frac{\varepsilon}{2}h_{jk})\sigma_j}\overline{\hat{G}_{t_0}}(h_{jk})\hat{f}(\omega_{jk}+\tfrac{\varepsilon}{2}h_{jk})\mathrm{d}\omega_{jk}\mathrm{d}h_{jk}, \end{aligned} \tag{3.4.2}$$

it is enough to compute the limits

$$u_M(\omega_1, \cdots, h_M) = \lim_{\varepsilon \downarrow 0} \mathbb{E}\{\prod_{k=1}^{M} R_1^\varepsilon(0, \omega_k + \tfrac{\varepsilon}{2} h_k)\overline{R_2^\varepsilon}(0, \omega_k - \tfrac{\varepsilon}{2} h_k)\}, \tag{3.4.3}$$

for M different frequencies $\omega_1, \ldots, \omega_M$ and M different increments $h_1, \ldots, h_M$, in order to obtain that:

$$\lim_{\varepsilon \downarrow 0} \mathbb{E}\{\big(B_{t_0}^{\varepsilon,\mathrm{TR}}(\sigma_1)\big)^{p_1} \cdots \big(B_{t_0}^{\varepsilon,\mathrm{TR}}(\sigma_l)\big)^{p_l}\} = \frac{1}{(2\pi)^{2M}} \int \cdots \int u_M(\omega_{11}, \cdots, h_{lp_l}) \prod_{\substack{j=1,l \\ k=1,p_j}} \mathrm{e}^{\mathrm{i}\omega_{jk}\sigma_j} \hat{f}(\omega_{jk}) \overline{\hat{G}_{t_0}}(h_{jk}) \mathrm{d}\omega_{jk} \mathrm{d}h_{jk} \tag{3.4.4}$$

Under the assumption of a totally reflecting termination, the application of the diffusion-approximation theorems presented in appendix A give us that

$$u_M(\omega_1, \cdots, h_M) = \lim_{z \to -\infty} V(z, \psi_1, \cdots, \psi_M; \omega_1, \cdots, h_M) \tag{3.4.5}$$

where V is obtained from the Kolmogorov backward equation:

$$\begin{cases} (\dfrac{\partial}{\partial z} + \mathcal{L})V = 0 \qquad z < 0 \\ V|_{z=0} = \mathrm{e}^{\mathrm{i}(\psi_1 + \cdots + \psi_M)} \end{cases} \tag{3.4.6}$$

with the infinitesimal generator given by

$$\mathcal{L} = \sum_{k=1}^{M} \mathcal{L}_k^0 + 4\frac{\gamma_{\delta m}(z)}{c_0(z)} \sum_{\substack{j,k=1 \\ j \neq k}}^{M} \omega_j \omega_k \partial^2_{\psi_j \psi_k} \tag{3.4.7}$$

where $\mathcal{L}_k^0$ corresponds to the infinitesimal generator $\mathcal{L}^0$ at a single frequency and increment, given by (2.4.10) or (2.4.38) in the strong or weak fluctuations case, respectively, after setting $\omega = \omega_k$, $h = h_k$ and $\psi = \psi_k$, $k = 1, \ldots, M$. The limit (3.4.5) exists if the coefficients of the generator (3.4.7) have an appropriate behavior as z approaches $-\infty$ as discussed in section 2.4.

Remark 3.4.3. From these results become apparent that the limiting finite-dimensional moments have a unique description, leading to the uniqueness of the limit finite-dimensional probability distributions and the weak limit of the family of random processes.

Limit finite-dimensional distribution

The analysis that lead us to the characterization of the limit finite-dimensional distribution is motivated by the fact that the study of stochastic partial differential equations simplifies the analysis and description of multiple-points trajectories of diffusion processes [44]. In accordance with this, we additionally use the structure of the infinitesimal generator (3.4.7) and the properties of solutions of stochastic differential equations (Itô formula).

Let us represent by B_s, a standard one-dimensional Brownian motion with $s \in [0, +\infty)$ defined on a complete probability space $(\tilde{\Omega}, \tilde{\mathcal{F}}, \tilde{\mathbb{P}})$. Define a new stochastic process $(\check{B}_z, z \in (-\infty, 0])$ by setting $\check{B}_z = B_{-z}$ almost surely, it is called a *backward (standard) one-dimensional Brownian motion.* It is a backward martingale, and therefore we can introduce a second order backward Itô stochastic partial differential equation [43, 44]:

$$\begin{cases} \mathrm{d}v + (\mathcal{L}^0 v)\mathrm{d}z + 2\omega\sqrt{\frac{2\gamma_{\delta m}(z)}{c_0(z)}}\,\partial_\psi v \overleftarrow{\mathrm{d}}\,\check{B}_z = 0, & \text{for } z < 0 \\ v|_{z=0} = \mathrm{e}^{\mathrm{i}\psi} \end{cases} \tag{3.4.8}$$

where $\overleftarrow{\mathrm{d}}\,\check{B}_z$ represents the backward Itô's differential of $\check{B}_z$. Or re-writing in integral form:

$$v(z,\psi) = \mathrm{e}^{\mathrm{i}\psi} + \int_z^0 (\mathcal{L}^0 v)\mathrm{d}s + 2\omega \int_z^0 \sqrt{\frac{2\gamma_{\delta m}(z)}{c_0(z)}}\,\partial_\psi v \overleftarrow{\mathrm{d}}\,\check{B}_s, \tag{3.4.9}$$

with the backward stochastic integral defined through a (forward) Itô's stochastic integral as

$$\int_{z_1}^{z_2} \xi(s) \overleftarrow{\mathrm{d}}\,\check{B}_s := -\int_{-z_2}^{-z_1} \xi(-s)\,\mathrm{d}B_s.$$

From [43, 44], we know that the stochastic equation (3.4.8) (or (3.4.9)) has a unique solution, which is a backward semimartingale (see Appendix C). Let $v_k(z,\psi_k) = v(z,\psi_k;\omega_k,h_k)$ be the solution of (3.4.8) (or (3.4.9)) when we set $\psi = \psi_k$, $\omega = \omega_k$ and $h = h_k$, for $k = 1,\ldots,M$.

Recall the Itô formula for backward semimartingales: if $F \in C^2(\mathbf{R}^M, \mathbf{R})$ then for

$F(v_1(z,\psi_1),\cdots,v_M(z,\psi_M))$ we have

$$\mathrm{d}F = \sum_{j=1}^{M} \partial_{v_j} F \,\mathrm{d}v_j - \tfrac{1}{2}\sum_{i,j=1}^{M} \partial^2_{v_i v_j} F \,\mathrm{d}\langle v_i, v_j\rangle_z .$$

where $\mathrm{d}\langle v_i, v_j\rangle_z$ represents the differential of the joint quadratic variation of the semimartingales v_i and v_j, for $i,j=1,\ldots,M$. For details on backward semimartingales and stochastic differential equations and integration, see the references above and [42].

For $U_M(z,\psi_1,\cdots,\psi_M;\omega_1,\cdots,h_M)=\prod_{j=1}^M v_j(z,\psi_j)$, by using that for $i\neq j$

$$\mathrm{d}\langle v_i, v_j\rangle_z = 8\omega_i\omega_j \tfrac{\gamma_{\delta m}(z)}{c_0(z)} (\partial^2_{\psi_i\psi_j} v_i v_j)\mathrm{d}z,$$

one gets the following backward stochastic partial differential equation:

$$\begin{cases} \mathrm{d}U_M + \big(\mathcal{L}U_M\big)\mathrm{d}z + 2\sqrt{\tfrac{2\gamma_{\delta m}(z)}{c_0(z)}}\Big(\sum_{j=1}^{M}\omega_j\partial_{\psi_j}\Big)U_M \overleftarrow{\mathrm{d}}\,\check{B}_z = 0 & \text{for } z<0, \\ U_M|_{z=0} = \mathrm{e}^{\mathrm{i}(\psi_1+\cdots+\psi_M)}. \end{cases}$$

Consequently, the function $\tilde{U}_M(z,\psi_1,\cdots,\psi_M)=\tilde{\mathbb{E}}\{U_M(z,\psi_1,\cdots,\psi_M)\}$, where $\tilde{\mathbb{E}}\{\cdot\}$ represents expectation with respect to the probability $\tilde{\mathbb{P}}$, satisfies the Kolmogorov backward equation (3.4.6). Introducing $v_0(\omega,h)=\lim_{z\to-\infty} v(z,\psi,\omega,h)$ (see Lemma C.2 of the Appendix C) one gets

$$u_M(\omega_1,\cdots,h_M) = \tilde{\mathbb{E}}\{\prod_{j=1}^{M} v_0(\omega_j,h_j)\}. \tag{3.4.10}$$

This is a great simplification, since $v_0(\omega_j,h_j)$ are functionals of a single Brownian motion while the initial Kolmogorov backward equation (3.4.6) is associated with a M-dimensional diffusion process.

Now, the substitution of (3.4.10) in (3.4.4) yields

$$\lim_{\varepsilon\downarrow 0}\mathbb{E}\{\big(B^{\varepsilon,\mathrm{TR}}_{t_0}(\sigma_1)\big)^{p_1}\cdots\big(B^{\varepsilon,\mathrm{TR}}_{t_0}(\sigma_l)\big)^{p_l}\} =$$

$$\frac{1}{(2\pi)^{2M}}\int\cdots\int \tilde{\mathbb{E}}\{\prod_{\substack{j=1,l\\k=1,p_j}} \mathrm{e}^{\mathrm{i}\omega_{jk}\sigma_j}\hat{f}(\omega_{jk})v_0(\omega_{jk},h_{jk})\overline{\hat{G}_{t_0}}(h_{jk})\mathrm{d}\omega_{jk}\mathrm{d}h_{jk}\}.$$

Finally, we get that

$$\lim_{\varepsilon\downarrow 0}\mathbb{E}\{\big(B^{\varepsilon,\mathrm{TR}}_{t_0}(\sigma_1)\big)^{p_1}\cdots\big(B^{\varepsilon,\mathrm{TR}}_{t_0}(\sigma_l)\big)^{p_l}\}=\tilde{\mathbb{E}}\{\big(B^{\mathrm{TR}}_{t_0}(\sigma_1)\big)^{p_1}\cdots\big(B^{\mathrm{TR}}_{t_0}(\sigma_l)\big)^{p_l}\}$$

where

$$B^{\mathrm{TR}}_{t_0}(\sigma)=\frac{1}{(2\pi)^2}\iint \mathrm{e}^{\mathrm{i}\omega\sigma}\hat{f}(\omega)\overline{\hat{G}_{t_0}}(h)v_0(\omega,h)\mathrm{d}\omega\mathrm{d}h.$$

Note that these allow us to identify the continuous random process $(B^{\mathrm{TR}}_{t_0}(\sigma),\sigma\in\mathbf{R})$ as the weak limit of $B^{\varepsilon,\mathrm{TR}}_{t_0}(\cdot)$ as ε goes to zero.

Remark 3.4.4. It should be noted that the limit time-reversed refocused reflection $B^{\mathrm{TR}}_{t_0}(\cdot)$ is a different random process for each medium fluctuations regime, this is a consequence of the fact that the differential operator $\mathcal{L}^0$ in (3.4.8) corresponds to the infinitesimal generators (2.4.10) or (2.4.38) in the case of strong or weak medium fluctuations, respectively.

3.4.3 Characterization of the refocused pulse

From the results above and noting that

$$\begin{aligned}B^{\mathrm{TR}}_{t_0}(\sigma)&=\frac{1}{2\pi}\int \mathrm{e}^{\mathrm{i}\omega\sigma}\hat{f}(\omega)\big(\lambda(\omega,\cdot)\star G_{t_0}(-\cdot)\big)(0)\mathrm{d}\omega\\&=\big(K^{\mathrm{TR}}_{t_0}(\cdot)\star f(-\cdot)\big)(\sigma)\end{aligned}\tag{3.4.11}$$

where

$$\widehat{\lambda(\omega,\cdot)}(h)=v_0(\omega,h),\tag{3.4.12a}$$

$$\widehat{K^{\mathrm{TR}}_{t_0}}(\omega)=\big(\lambda(\omega,\cdot)\star G_{t_0}(-\cdot)\big)(0)\tag{3.4.12b}$$

and $\star$, $\widehat{(\cdot)}$ stand for convolution and Fourier transform with respect to t, respectively. We can state the main result as:

Theorem 3.4.2. *The time-reversed acoustic pulse* $(u^{\mathrm{TR}}_{\mathrm{ref}}(0,t_0+\varepsilon\sigma),\, p^{\mathrm{TR}}_{\mathrm{ref}}(0,t_0+\varepsilon\sigma))$ *weakly converges (i.e. in distribution) as* ε *approaches zero to the random acoustic signal* $(\frac{1}{2}\zeta_0^{-1/2}(0)B^{\mathrm{TR}}_{t_0}(\sigma),\, \frac{1}{2}\zeta_0^{1/2}(0)B^{\mathrm{TR}}_{t_0}(\sigma))$ *where the time-reversed reflection*

$$B^{\mathrm{TR}}_{t_0}(\sigma)=\big(K^{\mathrm{TR}}_{t_0}(\cdot)\star f(-\cdot)\big)(\sigma)$$

with the time-reversal refocusing (random) convolution kernel $K_{t_0}^{\mathrm{TR}}$ *given by the relations* (3.4.12).

This theorem completely characterizes the probability distribution of the limiting refocused pulse as ε goes to zero. The weak convergence implies much more than the simple convergence of finite-dimensional distributions. In fact, for every continuous function F on $C(\mathbf{R})$ we have that $F(B_{t_0}^{\varepsilon,\mathrm{TR}}(\cdot))$ has the weak limit $F(B_{t_0}^{\mathrm{TR}}(\cdot))$. Therefore, the limiting signal $B_{t_0}^{\mathrm{TR}}(\cdot)$ can be used to get good approximations to the distributions of many interesting functionals of the refocused reflection $B_{t_0}^{\varepsilon,\mathrm{TR}}(\cdot)$. For example, we have that $\mathbb{P}\{\max_{|s|\leq T} B_{t_0}^{\varepsilon,\mathrm{TR}}(s) < x\} \approx \tilde{\mathbb{P}}\{\max_{|s|\leq T} B_{t_0}^{\mathrm{TR}}(s) < x\}$. Other useful examples are given by path functionals such as $\int_{-T}^{T} g(B_{t_0}^{\varepsilon,\mathrm{TR}}(s))\mathrm{d}s$.

Remark 3.4.5. A remarkable property of the limiting refocused pulse is that its description involves a single standard one-dimensional Brownian motion and a few statistical parameters of the random media fluctuations through the solution of the backward Itô stochastic partial differential equation (3.4.8).

A simple generalization of the computations performed in the previous paragraphs together with the application of the Riemann-Lebesgue Theorem (as we did in Proposition 3.3.1) leads to the conclusion that for $t_0 \neq t_1$ the process $(B_{t_0,t_1}^{\varepsilon,\mathrm{TR}}(\sigma), \sigma \in \mathbf{R})$, weakly converges to the null process as ε goes to zero. Moreover, since this limiting process is deterministic then the convergence is actually in probability [13]. This gives a stronger version of the refocusing property stated in Proposition 3.3.1 that we present as a theorem.

Theorem 3.4.3 (Strong refocusing property). *Let the recording and the observation times be different, i.e.* $t_1 \neq t_0$. *Then the limiting time-reversed reflected acoustic signal vanishes. More exactly, the acoustic signals* $u_{\mathrm{ref}}^{\mathrm{TR}}(0, t_1+\varepsilon\sigma)$ *and* $p_{\mathrm{ref}}^{\mathrm{TR}}(0, t_1+\varepsilon\sigma)$, $\sigma \in \mathbf{R}$ *converges in probability as* ε *goes to zero to the null process, meaning that for every* $\delta > 0$, $T > 0$

$$\lim_{\varepsilon\downarrow 0}\mathbb{P}\{\sup_{|\sigma|\leq T}\left|u_{\mathrm{ref}}^{\mathrm{TR}}(0, t_1+\varepsilon\sigma)\right| \geq \delta\} = \lim_{\varepsilon\downarrow 0}\mathbb{P}\{\sup_{|\sigma|\leq T}\left|p_{\mathrm{ref}}^{\mathrm{TR}}(0, t_1+\varepsilon\sigma)\right| \geq \delta\} = 0.$$

Remark 3.4.6. It should be noted that this theorem is also valid in the case where $L < +\infty$, since for applying the Riemann-Lebesgue Theorem we only need the uniform boundedness of the reflection coefficients.

3.4.4 Statistical stabilization of the refocused pulse

Recall that in standard time reversal experiments the refocused pulse has the remarkable property of statistical stabilization: its shape does not depend on the media realizations [19, 28, 66]. This property allows for a great potential of practical applications [25, 26].

However, when the medium is subjected to perturbations the statistical stabilization is lost: the limiting refocused pulse is (in general) a random function. Nevertheless from the computations above we can observe that in the case where $\gamma_{\delta m}(z) = 0$ the limit system of equations (3.4.8) is not stochastic anymore and consequently the refocused pulse is deterministic. This occurs for instance if the fluctuation $m(\cdot)$ remains unperturbed, that is $\delta m(\cdot) = 0$ almost surely.

More specifically, now the description goes as follows. The time reversed reflection is the deterministic signal given by

$$\begin{aligned} \tilde{B}^{\mathrm{TR}}_{t_0}(\sigma) &= \frac{1}{2\pi}\int e^{i\omega\sigma}\hat{f}(\omega)\big(\tilde{\lambda}(\omega,\cdot)\star G_{t_0}(-\cdot)\big)(0)d\omega \\ &= \big(\tilde{K}^{\mathrm{TR}}_{t_0}(\cdot)\star f(-\cdot)\big)(\sigma) \end{aligned} \tag{3.4.13}$$

where the deterministic convolution kernel $\tilde{K}^{\mathrm{TR}}_{t_0}$ is obtained through the relations

$$\widehat{\tilde{K}^{\mathrm{TR}}_{t_0}}(\omega) = \big(\tilde{\lambda}(\omega,\cdot)\star G_{t_0}(-\cdot)\big)(0) \tag{3.4.14a}$$

$$\widehat{\tilde{\lambda}(\omega,\cdot)}(h) = \tilde{v}_0(\omega,h) \tag{3.4.14b}$$

The function $\tilde{v}_0$ is determined solving the deterministic backward parabolic equation

$$\begin{cases} \big(\dfrac{\partial}{\partial z} + \mathcal{L}^0\big)V = 0, & \text{for } z < 0 \\ V|_{z=0} = e^{i\psi} \end{cases} \tag{3.4.15}$$

and computing the limit

$$\tilde{v}_0(\omega, h) = \lim_{z \to -\infty} V(z, \psi, \omega, h). \tag{3.4.16}$$

The differential operator $\mathcal{L}^0$ has the form

$$\mathcal{L}^0_{(\mathrm{s})} = \frac{2h}{c_0(z)}\partial_\psi + \frac{4\omega^2}{c_0(z)}\{\gamma_n(z)(1-\cos\psi) + \frac{1}{2}\gamma_{\delta n}(z)\}\partial^2_\psi \tag{3.4.17}$$

in the strong fluctuations regime, and

$$\mathcal{L}^0_{(\mathrm{w})} = 2\frac{h - \omega^2\gamma^s_{\delta n}(z,\omega)}{c_0(z)}\partial_\psi + \frac{4\omega^2}{c_0(z)}\{\gamma^c_n(z,\omega)(1-\cos\psi) + \frac{1}{2}\gamma^c_{\delta n}(z,\omega)\}\partial^2_\psi \tag{3.4.18}$$

for weak fluctuations. Summarizing we have the following theorem:

Theorem 3.4.4 (Refocused pulse stabilization). *If the medium is perturbed in such a way that $\gamma_{\delta m}(z) = 0$, then the refocused pulse converges in probability as ε goes to zero to a deterministic pulse. More exactly, we have that for every $\delta > 0$, $T > 0$,*

$$\lim_{\varepsilon\downarrow 0} \mathbb{P}\{\sup_{|s|\le T} \left|u^{\mathrm{TR}}_{\mathrm{ref}}(0, t_0 + \varepsilon s) - \tfrac{1}{2}\zeta_0^{-1/2}(0)\tilde{B}^{\mathrm{TR}}_{t_0}(s)\right| \ge \delta\} = 0$$

$$\lim_{\varepsilon\downarrow 0} \mathbb{P}\{\sup_{|s|\le T} \left|p^{\mathrm{TR}}_{\mathrm{ref}}(0, t_0 + \varepsilon s) - \tfrac{1}{2}\zeta_0^{1/2}(0)\tilde{B}^{\mathrm{TR}}_{t_0}(s)\right| \ge \delta\} = 0$$

where the time-reversed reflection signal has the deterministic form $\tilde{B}^{\mathrm{TR}}_{t_0}(s)$ defined through equations (3.4.13)–(3.4.16).

There is an obvious relation of this self-averaging time-reversed reflection and the limiting coherent time-reversed reflected signal (3.3.5), namely under the assumption $\gamma_{\delta m}(z) = 0$ we have that

$$\tilde{B}^{\mathrm{TR}}_{t_0}(s) = \langle B^{\mathrm{TR}}_{t_0}\rangle(s).$$

The case of a uniform random medium with strong fluctuations is very illustrative, since we can obtain simple expressions. Actually, when the cutoff function $G_{t_0} = \mathbf{1}_{[0,t_0]}$ (the indicator function of $[0, t_0]$) we get explicit formulas for the convolution kernel

$$\widehat{\tilde{K}^{\mathrm{TR}}_{t_0}}(\omega) = \frac{\tanh(2\sqrt{\alpha_0(1+\alpha_0)}\gamma_n\omega^2 t_0)}{2\sqrt{\alpha_0(1+\alpha_0)} + (1+2\alpha_0)\tanh(2\sqrt{\alpha_0(1+\alpha_0)}\gamma_n\omega^2 t_0)}$$

where $\alpha_0 = \frac{\gamma_{\delta n}}{4\gamma_n}$. Note the analogy with the equation (3.3.6) for the averaging convolution kernel. Furthermore, when we perform a total record experiment (i.e. $t_0 \to +\infty$) the convolution kernel becomes $(\sqrt{1+\alpha_0}+\sqrt{\alpha_0})^{-2}\delta(t)$ and the time reversal recovers an scaled version of the initial incident pulse.

3.5 Conclusions

In this chapter, we have analyzed how perturbations of a randomly layered half-space affect the outcome of a time reversal experiment. We presented an asymptotic theory that generalizes the analysis of the case where no perturbations of the medium occur. Under the hypothesis of independent perturbations we show that the time-reversed reflections still have a coherent structure. For a uniform random medium, we studied the coherently refocused pulse (averaged over media realizations), showed its connection with the initial pulse. We also gave bounds for the recovered energy. Furthermore, we characterized the refocused pulse as a stochastic process.

It is remarkable that the probability distribution of the limiting refocused pulse depends on the asymptotic behavior of the solution of an Itô stochastic partial differential equation driven by a single one-dimensional Brownian Motion, whose coefficients are connected with simple statistics of the random medium fluctuations and perturbations. This is an important difference in comparison with the standard time reversal theory where the refocused pulse is a deterministic object. This is known as statistical stabilization. Consequently, the statistical stabilization property is killed by the perturbations. However, for a certain class of perturbations one has statistical stabilization, since the above mentioned stochastic partial differential equation, under certain conditions, becomes deterministic.

It is worth noting that for a uniform random medium we arrived at explicit expressions for characterizing the coherently refocused pulse, which allows a better understanding of the phenomenon. Moreover, this will be specially useful for corroborating our theory by performing numerical experiments. These observations are the basis for the numerical experiments to be presented in the next chapter.

Chapter 4

Numerical study of time reversal refocusing

4.1 Introduction

This chapter is concerned with the numerical study of time reversal. Our aim is to show the agreement of the numerical results and the asymptotics developed in the previous chapter. Moreover, other features of the propagation of waves in a highly heterogeneous medium such as localization effects and the O'Doherty-Anstey approximation, are also illustrated.

The exposition is organized as follow. In section 4.2 the basic equations for one-dimensional acoustic are recast in a lagrangian formulation. Some numerical schemes that take advantage of the lagrangian formulation are derived in section 4.3 and the analogy with a discrete Goupillaud medium is remarked. The results of some numerical tests are presented in section 4.4, showing a noticeable agreement with the theory developed in chapter 3. Finally, section 4.5 is dedicated to present the concluding remarks of this chapter.

4.2 Lagrangian formulation of the one-dimensional acoustic equations

Recall that the governing equations for waves propagating through a one-dimensional acoustic medium are given by (2.2.1). We shall re-write this equations in a form more suitable for the treatment of reflection-transmission problems by following [18].

The 'local' acoustic sound speed, i.e. the speed of propagation of small disturbances in the medium, is given by

$$c(z) = \sqrt{\frac{\kappa(z)}{\varrho(z)}}. \tag{4.2.1}$$

By introducing as a new 'spatial' coordinate the travel time from the origin

$$x = \int_0^z \frac{ds}{c(s)}, \tag{4.2.2}$$

we can recast the equations (2.2.1) in the form:

$$\begin{cases} \zeta(x)\dfrac{\partial}{\partial t}u(x,t) + \dfrac{\partial}{\partial x}p(x,t) = 0 \\ \dfrac{\partial}{\partial t}p(x,t) + \zeta(x)\dfrac{\partial}{\partial x}u(x,t) = 0 \end{cases} \tag{4.2.3}$$

where $\zeta(x)$ is the 'local' acoustic impedance of the medium defined as

$$\zeta(x) = \sqrt{\varrho(x)\kappa(x)}.$$

Remark 4.2.1. It should be noted that the 'local' sound speed and acoustic impedance introduced above also take into account the heterogeneities of the medium at the micro-scale level, i.e. the random fluctuations. In contrast, the definitions given by (2.2.5) correspond to the sound speed and impedance of the effective or 'locally' homogenized medium (the underlying background medium) and consequently are independent of the random fluctuations.

After the change of variable (4.2.2) the characteristic curves for the system (4.2.3) take the simple form:

$$C^{\pm} : \frac{\mathrm{d}x}{\mathrm{d}t} = \pm 1. \tag{4.2.4}$$

Moreover, in the homogeneous case where $\zeta(x) = \text{const}$, one has the Riemann invariants:

$$\begin{cases} D = \zeta^{\frac{1}{2}}u + \zeta^{-\frac{1}{2}}p \\ U = -\zeta^{\frac{1}{2}}u + \zeta^{-\frac{1}{2}}p \end{cases} \tag{4.2.5}$$

representing down- and up-going waves respectively [18, 73]. Furthermore, when the medium is heterogeneous by defining new variables through the 'frozen Riemann invariants' given by (4.2.5) (after substitution in (4.2.3)) we obtain the new equations:

$$\begin{cases} (\partial_t + \partial_x)D = -rU \\ (\partial_t - \partial_x)U = rD \end{cases} \tag{4.2.6}$$

with the reflectivity coefficient

$$r(x) = \frac{\zeta'(x)}{2\zeta(x)} = \tfrac{1}{2}(\log \zeta(x))' = \frac{(\zeta(x)^{1/2})'}{\zeta(x)^{1/2}}. \tag{4.2.7}$$

Recall that the conservation of mechanical energy is an important feature concerning acoustic waves propagation. Namely, for the solutions of (2.2.1) one has

$$E(t) = \tfrac{1}{2} \int (\rho u^2 + \frac{1}{\kappa}p^2)\mathrm{d}z = \text{const} \tag{4.2.8}$$

and according with the transformations introduced above, in the new variables it reads:

$$E(t) = \tfrac{1}{4} \int (D^2 + U^2)\mathrm{d}x = \text{const}. \tag{4.2.9}$$

Thus in the new variables the energy norm coincides with the L^2-norm of the 'invariants'.

Remark 4.2.2. Note that after these transformations the acoustic equations take a simple form, in which two main effects are apparent: transport along characteristics and scattering by the heterogeneities. More exactly, each 'frozen Riemann invariant' is transported along the corresponding characteristic while the interaction with the heterogeneities transfers energy from one 'invariant' to the other.

4.3 Numerical methods

We shall develop numerical schemes for the solution of the system (2.2.1), basing our analysis on the equivalent equations (4.2.6) formulated in terms of the down- and up-travelling waves that are more suitable for the study of reflection-transmission problems. Furthermore, in case one is interested in the velocity and pressure wave fields, since the transformation (2.2.9) can be easily inverted, these quantities can be readily computed. Concerning the change of variable (4.2.2) note that it can be carried out accurately by applying an appropriate integration method. Nevertheless, for simplicity we consider that this coordinate change has been exactly performed.

4.3.1 Lagrangian schemes

The lagrangian approach in the computation of highly oscillatory solutions to hyperbolic differential equations has been successfully used. An important reason for this, is its ability to perform the correct advection of high frequency modes, eliminating one of the main sources of problems in the discretizations of the equations [22, 24]. We shall follow this approach for the discretization of (4.2.6).

Let us consider the grid $\{(x_j, t_n),\ j \in \mathbf{Z},\ n \in \mathbf{Z}_+\}$ with $\Delta x = \Delta t = h$ and use the representation

$$D_j^n = D(x_j, t_n) \quad \text{and} \quad U_j^n = U(x_j, t_n)$$

where $(x_j, t_n) = (jh, nh)$.

We approximate equation (4.2.6) at the midpoints $(x_{j-1/2}, t_{n+1/2})$ of the grid (see figure 4.1). The transport operators $\partial_t \pm \partial_x$ are discretized by considering them as directional derivatives along the characteristics $C^{\pm}$ respectively, using a central difference approximation. In the right hand side the unknowns D, U are approximated by averaging along the characteristics $C^{\pm}$, respectively, and the reflectivity coefficient (4.2.7) using a finite difference approximate derivative supported on the space mesh

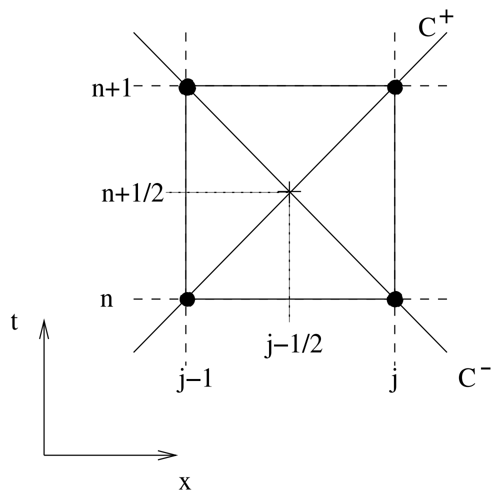

Figure 4.1: Characteristic curves and grid.

points. After some manipulations we finally obtain:

$$\begin{cases} \dfrac{D_j^{n+1} - D_{j-1}^n}{h} & = -\tilde{r}_{j-1/2}\Big(\dfrac{U_{j-1}^{n+1} + U_j^n}{2}\Big) \\ \dfrac{U_{j-1}^{n+1} - U_j^n}{h} & = \tilde{r}_{j-1/2}\Big(\dfrac{D_j^{n+1} + D_{j-1}^n}{2}\Big) \end{cases} \tag{4.3.1}$$

where $\tilde{r}_{j-1/2}$ represents the approximate reflectivity coefficient. For instance, we can use one of the following approximations:

$$\tilde{r}_{j-1/2} = \frac{1}{2h}\log\Big(\frac{\zeta_j}{\zeta_{j-1}}\Big) \tag{4.3.2}$$

or

$$\tilde{r}_{j-1/2} = \frac{2}{h}\Big(\frac{\zeta_j^{1/2} - \zeta_{j-1}^{1/2}}{\zeta_j^{1/2} + \zeta_{j-1}^{1/2}}\Big) \tag{4.3.3}$$

that formally lead to second-order numerical schemes.

Rearranging we get a set of reflection-transmission cell problems:

$$\begin{pmatrix} D_j^{n+1} \\ U_{j-1}^{n+1} \end{pmatrix} = \begin{pmatrix} \tilde{\tau}_{j-1/2} & -\tilde{\sigma}_{j-1/2} \\ \tilde{\sigma}_{j-1/2} & \tilde{\tau}_{j-1/2} \end{pmatrix} \begin{pmatrix} D_{j-1}^n \\ U_j^n \end{pmatrix} \tag{4.3.4}$$

where

$$\tilde{\sigma}_{j-1/2} = \frac{h^2 \tilde{r}_{j-1/2}^2}{1 + \frac{h^2}{4}\tilde{r}_{j-1/2}^2} \quad \text{and} \quad \tilde{\tau}_{j-1/2} = \frac{1 - \frac{h^2}{4}\tilde{r}_{j-1/2}^2}{1 + \frac{h^2}{4}\tilde{r}_{j-1/2}^2},$$

are the reflection and transmission coefficients of the cell centered at $x_{j-1/2}$, respectively, and the matrix above defines the reflection-transmission matrix for this cell.

Since these matrices are orthogonal we obtain the following discrete analog for the energy conservation law (4.2.9)

$$\frac{\Delta x}{4} \sum_{j \in \mathbf{Z}} \Big((D_j^{n+1})^2 + (U_j^{n+1})^2 \Big) = \frac{\Delta x}{4} \sum_{j \in \mathbf{Z}} \Big((D_j^{n})^2 + (U_j^{n})^2 \Big). \tag{4.3.5}$$

This ensures that the presented schemes are conservative and stable in the L^2-norm, so their convergence follows.

Remark 4.3.1. We point out that since we deal with rapidly varying acoustic media and high frequency wave fields (cf. (2.2.4)) the consistency-accuracy analysis imposes very restrictive conditions on the mesh size, namely $h = o(\lambda)$ where λ is the typical wavelength [23].

Remark 4.3.2. Other important remark that should be stressed is the analogy of the reflection-transmission cell problems above with the equations for a Goupillaud acoustic medium (D.2) (see appendix D). Moreover, using the approximation (4.3.3), the reflection-transmission matrices of the scheme and the Goupillaud medium are the same, and in this case the numerical scheme can be interpreted as an approximation of the acoustic medium by a Goupillaud one.

4.3.2 Operator splitting scheme

System (4.2.6) can be re-written in the following form:

$$\partial_t \mathbf{a} = \mathbf{H}(x, \partial_x)\mathbf{a} \tag{4.3.6}$$

where

$$\mathbf{a} = \begin{pmatrix} D \\ U \end{pmatrix} \quad \text{and} \quad \mathbf{H}(x, \partial_x) = \begin{pmatrix} -\partial_x & -r(x) \\ r(x) & \partial_x \end{pmatrix}. \tag{4.3.7}$$

The differential operator $\mathbf{H}$ can be decomposed into a sum of the constant-coefficient diagonal hyperbolic operator $\mathbf{H_0}$ and the multiplicative operator $\mathbf{M}$ defined as

$$\mathbf{H_0}(\partial_x) = \begin{pmatrix} -\partial_x & 0 \\ 0 & \partial_x \end{pmatrix} \quad \text{and} \quad \mathbf{M}(x) = \begin{pmatrix} 0 & -r(x) \\ r(x) & 0 \end{pmatrix}, \tag{4.3.8}$$

with associated evolutionary equations

$$\partial_t \mathbf{a} = \mathbf{H_0}\mathbf{a} \qquad \text{and} \qquad \partial_t \mathbf{a} = \mathbf{M}\mathbf{a}, \tag{4.3.9}$$

respectively. We assume that $r(x)$ and its derivatives are sufficiently regular. Then the corresponding solution operators $\mathcal{H}_0$ and $\mathcal{M}$ are unitary by the Stone's theorem [58]. Their computation is straightforward and we get

$$\begin{aligned} \mathcal{H}_0(t) \begin{pmatrix} D^0(x) \\ U^0(x) \end{pmatrix} &= \begin{pmatrix} D^0(x-t) \\ U^0(x+t) \end{pmatrix}, \\ \mathcal{M}(t) \begin{pmatrix} D^0(x) \\ U^0(x) \end{pmatrix} &= \begin{pmatrix} \cos(r(x)t) & -\sin(r(x)t) \\ \sin(r(x)t) & \cos(r(x)t) \end{pmatrix} \begin{pmatrix} D^0(x) \\ U^0(x) \end{pmatrix}. \end{aligned}$$

Introducing a time discretization with time step Δt and using the Strang splitting [68], we obtain the semi-discrete conservative scheme

$$\mathbf{a}^{n+1}(x) = \mathcal{H}_0(\tfrac{\Delta t}{2})\mathcal{M}(\Delta t)\mathcal{H}_0(\tfrac{\Delta t}{2})\mathbf{a}^n(x) \tag{4.3.10}$$

which for initial data sufficiently regular is formally second order accurate in time and exact in space. More general, if $r(x)$ is continuous and bounded then the scheme is consistent and its convergence in the L^2-norm follows.

However, in applications we use a full discretization introducing the spatial mesh $\{x_j = j\Delta x | \, j \in \mathbf{Z}\}$ and approximate values $\tilde{r}(x)$ for the reflectivity coefficient. From this, we obtain the approximate solution operator $\tilde{\mathcal{M}}$ and after replacing it in (4.3.10) we get the scheme

$$\mathbf{a}^{n+1}(x_j) = \mathcal{H}_0(\tfrac{\Delta t}{2})\tilde{\mathcal{M}}(\Delta t)\mathcal{H}_0(\tfrac{\Delta t}{2})\mathbf{a}^n(x_j). \tag{4.3.11}$$

This scheme is also conservative, but inherits truncation errors from the space discretization. For instance, using a central difference approximation for the reflectivity coefficient it becomes second order in space and time. By using a time step $\Delta t = \Delta x$ we avoid the introduction of interpolation errors and after some rearranging the scheme is re-written as:

$$\begin{pmatrix} D_j^{n+1} \\ U_{j-1}^{n+1} \end{pmatrix} = \begin{pmatrix} \cos(\tilde{r}_{j-1/2}\Delta t) & -\sin(\tilde{r}_{j-1/2}\Delta t) \\ \sin(\tilde{r}_{j-1/2}\Delta t) & \cos(\tilde{r}_{j-1/2}\Delta t) \end{pmatrix} \begin{pmatrix} D_{j-1}^{n} \\ U_j^{n} \end{pmatrix}. \tag{4.3.12}$$

Again a set of reflection-transmission problems arises with the corresponding reflection-transmission matrix for each cell given above. Moreover, using a second order Padé approximation for $\cos(\tilde{r}_{j-1/2}\Delta t)$ and $\sin(\tilde{r}_{j-1/2}\Delta t)$ we obtain the scheme (4.3.4).

4.4 Time-reversal experiments

In this section we describe how the forward and time-reversal experiments were performed. The numerical results illustrate some features of wave propagation through a highly heterogeneous medium and the refocusing of time-reversed reflections in the standard and generalized setting, in the regime of strong fluctuations.

The numerical experiments take advantage of the presented lagrangian framework through a complete control of the down- and up-travelling waves. More exactly, the experiments are conducted as follows:

1. a pulse-shaped wave impinges upon a random medium from a homogeneous half-space and the wave reflected at the interface is recorded as a time signal

2. this scattered signal is time-reversed and re-entered into the medium by considering it as a time dependent boundary condition.

Moreover, since we shall compute the approximate solution for finite time, from the hyperbolicity of the equations follows that one needs only to consider a slab from the heterogeneous half-space. After that the computational domain is obtained by surrounding the heterogeneous slab of interest by a homogeneous region in which we can exactly manage the radiation boundary conditions.

An equivalent procedure frequently used consists of capturing a spatial segment of the reflected wave field travelling upward in the homogeneous half-space at a particular time instant; 'freezing' this piece, and sending it back into the heterogeneous medium by considering it as an initial condition after inverting the velocity direction.

In our approach the size of the computational domain is almost the same as the random slab independently of the recording time which can be as long as we wish. However in the alternative procedure outlined above the computational domain should increase its size along with the recording time in order to place the 'frozen' wave field.

4.4.1 Random media, scaling and discretization

As stated before in the numerical experiments we only need to consider a random slab. Let the heterogeneities be localized in the interval $[z_I, z_F]$, $0 < z_I < z_F$ and $L = z_F - z_I$ is the random slab length. Concerning the medium properties for simplicity, we take a uniform background with $\varrho_0 = 1$ and $\kappa_0 = 1$ and only allow fluctuations of the density. More specifically, we define the fluctuations of the density by setting $\eta(z_j) = \sigma Y_j^{(1)}$ at the points $z_j = z_I + j\varepsilon$, $j = 0, \ldots, J = [\frac{L}{\varepsilon}]$ and extending by linear interpolation to the whole random slab; where we have introduced a small parameter ε and $[x]$ represents the integer part of x. Moreover, $\{Y_j^{(1)}\}_{j=1,\ldots,J}$ is a sequence of independent identically distributed (i.i.d.) random variables, in fact they are obtained by a pseudo-random number generator using a uniform distribution over $[-1, 1]$ and $\sigma < 1$ is a constant that controls the random fluctuations' strength. Note that the fluctuations correlation length will be of order $O(\varepsilon)$.

For modelling the perturbed medium an independent sequence of i.i.d. random variables $\{Y_j^{(2)}\}_{j=1,\ldots,J}$ uniformly distributed over $[-1, 1]$ is generated, we set $\delta\eta(z_j) = p\sigma Y_j^{(2)}$ and extend it as before to the whole slab by linear interpolation. The parameter p represents the relative random media mismatch introduced by the perturbation and its value is restricted by the inequality $\sigma(p + 1) < 1$, furthermore it is related to the perturbation intensity through the relation $\alpha = \frac{3}{4}p^2$. In all the experiments we have chosen $\sigma = 0.6$ allowing us to introduce perturbations with a mismatch over 50%.

We consider as an impinging pulse the scaled derivative of a Gaussian:

$$D_0(z) = -2a(z - z_0)\mathrm{e}^{-\frac{(z-z_0)^2}{2c^2}} \quad \text{and} \quad U_0(z) = 0. \tag{4.4.1}$$

The choice $a = 7$ and $c^2 = 0.05$ gives roughly a unit amplitude acoustic pulse effectively supported on the interval $(z_0 - 0.5, z_0 + 0.5)$. This ensures that the inhomogeneity correlation length to typical pulse wavelength ratio is of $O(\varepsilon)$. Moreover, when the ratio of the typical wavelength to propagation distance is $O(\varepsilon)$, i.e. for propagation distance $O(\frac{1}{\varepsilon})$, the situation corresponds to the strong fluctuations regime. Actually, in the new variables t', z' defined by $t = \frac{t'}{\varepsilon}$ and $t = \frac{z'}{\varepsilon}$, one has the scaling associated to this regime.

Recall that to perform the numerical experiments, using the schemes presented in the previous section, one needs to apply the change of coordinate (4.2.2). More exactly, let us introduce a discretization of the x-domain: $x_k = kh$, $k = 0, \ldots, K$ with mesh size h. Consequently, one needs the medium properties at these mesh points, in our case $\varrho_k = \varrho(z_k)$ where z_k maps to x_k under the transformation (4.2.2). In other words, for determining ϱ_k one needs to perform the inverse map $x \mapsto z$ at the mesh points x_k. In practice, we just find approximated values $\tilde{z}_k$ and set $\varrho_k = \varrho(\tilde{z}_k) \approx \varrho(z_k)$.

The inverse map approximation is performed as follows. Let us introduce a fine mesh $\bar{z}_l = l\varepsilon_1$, $l = 0, \ldots, N$ in the z-domain with $\varepsilon_1 \ll \varepsilon$, and analytically compute its image $\bar{x}_l$, $l = 0, \ldots, N$ under the transformation (4.2.2). Further by interpolating the data $(\bar{x}_l, \bar{z}_l)$ at the points $x_k = kh$, $k = 0, \ldots, K$ one gets the corresponding approximates values $\tilde{z}_k$, $k = 0, \ldots, K$ for the inverse map. The whole approximation procedure appears to be very robust with respect to different methods of interpolation when the mesh $\bar{z}_l$, $l = 0, \ldots, N$ is sufficiently fine.

Concerning the mesh size h, a choice of 5-10 mesh points per layer gives excellent results. This is in agreement with the remarks on the numerical experiments presented in [4]. In [31] a spatial discretization with mesh size equal ε also produced very good results. The heuristic reasoning below can help us understand why the choice $h = c_1\varepsilon$, with a constant $c_1 < 1$, give us accurate results despite the fact that the conditions imposed by a classical consistency-accuracy analysis (see [23]) are not fulfilled. for waves with wavelength comparable to the layers size but sufficient to.

Recall that according to the homogenization theory, for distances of the order of several typical wavelengths the pulse shape effectively does not change nor reflection is generated [3], thus a discretization that resolves the initial pulse is enough for a good representation of the effectively transmitted wave. In the other extreme for long propagation distances the pulse attenuates and spreads out as predicted by the O'Doherty-Anstey theory [3, 50, 67], so again there is no need to increase resolution to capture the transmitted wave front. Additionally a lot of energy is transferred to the coda and reflected back. More specifically, the power spectrum of the scattered wave at the interface has a maximum expected spectral power at the frequency $\tilde{\omega} = \frac{1}{\sqrt{\gamma_n t}}$ (in the frequency domain associated with the initial signal time-scale) [3, 65, 72] which is $O(1)$. Therefore properly resolving the initial pulse warrants a good resolution of the scattered signal at the interface. Moreover, when $h = c_1\varepsilon$ also the typical sub-wavelength scale reflected waves mainly associated with high-order multiple scattering are well resolved.

4.4.2 Forward propagation and standard time reversal

In all the experiments that follows we take $\varepsilon = 0.1$ and a mesh size $h = 0.01$. The heterogeneous slab extends from $z_I = 5$ and has a length L (i.e. $z_F = L + 5$) that will change in the different experiments. The cutoff function for the time-reversal mirror is the indicator of the time interval $[0, t_0]$ and generally we take $t_0 \approx L$.

Complete refocusing and localization

In our first test an heterogeneous slab of length $L = 405$ was used, and the time reversal procedure ran up to $t_0 = 500$. Figure 4.2 shows the forward experiment. At the bottom the incident pulse is plotted (a derivative of a Gaussian). Above are snapshots of the propagated pulse at different times are shown. In the plots corresponding to time $t = 125, 250$ and 375, one sees that the transmitted pulse is clearly subjected to the attenuation and spreading effects predicted by the O'Doherty-Anstey approximation. The plot at the top ($t = 500$) shows that the pulse left the computational domain without generating any reflected wave, demonstrating that the radiation conditions are correctly implemented.

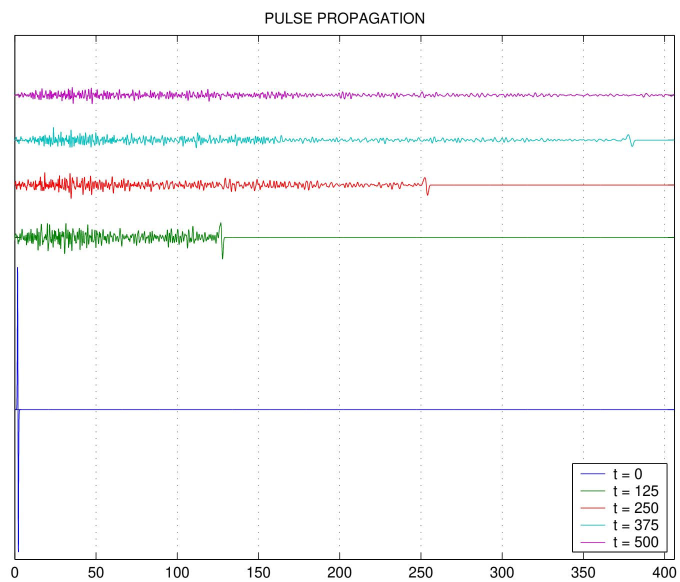

Figure 4.2: The direct experiment and the O'Doherty-Anstey approximation. Propagated pulse for different times, from bottom up $t = 0$, 125, 250, 375 and 500.

In figure 4.3, we show the back-propagation of the time-reversed signal for different times. Note the noisy propagating waves corresponding to time $t = 125$, 250 and 375, and the refocused pulse at the top trace generated by the recompression of the incoherent signal. Furthermore, one sees that the waves penetrating into the random slab stay localized at the left extreme as predicted by the localization theory. Actually, the scattered signal at the interface obtained in the forward propagation experiment contains mainly high-frequency waves early on, and as time goes on the frequency content is gradually shifted to low frequencies but effectively stays apart from zero.

Therefore when this signal is time-reversed and re-emitted back the low-frequency waves interact first and stay localized, later on high-frequency waves gradually impinge upon the random medium and penetrate into it. Eventually, all the dynamics occurs in a localized region at the left extreme of the random slab until the generation of the recompressed pulse.

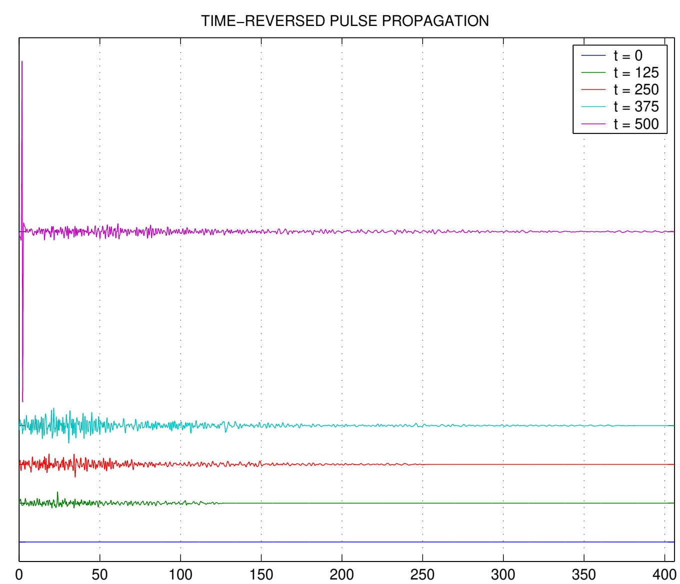

Figure 4.3: Localization in the time-reversal experiment. Time-reversed and back-propagated pulse for different times, from bottom up $t = 0$, 125, 250, 375 and 500. Note the refocused pulse, at the top trace, generated by the recompression of the incoming incoherent signal.

Our second test is aimed to a more detailed presentation of the refocusing effect. We perform two experiments for an heterogeneous slab with $L = 405$ and $t_0 = 410, 820$ respectively. In figure 4.4 we show the refocused and the initial pulses. Note that as stated in remark 3.3.1 as t_0 increases the refocused pulse shape becomes closer to the initial one. Our experiments show an effectively complete refocusing, which leads to a sharp reconstruction of the initial pulse shape. Moreover, doubling the recording time does not increase too much the accuracy of the recovered pulse.

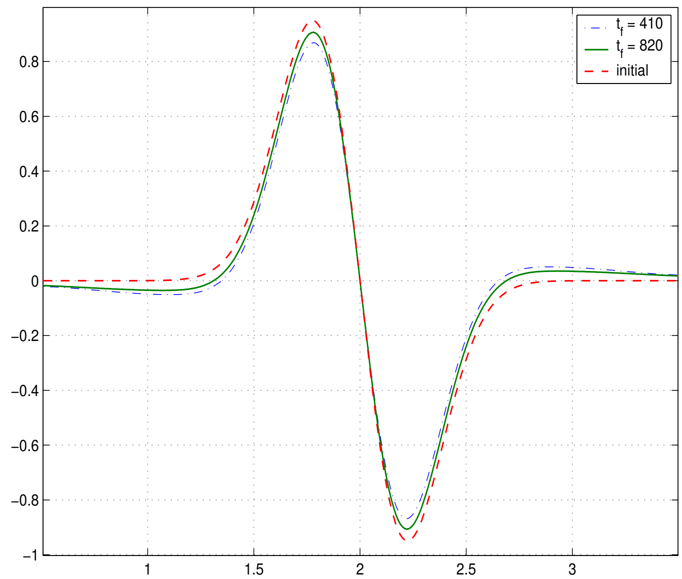

Figure 4.4: Initial (dashed line) and refocused pulses for $t_0 = 410$ (dashed-dotted line) and $t_0 = 820$ (solid line). Note that the initial pulse shape is accurately recovered.

Refocused pulse stabilization

In the next experiments we set $t_0 = 70$ and $L = 50$ and demonstrate the statistical stabilization property (self-averaging) of the refocused pulse. The resulting refocused pulses for 10 realizations of the heterogeneous slab are shown in figure 4.5. It is apparent that, with a high accuracy, the refocused pulse shape is independent of the medium realization. This is in complete agreement with the statistical stabilization property, and the observed disordered reflections about the pulse and variations of the pulse amplitude reflects the fact that we have a finite ε. It should be noted that the pulse center positions agree with the high accuracy. In the present case they are totally correct, since the pulse symmetry is also valid for $\varepsilon \neq 0$ (cf. equation (3.3.4)).

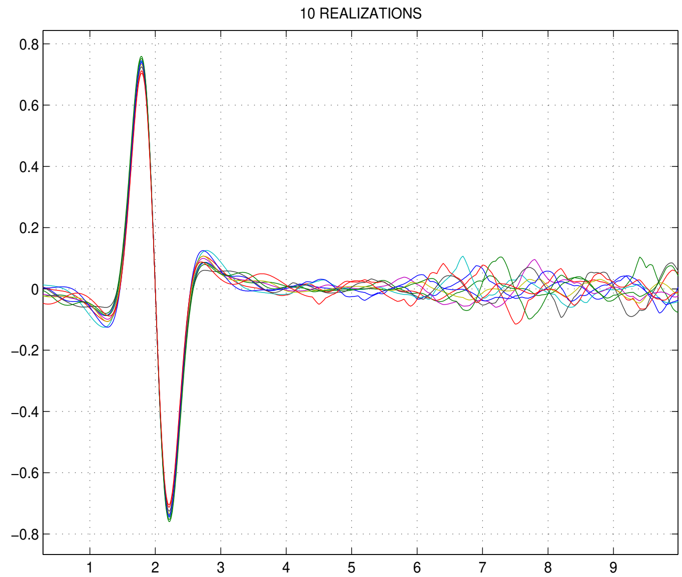

Figure 4.5: Self-averaging of the refocused pulses over 10 realizations of the medium.

Wave train refocusing

In this experiment the refocusing of a wave train is demonstrated. We use a heterogeneous slab of length $L = 200$ in a computational mesh from $z_I = 0$ to $z_F = 202$, set $t_0 = t_1 = 485$, and perform the time reversal procedure recording the reflected wave as a time signal at the left extreme. Note that we do not need to allocate the reflected and refocused signals on the computational mesh, thus the numerical experiment is performed in an efficient way.

In figure 4.6 (from top to bottom) the initial wave train, reflected signal and refocused wave train are shown. It is apparent that the refocused signal is a reduced copy of the initial wave train in which each pulse of the wave train is sharply identified. We draw attention to the reflected signal, it is very noisy but has a clear large time-scale modulation. This can be easily explained since for a single pulse and fixed t an expected bound of the reflected signal strength is $O(t^{-1/2})$ (see [72]) and consequently the large time modulation is associated with the function $t^{-1/2}$.

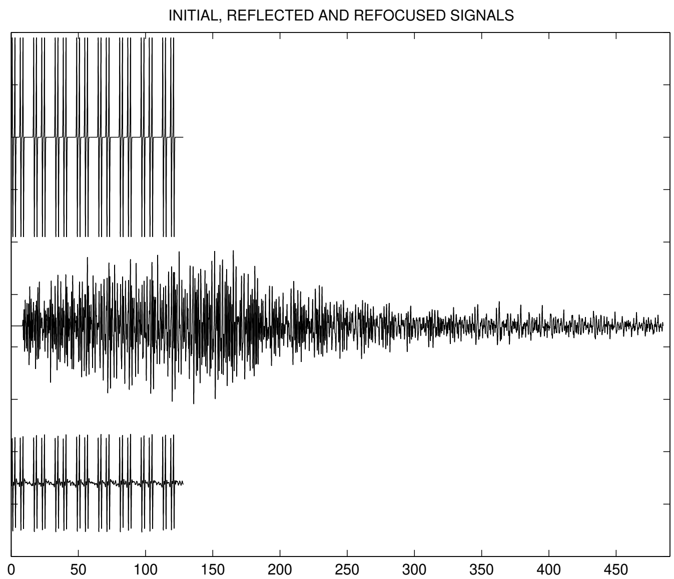

Figure 4.6: Wave train refocusing. From top to bottom the initial wave train, reflected signal and refocused wave train are shown. Note that the refocused wave train is a sharply reduced copy of the initial one.

4.4.3 Time reversal in a perturbed medium

The next numerical experiments illustrate the theory developed in chapter 3. The numerical results obtained show a qualitative behavior in full agreement with the theory. Furthermore, we perform a comparison of the coherent refocused pulses, corresponding to asymptotic theory, and numerical experiments, respectively. The former is given by expression (3.3.5) with the convolution kernel (3.3.6) and the latter is computed by applying a simple Monte Carlo simulation. The necessary statistical parameters are determined theoretically. Namely, the perturbation intensity α is related to the relative mismatch of the random media p by the expression $\alpha = \frac{3}{4}p^2$, and γ_n is obtained as in reference [31].

Small perturbations effect

In the first experiment the perturbation percentage is $p = 0.1$. In figure 4.7 we show the result for 50 generalized time reversal experiments. The refocusing is very clear. Note however, that the center of the refocused pulse is not determined with the same accuracy as in standard experiments. Moreover, the variation of the pulse amplitude is larger than in standard experiments. This is a direct consequence of the lack of statistical stabilization. In the figure 4.8, the average of the time-reversed reflection over 100 realizations is compared to the coherent refocused pulse obtained by (3.3.5) and (3.3.6), and a remarkable agreement is shown.

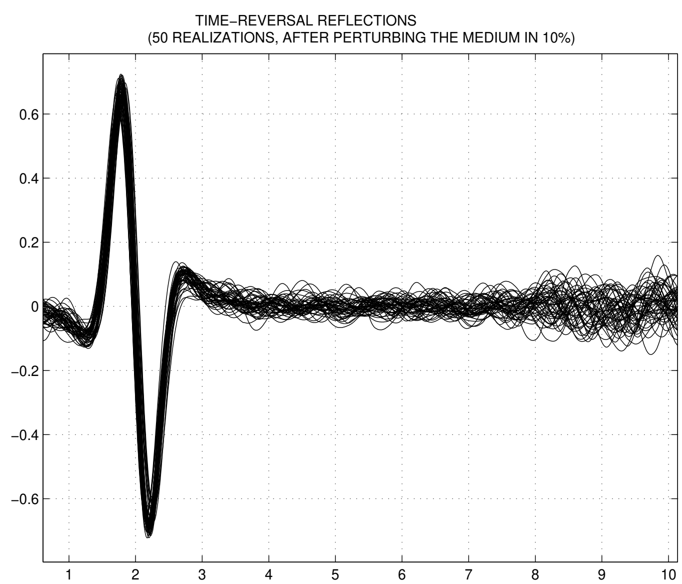

Figure 4.7: Time-reversed reflections for a medium perturbed in 10% (corresponds to a perturbation intensity $\alpha = 0.0075$). A coherent refocused pulse is clearly observed in all experiments.

Increasing the perturbation

In the second set of experiments we have increased the perturbation percentage to $p = 0.3$. For individual realizations the quality of the refocused signal has decreased,

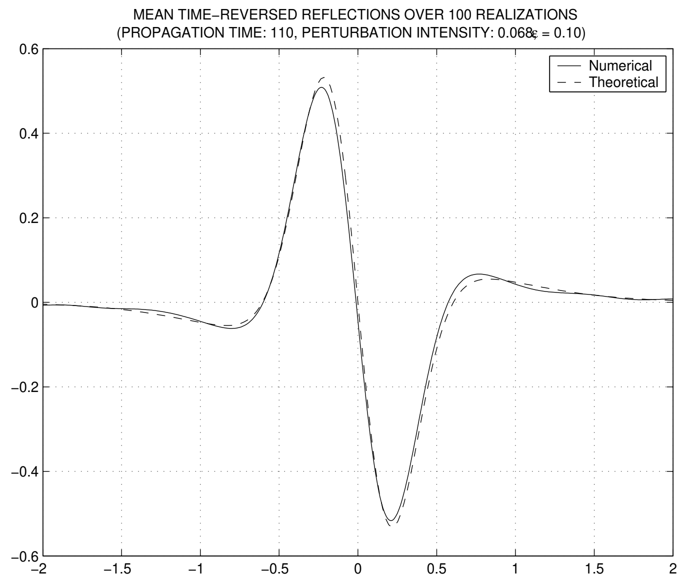

Figure 4.8: Average time-reversed reflections. Comparison with the asymptotic theory result.

the pulse looses its symmetry, presents strong amplitude variations and the refocusing center spreads out (see fig.4.9). This is a clear evidence of the statistical stabilization loss: the refocused pulse is a random function. However, a coherent structure remains visible anyway. Thus, the qualitative behavior predicted by the asymptotic theory is observed in the numerical experiments. In fig.4.10 the averaged signal, now over 40 realizations, is compared to the theoretical coherent refocused pulse and an excellent agreement is noticeable.

4.5 Conclusions

In this chapter, we have performed the numerical validation of the theory developed in the previous chapters (figures 4.7-4.10). First, we presented the numerical scheme remarking the characteristics that allow an accurate and efficient numerical study of

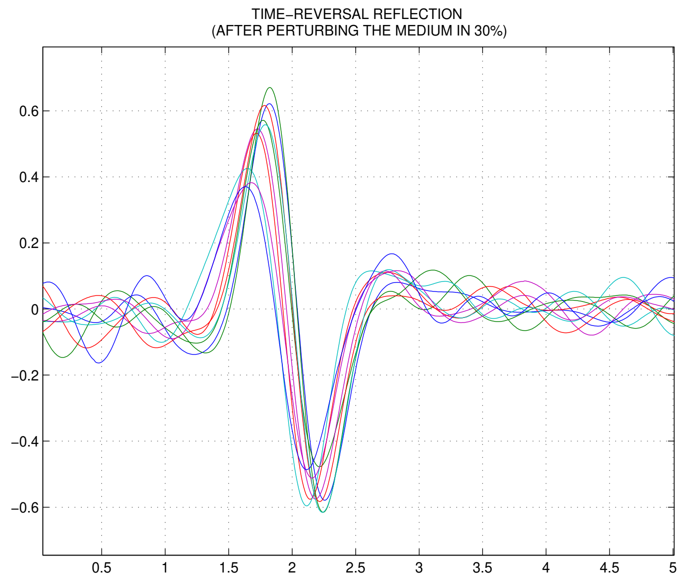

Figure 4.9: Time-reversed reflections for a medium perturbed in 30% (corresponds to a perturbation intensity $\alpha = 0.068$). We still see the coherent refocused reflections.

time reversal experiments. Namely, we show that it is related to a set of reflection-transmission cell problems and a discrete type of layered medium called a Goupillaud medium.

We performed experiments that showed different features of wave propagation in a heterogeneous medium, as the O'Doherty-Anstey approximation, the localization of waves and the standard time reversal. A complete agreement with the corresponding theories is remarkable. Concerning the generalized time reversal experiments, we validated the developed theory by showing the agreement of the numerical results with the explicit formulas obtained in the previous chapter. Moreover, the expected qualitative behavior is observed in all the experiments. The scope of the theory was tested allowing general models for the random media, a remarkable robustness of the theory is observed.

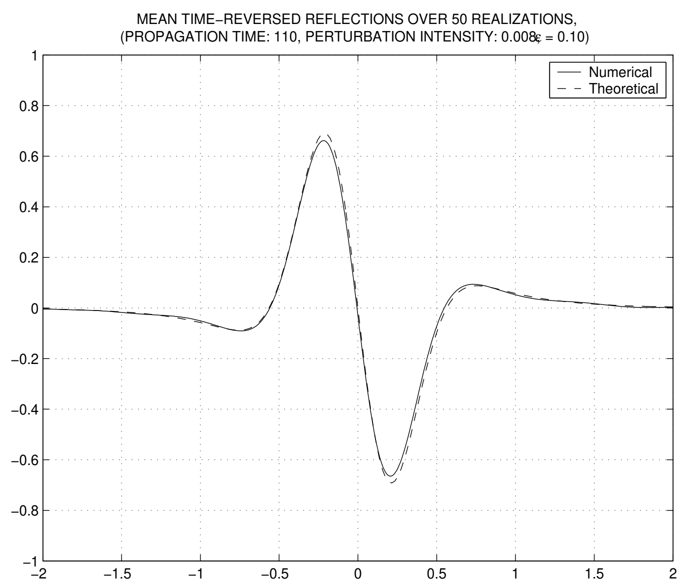

Figure 4.10: Average time-reversed reflections. Comparison with the asymptotic theory result.

Appendix A

Diffusion-approximation theorems

In this appendix we briefly review some results on the asymptotic analysis of stochastic differential equations that are used in this thesis. It is an extensively studied topic, so we shall concentrate on results and references that are the most relevant for our purpose. A self-contained and compact exposition of the subject can be found in [51]. An extensive account of the theory, along with the different techniques involved and applications are given in [46]. Some convergence theorems for stochastic equations are presented in the book [44] which generalizes the results in [39, 53, 54].

The origin of the asymptotic analysis goes back to the work of Stratonovich [69] and the theorems first proved by Khazminskii in [40]. Extensive use of asymptotics for wave propagation problems is made in Klyatskin's book [41].

Now, we formulate the fundamental theorems used in this work. They concern asymptotics of solutions of differential equations with oscillatory components that are driven by a Markov process with slowly varying parameters.

Let $\mathbf{S}$ be a compact metric space and $q(x, s)$ with values in $\mathbf{S}$ be, for each fixed x, a stationary ergodic Markov process. By ergodicity $q(x, \cdot)$ has an invariant probability measure $\mathbb{P}_x$.

Theorem A.1. *Define the* $\mathbf{R}^m$*-valued random process* $(Y^\varepsilon(x),\, x \geq 0)$ *as the solution* *of the system of differential equations*

$$\begin{cases} \dfrac{\mathrm{d}}{\mathrm{d}x} Y^\varepsilon(x) = \dfrac{1}{\varepsilon} F(Y^\varepsilon(x), x, \dfrac{\tau(x)}{\varepsilon}, q(x, \dfrac{x}{\varepsilon^2})) + G(Y^\varepsilon(x), x, \dfrac{\tau(x)}{\varepsilon}, q(x, \dfrac{x}{\varepsilon^2})) \\ \quad Y^\varepsilon(0) = y_0 \end{cases} \tag{A.1}$$

where the functions $\tau : \mathbf{R}_+ \to \mathbf{R}_+$, *and* F, G *mapping* $\mathbf{R}^m \times \mathbf{R}_+^2 \times \mathbf{S}$ *into* $\mathbf{R}^m$ *have the following properties:*

1. $\tau(0) = 0$, $\tau'(x) > 0$ *for* $0 \leq x < +\infty$

2. $F(y, x, \mu, q)$ *and* $G(y, x, \mu, q)$ *are smooth in* y *and periodic in* μ

3. F *is centered with respect to the invariant probability measure* $\mathbb{P}_x$, *i.e.*

$$\int_{\mathbf{S}} F(y, x, \mu, q) \mathbb{P}_x(\mathrm{d}q) = 0.$$

Then, if all the integrals in (A.2) *below are correctly defined, the process* $Y^\varepsilon(x)$ *converges in distribution as* $\varepsilon \downarrow 0$ *to the* m*-dimensional Markov process* $(Y(x),\ x \geq 0)$ *which admits the following infinitesimal generator:*

$$\mathcal{L}_x = \int_0^{+\infty} \langle \mathbb{E}\{F(y, x, \mu, q(x, 0)\} \cdot \nabla_y \big(F(y, x, \mu, q(x, r) \cdot \nabla_y)\big) \rangle_\mu \mathrm{d}r \\ + \langle \mathbb{E}\{G(y, x, \mu, q(x, 0))\} \cdot \nabla_y \rangle_\mu \tag{A.2}$$

where the expectation $\mathbb{E}\{\cdot\}$ *is relative to the stationary process* $q(x, \cdot)$ *and* $\langle \cdot \rangle_\mu = \lim_{\mu \to +\infty} \mu^{-1} \int_0^\mu \cdot \, \mathrm{d}\mu'$ *stands for averaging with respect to the fast phase* μ.

It should be noted that in equation (A.1) the disordered fluctuations (randomness) are varying in a faster scale than the oscillatory components, and consequently the averaging with respect to randomness and oscillations in the infinitesimal generator (A.2) are decoupled. In the next theorem we analyze the case where randomness and oscillations are varying in the same scale, as a result the averaging of these rapid fluctuations is performed in a coupled manner (cf. equation (A.3) and the expression for the infinitesimal generator (A.4) below).

Theorem A.2. *Consider the $\mathbf{R}^m$-valued random process $(Y^\varepsilon(x),\, x \geq 0)$ satisfying the system of differential equations*

$$\begin{cases} \dfrac{\mathrm{d}}{\mathrm{d}x} Y^\varepsilon(x) = \dfrac{1}{\varepsilon} F(Y^\varepsilon(x), x, \dfrac{\tau(x)}{\varepsilon^2}, q(x, \dfrac{x}{\varepsilon^2})) + G(Y^\varepsilon(x), x, \dfrac{\tau(x)}{\varepsilon^2}, q(x, \dfrac{x}{\varepsilon^2})) \\ \qquad Y^\varepsilon(0) = y_0 \end{cases} \tag{A.3}$$

where the functions τ, F and G satisfy the same assumptions of the previous theorem.

Then, if all the integrals in (A.4) *below are correctly defined, the process $Y^\varepsilon(x)$ converges in distribution as $\varepsilon \downarrow 0$ to the m-dimensional Markov process $(Y(x),\, x \geq 0)$ whose infinitesimal generator is:*

$$\mathcal{L}_x = \int_0^{+\infty} \langle \mathbb{E}\{F(y, x, \mu, q(x,0)\} \cdot \nabla_y \big(F(y, x, \mu + r\tau'(x), q(x, r)) \cdot \nabla_y \big) \rangle_\mu \mathrm{d}r \\ + \langle \mathbb{E}\{G(y, x, \mu, q(x,0))\} \cdot \nabla_y \rangle_\mu \tag{A.4}$$

For a proof see, for example, [51, section 7, pp. 142–147]. Similar results can be proved in the case where F and G satisfy some mixing conditions, see for instance [53, 54] and also [44, 46].

Appendix B

Computation of $\Lambda_{12}(t,\omega)$ in the strong fluctuations regime

In this appendix we shall compute the normalized joint correlation spectral density $\Lambda_{12}(t,\omega)$ in the case where the random medium is uniform, i.e. when $c_0(z) = c_0 =$ const., $\gamma_n(z) = \gamma_n =$ const. and $\tilde{\gamma}_{m,n}(z) = \tilde{\gamma}_{m,n} =$ const. in order to obtain the expression (2.4.26). The computation is similar to that in [16].

Recall that

$$\Lambda_{12}(t,\omega) = \frac{1}{2\pi}\int e^{-\mathrm{i}ht} u_{12}(\omega,h)\mathrm{d}h, \tag{B.1}$$

where u_{12} is obtained by solving the Kolmogorov backward equation

$$\begin{cases} \Big\{\dfrac{\partial}{\partial z} + \dfrac{2h}{c_0}\dfrac{\partial}{\partial \psi} + \dfrac{4\omega^2}{c_0}\big(\gamma_n(1-\cos\psi) + \tilde{\gamma}_{m,n}\big)\dfrac{\partial^2}{\partial\psi^2}\Big\}V = 0, \qquad \text{for } z<0 \\ V|_{z=0} = \mathrm{e}^{\mathrm{i}\psi} \end{cases}$$

and using the limiting relation

$$u_{12}(\omega,h) = \lim_{z\to-\infty} V(z,\psi,\omega,h).$$

These equations correspond to the large time behavior of the expected value of a diffusion process on the circle associated with the Itô stochastic differential equation

$$\mathrm{d}\psi_z = \frac{2h}{c_0}\mathrm{d}z + 2\omega\sqrt{\frac{2}{c_0}\big(\gamma_n(1-\cos\psi_z) + \tilde{\gamma}_{m,n}\big)}\,\mathrm{d}B_z, \tag{B.2}$$

where $z \in [-\infty, 0]$ plays the role of time and B_z is a standard one-dimensional Brownian motion beginning at $z = -\infty$. Using ergodicity we get that

$$u_{12}(\omega, h) = \int_{-\pi}^{\pi} \mathrm{e}^{\mathrm{i}\psi} p_{\omega,h}(\psi) \mathrm{d}\psi \tag{B.3}$$

where $p_{\omega,h}(\psi)$ is the invariant probability density corresponding to the diffusion process. This probability density is a 'time'-independent solution of the associated Fokker-Planck equation (the differential equation adjoint to the Kolmogorov backward equation), which after eliminating the 'time' dependence, and introducing the change of variable $\xi = \cot(\psi/2)$, becomes the ordinary differential equation

$$h\frac{\mathrm{d}}{\mathrm{d}\xi}\big((1+\xi^2)p_{\omega,h}\big) + 2\omega^2\frac{\mathrm{d}}{\mathrm{d}\xi}\Big\{(1+\xi^2)\frac{\mathrm{d}}{\mathrm{d}\xi}\big[\big(\gamma_n + \frac{\tilde{\gamma}_{m,n}}{2}(1+\xi^2)\big)p_{\omega,h}\big]\Big\} = 0.$$

By solving this equation, applying boundary conditions and normalizing to a unit mass one gets:

$$\begin{aligned} p_{\omega,h}(\xi) = \frac{\mathrm{e}^{-\frac{\beta}{\sqrt{\alpha(1+\alpha)}}\arctan(\sqrt{\frac{\alpha}{1+\alpha}}\xi)}}{\pi(1+\alpha(1+\xi^2))}\Big\{ & \frac{\beta \mathrm{e}^{\frac{\pi\beta}{2\sqrt{\alpha(1+\alpha)}}}}{2\sinh(\frac{\pi\beta}{2\sqrt{\alpha(1+\alpha)}})}\int \frac{\mathrm{e}^{\frac{\beta}{\sqrt{\alpha(1+\alpha)}}\arctan(\sqrt{\frac{\alpha}{1+\alpha}}s)}}{1+s^2}\mathrm{d}s \\ & - \beta\int_{\xi}^{+\infty}\frac{\mathrm{e}^{\frac{\beta}{\sqrt{\alpha(1+\alpha)}}\arctan(\sqrt{\frac{\alpha}{1+\alpha}}s)}}{1+s^2}\mathrm{d}s\Big\} \end{aligned} \tag{B.4}$$

where $\alpha = \frac{\tilde{\gamma}_{m,n}}{2\gamma_n}$ and $\beta = \frac{2h}{\gamma_n\omega^2}$.

From the equation above follows that $p_{\omega,-h}(\xi) = p_{\omega,h}(-\xi)$ and since

$$u_{12}(\omega, h) = \int_{-\infty}^{+\infty}\big(\frac{\xi+\mathrm{i}}{\xi-\mathrm{i}}\big)p_{\omega,h}(\xi)\mathrm{d}\xi$$

we have that $u_{12}(\omega, -h) = \overline{u_{12}(\omega, h)}$, where $\bar{x}$ represents the complex conjugate of x. Moreover, using (B.4) we can write $\overline{u_{12}(\omega, h)} = \tilde{v}^0(\omega, h) + \tilde{v}^1(\omega, h)$ with

$$\begin{aligned} \tilde{v}^0(\omega, h) = \frac{\beta \mathrm{e}^{-\frac{\pi\beta}{2\sqrt{\alpha(1+\alpha)}}}}{2\sinh(\frac{\pi\beta}{2\sqrt{\alpha(1+\alpha)}})} & \int \frac{\mathrm{e}^{-\frac{\beta}{\sqrt{\alpha(1+\alpha)}}\arctan(\sqrt{\frac{\alpha}{1+\alpha}}s)}}{1+s^2}\mathrm{d}s \\ & \times\int\big(\frac{\xi+\mathrm{i}}{\xi-\mathrm{i}}\big)\frac{\mathrm{e}^{\frac{\beta}{\sqrt{\alpha(1+\alpha)}}\arctan(\sqrt{\frac{\alpha}{1+\alpha}}\xi)}}{1+\alpha(1+\xi^2)}\mathrm{d}\xi \end{aligned}$$

and

$$\tilde{v}^1(\omega,h) \;=\; \frac{\beta}{\pi}\int (\frac{\xi+\mathrm{i}}{\xi-\mathrm{i}})\frac{\mathrm{e}^{\frac{\beta}{\sqrt{\alpha(1+\alpha)}}\arctan(\sqrt{\frac{\alpha}{1+\alpha}}\xi)}}{1+\alpha(1+\xi^2)}\Big(\int_{\xi}^{+\infty}\frac{\mathrm{e}^{-\frac{\beta}{\sqrt{\alpha(1+\alpha)}}\arctan(\sqrt{\frac{\alpha}{1+\alpha}}s)}}{1+s^2}\,\mathrm{d}s\Big)\mathrm{d}\xi.$$

From (B.1) we have that

$$\Lambda_{12}(t,\omega)=\frac{1}{\pi}\mathrm{Re}\Big\{\int_0^{+\infty}\mathrm{e}^{\mathrm{i}ht}\overline{u_{12}(\omega,h)}\mathrm{d}h\Big\}.$$

By introducing the decomposition $\Lambda_{12}(t,\omega)=\Lambda_{12}^0(t,\omega)+\Lambda_{12}^1(t,\omega)$ associated with the decomposition for $\overline{u_{12}}$ above, after some elementary transformations and changing the order of integration one gets

$$\Lambda_{12}^0(t,\omega)=\frac{2\alpha\gamma_n\omega^2}{\pi^4}\mathrm{Re}\Big\{\iint(\frac{\xi+\mathrm{i}a}{\xi-\mathrm{i}a}) \Psi^{(1)}(1+\frac{1}{\pi}\arctan s-\frac{1}{\pi}\arctan\xi-\mathrm{i}\frac{t'}{\pi})\frac{\mathrm{d}s}{s^2+a^2}\frac{\mathrm{d}\xi}{1+\xi^2}\Big\}$$

and

$$\Lambda_{12}^1(t,\omega)=\frac{\alpha\gamma_n\omega^2}{\pi^2}\iint(\frac{\xi+\mathrm{i}a}{\xi-\mathrm{i}a})\frac{1}{(\arctan s-\arctan\xi-\mathrm{i}t')^2}\frac{\mathrm{d}s}{s^2+a^2}\frac{\mathrm{d}\xi}{1+\xi^2},$$

where $a=\sqrt{\frac{\alpha}{1+\alpha}}$, $t'=2\sqrt{\alpha(1+\alpha)}\gamma_n\omega^2 t$ and $\Psi^{(1)}(\cdot)$ represents the polygamma function of order 1 (see [1] for definition and properties). Furthermore, using the properties of the polygamma function and performing some elementary transformations we have

$$\Lambda_{12}(t,\omega)=\frac{\alpha\gamma_n\omega^2}{\pi^2}\iint(\frac{\xi+\mathrm{i}a}{\xi-\mathrm{i}a})\frac{\mathrm{d}}{\mathrm{d}\xi}\cot(\arctan s-\arctan\xi-\mathrm{i}t')\frac{\mathrm{d}s}{s^2+a^2}\,\mathrm{d}\xi.$$

After integrating by parts and using the Cauchy Theorem of residues for computing the integrals, we finally get the desired result for the joint correlation spectral density:

$$\Lambda_{12}(t,\omega)=\gamma_n\omega^2\frac{1-\tanh^2(2\sqrt{\alpha(1+\alpha)}\gamma_n\omega^2 t)}{\big(1+\frac{1+2\alpha}{2\sqrt{\alpha(1+\alpha)}}\tanh(2\sqrt{\alpha(1+\alpha)}\gamma_n\omega^2 t)\big)^2} \tag{B.5}$$

where $\alpha=\frac{\tilde{\gamma}_{m,n}}{2\gamma_n}$.

Appendix C

Asymptotic behavior of the backward Itô stochastic parabolic equation

In this appendix we present some properties of the solutions of the backward stochastic differential equation (3.4.8) and their asymptotic behavior for large depth (i.e. $z \to -\infty$). This results are used in chapter 3

Recall that this backward Itô stochastic differential equation reads

$$\begin{cases} \mathrm{d}v + (\mathcal{L}^0 v)\mathrm{d}z + 2\omega\sqrt{\frac{2\gamma_{\delta m}(z)}{c_0(z)}}\,\partial_\psi v \overleftarrow{\mathrm{d}}\,\check{B}_z = 0, & \text{for } z < 0 \\ v|_{z=0} = \mathrm{e}^{\mathrm{i}\psi} \end{cases} \tag{C.1}$$

where $\overleftarrow{\mathrm{d}}\,\check{B}_z$ represents the backward Itô's differential of $\check{B}_z$. The partial differential operator $\mathcal{L}^0$ has the following form $\mathcal{L}^0 = b(z)\partial_\psi + \frac{1}{2}a(z,\psi)\partial_\psi^2$, where

$$b(z) = \frac{2h}{c_0(z)}, \qquad a(z,\psi) = \frac{8\omega^2}{c_0(z)}\{\gamma_n(z)(1-\cos\psi) + \tilde{\gamma}_{m,n}(z)\} \tag{C.2a}$$

for strong fluctuations, and

$$b(z) = 2\frac{h - \omega^2\gamma^s_{\delta n}(z,\omega)}{c_0(z)}, \quad a(z,\psi) = \frac{8\omega^2}{c_0(z)}\{\gamma^c_n(z)(1-\cos\psi) + \check{\gamma}_{m,n}(z,\omega)\} \tag{C.2b}$$

in the regime of weak fluctuations.

It is a well-known fact that under very general assumptions the solution of parabolic stochastic partial differential equations are connected with solutions of *random* parabolic partial differential equations (i.e. with random coefficients) [44]. For equation (C.1) this relation is extremely simple and it is stated in Lemma C.1.

Let us define the stochastic flows

$$\xi(z,\psi) = \psi - 2\omega \int_z^0 \sqrt{\tfrac{2\gamma_{\delta m}(s)}{c_0(s)}} \overleftarrow{\mathrm{d}}\, \check{B}_s \tag{C.3}$$

$$\tilde{\xi}(z,\psi) = \psi + 2\omega \int_z^0 \sqrt{\tfrac{2\gamma_{\delta m}(s)}{c_0(s)}} \overleftarrow{\mathrm{d}}\, \check{B}_s \tag{C.4}$$

for $z \le 0$ and represent by $\tilde{v}(z,\psi)$ the solution of the random parabolic partial differential equation

$$\begin{cases} \partial_z \tilde{v} + \{b(z)\partial_\psi + \frac{1}{2}\tilde{a}(z,\psi)\partial_\psi^2\}\tilde{v} = 0, & \text{for } z < 0 \\ \tilde{v}|_{z=0} = \mathrm{e}^{\mathrm{i}\psi}. \end{cases} \tag{C.5}$$

where the random coefficient

$$\begin{aligned} \tilde{a}(z,\psi) &= a(z,\tilde{\xi}(z,\psi)) - 8\omega^2 \frac{\gamma_{\delta m}(z)}{c_0(z)} \\ &= \frac{8\omega^2}{c_0(z)}\{\gamma_n(z)(1-\cos\tilde{\xi}(z,\psi)) + \tfrac{1}{2}\gamma_{\delta n}(z)\} \end{aligned} \tag{C.6a}$$

for strong fluctuations, and

$$= \frac{8\omega^2}{c_0(z)}\{\gamma_n^c(z)(1-\cos\tilde{\xi}(z,\psi)) + \tfrac{1}{2}\gamma_{\delta n}^c(z,\omega)\} \tag{C.6b}$$

in the regime of weak fluctuations. Note that this coefficient is in $C^{(\alpha,2)}((-\infty,0]\times\mathbf{R})$[1] almost surely with $0 \le \alpha < \frac{1}{2}$. Moreover, $\tilde{a}(z,\psi) > 0$, so (C.5) is a well posed problem almost surely [33] (it is enough that $\alpha = 0$, i.e. just continuity in all variables of the second order derivative with respect to the second variable).

[1] $C^{(\alpha,m)}((-\infty,0]\times\mathbf{R})$ denotes the space of functions continuous in all variables having derivatives up to order m with respect to the second variable which are Hölder continuous of order α in the first variable

Lemma C.1. *The solution of the stochastic partial differential equation* (C.1) *satisfies* $v(z,\psi) = \tilde{v}(z,\xi(z,\psi))$ *almost surely, where* $\tilde{v}(\cdot,\cdot)$ *is the solution of the random partial differential equation* (C.5) *and* $\xi(z,\psi)$ *is defined by* (C.4).

Proof. The proof is based on the application of the Itô-Wenttsel' formula [60] (or generalized Itô formula [44]). First we recall its formulation in the one dimensional case for backward semimartingales.

Suppose that the semimartingale defined by $\mathrm{d}u(z,x) = J(z,x)\mathrm{d}z + H(z,x) \overleftarrow{\mathrm{d}}\, \check{B}_z$ is $C^{(0,2)}((-\infty,0] \times \mathbf{R})$ almost surely and adapted to the family $\mathcal{F}_z$ of σ-algebras generated by $\check{B}_z$. Furthermore, assume that $J(z,x)$ is $C^{(0,1)}((-\infty,0]\times\mathbf{R})$ and $H(z,x)$ is $C((-\infty,0] \times \mathbf{R})$ almost surely. Suppose that $\xi(z)$ is a continuous semimartingale having the representation

$$\xi(z) = \xi_0 + \int_z^0 A(s)\mathrm{d}s + \int_z^0 B(s) \overleftarrow{\mathrm{d}}\, \check{B}_s$$

where $A(z)$ and $B(z)$ are $\mathcal{F}_z$-adapted random processes and ξ_0 is a $\mathcal{F}_0$ measurable almost surely finite random variable. Then

$$\begin{aligned} \mathrm{d}u(z,\xi(z)) = J(z,\xi(z))\,\mathrm{d}z + H(z,\xi(z)) \overleftarrow{\mathrm{d}}\, \check{B}_z + \partial_x u(z,\xi(z))\,\mathrm{d}\xi(z) \\ - \tfrac{1}{2}\partial_x^2 u(z,\xi(z))B^2(z)\,\mathrm{d}z - H(z,\xi(z))B(z)\,\mathrm{d}z. \quad \text{(C.7)} \end{aligned}$$

Let us now apply this formula. Note that as $b(z)$ is deterministic and $\tilde{a}(z,\psi)$ is $\mathcal{F}_z$-adapted for fixed ψ, $\tilde{v}(z,\psi)$ satisfies the needed assumptions where

$$J(z,\psi) = -\{b(z)\partial_\psi + \tfrac{1}{2}\tilde{a}(z,\psi)\partial_\psi^2\}\tilde{v}(z,\psi) \quad \text{and} \quad H(z,\psi) = 0 \quad \text{almost surely.}$$

Further, we take the process $\xi(z) = \xi(z,\tilde{\psi})$ with $\xi(\cdot,\cdot)$ defined by (C.4). Then after substitution in (C.7) we get

$$\begin{aligned} \mathrm{d}\tilde{v}(z,\xi(z,\tilde{\psi})) + b(z)\partial_\psi\tilde{v}(z,\xi(z,\tilde{\psi})) + \left\{\tfrac{1}{2}\tilde{a}(z,\xi(z,\tilde{\psi})) + 4\omega^2\tfrac{\gamma_{\delta m}(z)}{c_0(z)}\right\}\partial_\psi^2\tilde{v}(z,\xi(z,\tilde{\psi})) \\ + 2\omega\sqrt{\tfrac{2\gamma_{\delta m}(z)}{c_0(z)}}\,\partial_\psi\tilde{v}(z,\xi(z,\tilde{\psi}))\overleftarrow{\mathrm{d}}\, \check{B}_z = 0. \quad \text{(C.8)} \end{aligned}$$

Now noting that $\tilde{a}(z,\xi(z,\tilde{\psi})) = a(z,\tilde{\psi})$ and for $v(z,\tilde{\psi}) = \tilde{v}(z,\xi(z,\tilde{\psi}))$ one has $\partial_{\tilde{\psi}}^m v(z,\tilde{\psi}) = \partial_{\tilde{\psi}}^m \tilde{v}(z,\xi(z,\tilde{\psi}))$ we see that the above relation (C.8) resembles equation

(C.1). Furthermore, since the involved sets of zero probability measure are independent of ψ, it is clear that $v(z, \tilde{\psi})$ satisfies the backward stochastic parabolic partial differential equation (C.1) for every ψ. $\square$

As an application of the proved Lemma we will establish an assertion on the asymptotic behavior of the solution of equation (C.1). Namely, we have the following result.

Lemma C.2. *Let $v(z, \psi, \omega, h)$ be the solution of the stochastic partial differential equation* (C.1) *with $\omega \neq 0$. Further suppose that the coefficients $b(z)$, $\tilde{a}(z, \psi)$ given by* (C.2) *and* (C.6) *respectively, are bounded and that $\frac{\gamma_{\delta n}(z)}{c_0(z)} \geq \beta_0 > 0$, for $z \leq 0$ in the case of strong fluctuations (or $\frac{\gamma^c_{\delta n}(z,\omega)}{c_0(z)} \geq \beta_1(\omega) > 0$, for $z \leq 0$, $\omega \neq 0$ in the regime of weak fluctuations). Then there exists a complex valued random field v_0 on $\Pi = \{(\omega, h) \in \mathbf{R}^2 | \omega \neq 0\}$ such that $v(z, \psi, \omega, h)$ converges to $v_0(\omega, h)$ almost surely as $z \to -\infty$ on Π.*

Proof. Suppose that $\omega \neq 0$, h are fixed. We notice that $\tilde{v}(z, \psi)$ (the solution of equation (C.5)) can be defined in all the probability space but excluding a set of zero probability measure. Further from the results in [35] one knows that at each fixed point of the probability space $\tilde{v}(z, \psi)$ converges to μ as $z \to -\infty$ uniformly in $\psi \in \mathbf{R}/2\pi\mathbf{Z}$, consequently we have that $\lim_{z \to -\infty} v(z, \psi) = \lim_{z \to -\infty} \tilde{v}(z, \xi(z, \psi)) = \mu$. Moreover, since the excluded sets with zero probability measure do not depend on $\omega \neq 0$, h, the statement of the Lemma follows. $\square$

Appendix D

The Goupillaud layered medium

Due to the analogy of the proposed numerical schemes and the reflection-transmission relations for a Goupillaud layered medium mentioned in section 4.3, in this appendix we will make a brief description of the so-called Goupillaud layered medium (see [18] and references within). A Goupillaud acoustic medium is characterized by piecewise constant density and bulk modulus $\varrho(z)$ and $\kappa(z)$, whose jump discontinuities interfaces are distributed in such a way that the travel time across every layer is the same.

Therefore in the x coordinate defined through (4.2.2) the interfaces are uniformly spaced at intervals of Δx and without loss of generality we can consider the interfaces positioned at points $x_{j-1/2} = (j-1/2)\Delta x$, $j \in \mathbf{Z}$. By assuming the continuity of the pressure and velocity wave fields, from equations (4.2.5) we get the following jump condition for the down- and up-ward limits of $D(x,t)$ and $U(x,t)$, respectively, at the interface $x = x_{j-1/2}$

$$\begin{pmatrix} \zeta_{j-1}^{-\frac{1}{2}} & -\zeta_{j-1}^{-\frac{1}{2}} \\ \zeta_{j-1}^{\frac{1}{2}} & \zeta_{j-1}^{\frac{1}{2}} \end{pmatrix} \begin{pmatrix} D_{j-1/2-0}(t) \\ U_{j-1/2-0}(t) \end{pmatrix} = \begin{pmatrix} \zeta_{j}^{-\frac{1}{2}} & -\zeta_{j}^{-\frac{1}{2}} \\ \zeta_{j}^{\frac{1}{2}} & \zeta_{j}^{\frac{1}{2}} \end{pmatrix} \begin{pmatrix} D_{j-1/2+0}(t) \\ U_{j-1/2+0}(t) \end{pmatrix}. \tag{D.1}$$

Moreover, since in each layer the underlying medium is homogeneous the Riemann invariants are conserved along the segments of characteristic lines between the interfaces, and by continuity

$$D_{j-1/2-0}(t+\tfrac{1}{2}\Delta t) = D_{j-1}(t), \qquad D_{j-1/2+0}(t+\tfrac{1}{2}\Delta t) = D_j(t+\Delta t)$$
$$U_{j-1/2-0}(t+\tfrac{1}{2}\Delta t) = U_{j-1}(t+\Delta t), \qquad U_{j-1/2+0}(t+\tfrac{1}{2}\Delta t) = U_j(t)$$

where we have set $\Delta t = \Delta x$. Finally, by evaluating in (D.1) for time $t + \Delta t/2$ and using the relations above we obtain the system

$$\begin{pmatrix} D_j(t+\Delta t) \\ U_{j-1}(t+\Delta t) \end{pmatrix} = \begin{pmatrix} \tau_{j-1/2} & -\sigma_{j-1/2} \\ \sigma_{j-1/2} & \tau_{j-1/2} \end{pmatrix} \begin{pmatrix} D_{j-1}(t) \\ U_j(t) \end{pmatrix} \tag{D.2}$$

where the matrix standing in the right hand side is the so-called reflection-transmission matrix of the interface $x_{j-1/2}$, with the reflection and transmission coefficients defined by

$$\sigma_{j-1/2} = \frac{\zeta_j - \zeta_{j-1}}{\zeta_j + \zeta_{j-1}} \quad \text{and} \quad \tau_{j-1/2} = \frac{2\sqrt{\zeta_j \zeta_{j-1}}}{\zeta_j + \zeta_{j-1}}, \tag{D.3}$$

respectively. Since $\tau_{j-1/2}^2 + \sigma_{j-1/2}^2 = 1$, the transmission-reflection matrices are orthogonal and we get a semi-discrete version of the energy conservation law in the form

$$\tfrac{\Delta x}{4} \sum_{j\in\mathbf{Z}} \big([D_j(t+\Delta t)]^2 + [U_j(t+\Delta t)^2]\big) = \tfrac{\Delta x}{4} \sum_{j\in\mathbf{Z}} \big([D_j(t)]^2 + [U_j(t)]^2\big). \tag{D.4}$$

These equations allow us to compute the solution at discrete points of space and time. More precisely, we get the solution at the midpoint of the layers by steps in time equal to the travel time between interfaces. Furthermore, all the analysis above can be made by setting Δx equal to an integer fraction of the travel time across the layers, obtaining similar equations for computing the solution with a better resolution in space and time.

Bibliography

[1] M. Abramowitz and I. Stegun, *Handbook of mathematical functions*, Dover, New York, 1965.

[2] D.G. Alfaro Vigo, J.-P. Fouque, J. Garnier, and A. Nachbin, *Robustness of time reversal for waves in time-dependent random media*, Stoch. Processes Appl. **113** (2004), no. 2, 289–313.

[3] M. Asch, W. Kohler, G. Papanicolaou, M. Postel, and B. White, *Frequency content of randomly scattered signals*, SIAM Review **33** (1991), 519–626.

[4] M. Asch, G. Papanicolaou, M. Postel, P. Sheng, and B. White, *Frequency content of randomly scattered signals. Part I*, Wave Motion **12** (1990), 429–450.

[5] G. Bal, G. Papanicolaou, and L. Ryzhik, *Self-averaging in time reversal for the parabolic wave equation*, Stochastics and Dynamics **2** (2002), 507–531.

[6] G. Bal and L. Ryzhik, *Time reversal for classical waves in random media*, C.R. Acad. Sci. Paris **333** (2001), 1041–1046.

[7] ———, *Time reversal and refocusing in random media*, SIAM J. Appl. Math. **63** (2003), no. 5, 1475–1498.

[8] ———, *Stability of time reversal waves in changing media*, to appear in Disc. and Contin. Dynam. Syst. B, 2004.

[9] G. Bal and R. Verástegui, *Time-reversal in changing environment*, to appear in Multiscale Model. Simul., 2004.

[10] R. Bellman and G.M. Wing, *An introduction to invariant imbedding*, SIAM, Philadelphia, 1992.

[11] A. Bensoussan, J.-L. Lions, and G. Papanicolaou, *Asymptotic analysis for periodic structures*, North-Holland, Amsterdam, 1978.

[12] J. Berryman, L. Borcea, G. Papanicolaou, and C. Tsogka, *Statistically stable ultrasonic imaging in random media*, J. Acoust. Soc. Am. **112** (2002), 1509–1522.

[13] P. Billingsley, *Convergence of probability measures*, Wiley & Sons, New York, 1968.

[14] P. Blomgren, G. Papanicolaou, and H. Zhao, *Super-resolution in time-reversal acoustics*, J. Acoust. Soc. Am. **111** (2002), 230–248.

[15] L. Borcea, C. Tsogka, G. Papanicolaou, and J. Berryman, *Imaging and time reversal in random media*, Inverse Problems **18** (2002), 1247–1279.

[16] R. Burridge, G. Papanicolaou, P. Sheng, and B. White, *Probing a random medium with a pulse*, SIAM J. Appl. Math. **49** (1989), 582–607.

[17] R. Burridge, G. Papanicolaou, and B. White, *Statistics for pulse reflection from a randomly layered medium*, SIAM J. Appl. Math. **47** (1987), 146–168.

[18] ———, *One-dimensional wave propagation in a highly discontinuos medium*, Wave Motion **10** (1988), 19–44.

[19] J.F. Clouet and J.-P. Fouque, *A time-reversal method for an acoustical pulse propagating in randomly layered media*, Wave Motion **25** (1997), 361–368.

[20] A. Derode, A. Tourin, J. De Rosny, M. Tanter, S. You, and M. Fink, *Taking advantadge of multiple scattering to communicate with time reversal antennas*, Phys. Rev. Lett. **90** (2001), 014301.

[21] G.F. Edelman, T. Akal, W.S. Hodgkiss, S. Kim, W.A. Kuperman, and H.C. Song, *An initial demonstration of underwater acoustic communications using time reversal*, IEEE J. Oceanic Eng. **27** (2002), 602–609.

[22] B. Engquist, *Computation of oscillatory solutions to hyperbolic differential equations*, Nonlinear Hyperbolic Problems (C. Carasso, P.-A. Raviart, and D. Serre, eds.), Lectures Notes in Mathematics, vol. 1270, Springer-Verlag, New York, 1987, pp. 10–22.

[23] B. Engquist and T.Y. Hou, *Computation of oscillatory solutions to hyperbolic differential equations using particle methods*, Lectures Notes in Mathematics, vol. 1360, pp. 68–82, Springer-Verlag, New York, 1988.

[24] ______, *Particle method approximation of oscillatory solutions to hyperbolic differential equations*, SIAM J. Numer. Anal. **26** (1989), 289–319.

[25] M. Fink, *Time-reversal mirrors*, J. Phys. D: Appl. Phys. **26** (1993), 1333–1350.

[26] M. Fink, *Time-reversed acoustics*, Sci. Am. (November, 1999), 91–97.

[27] M. Fink and C. Prada, *Acoustic time-reversal mirrors*, Inverse Problems **17** (2001), no. 1, R1–R38.

[28] J.-P. Fouque, *Acoustic pulses propagating in randomly layered media*, Diffuse Waves in Complex Media (J.-P. Fouque, ed.), Kluwer Academic Publishers, The Netherlands, 1999, pp. 319–345.

[29] J.-P. Fouque, J. Garnier, and A. Nachbin, *Shock structure due to stochastic forcing and the time reversal of nonlinear waves*, submitted, 2003.

[30] ______, *Time reversal for dispersive waves in random media*, submitted, 2003.

[31] J.-P. Fouque and A. Nachbin, *Time-reversed refocusing of surface water waves*, Multiscale Model. Simul. **1** (2003), no. 4, 609–629.

[32] J.-P. Fouque and K. Sølna, *Time-reversal aperture enhancement*, Multiscale Model. Simul. **1** (2003), 239–259.

[33] A. Friedman, *Partial differential equations of parabolic type*, Prentice-Hall, Inc., Englewood Cliffs, N.J., 1964.

[34] W.S. Hodgkiss, H.C. Song, W.A. Kuperman, T. Akal, C. Ferla, and D.R. Jackson, *A long range and variable focus phase-conjugation experiment in a shallow water*, J. Acoust. Soc. Am. **105** (1999), 1597–1604.

[35] A.M. Ilin' and R. Z. Has'minskii, *Asymptotic behavior of solutions of parabolic equations and an ergodic property of nonhomogeneous diffusion processes*, Amer. Math. Soc. Transl. Series 2 (1966), no. 49, 241–268.

[36] O. Kallenberg, *Foundations of modern probability*, second ed., Springer series in statistics: Probability theory and its applications, Springer-Verlag, New York, 2002.

[37] J.B. Keller, *Wave propagation in random media*, Proc. Symp. Appl. Math., vol. XIII, pp. 227–246, McGraw-Hill, Amer. Math. Soc., New York, 1962.

[38] ______, *Stochastic equations and wave propagation in random media*, Proc. Symp. Appl. Math., vol. XVI, pp. 145–170, McGraw-Hill, Amer. Math. Soc., New York, 1964.

[39] H. Kesten and G. Papanicolaou, *A limit theorem for turbulent diffusion*, Comm. Math. Phys. **65** (1979), 97–128.

[40] R.Z. Khazminskii, *A limit theorem for solutions of stochastic differential equations with a random right-hand side*, Theor. Prob. Appl. **11** (1966), 390–406.

[41] V.I. Klyatskin, *Stochastic equations and waves in random media*, Nauka, Moscow, 1980.

[42] N.V. Krylov, *An analytic approach to spdes*, Stochastic Partial Differential Equations: Six Perspectives (Rene A. Carmona and Boris Rozovskii, eds.), Mathematical Surveys and Monographs, vol. 64, Amer. Math. Soc., 1999, pp. 185–242.

[43] N.V. Krylov and B.L. Rozovskii, *Stochastic partial differential equations and diffusion processes*, Uspekhi Mat. Nauk **37** (1982), no. 6, 75–95, transl. in Russian Math. Surveys, **37**:6(1982).

[44] H. Kunita, *Stochastic flows and stochastic differential equations*, Cambridge Studies in Advanced Mathematics, vol. 24, Cambridge University Press, Cambridge, 1990.

[45] W.A. Kuperman, W.S. Hodgkiss, H.C. Song, T. Akal, C. Ferla, and D.R. Jackson, *Phase conjugation in the ocean: experimental demonstration of an acoustic time-reversal mirror*, J. Acoust. Soc. Am. **103** (1997), 25–40.

[46] H. Kushner, *Approximation and weak convergence methos for random processes, with applications to stochastic system theory*, Series in signal processing, optimization, and control, MIT Press, Cambridge, Massachusetts, 1984.

[47] J.C. Muñoz Grajales and A. Nachbin, *Dispersive pulse stabilization and solitary wave refocusing*, in preparation, 2003.

[48] J. Ndzié Ewodo, *Refocusing of a time-reversed acoustic pulse propagating in randomly layered media*, J. Stat. Phys. **104** (2001), no. 5-6, 1253–1272.

[49] ———, *Some properties of time-reversed pulses in layered random media*, Stoch. Analysis Appl. **20** (2002), no. 1, 93–104.

[50] R.F. O'Doherty and N.A. Anstey, *Reflections on amplitudes*, Geophysical Prospecting **19** (1971), 430–458.

[51] G. Papanicolaou, *Asymptotic analysis of stochastic equations*, Studies in probability theory (M. Rosenblatt, ed.), MAA Studies in mathematics, vol. 18, Math. Assoc. of America, Washington, DC, 1978, pp. 111–179.

[52] ______, *Mathematical problems in geophysical wave propagation*, Documenta Mathematica, Extra volume ICM 98-I, (1998), 241–265.

[53] G. Papanicolaou and W. Kohler, *Asymptotic theory of mixing stochastic ordinary differential equations*, Comm. Pure Appl. Math. **27** (1974), 641–668.

[54] ______, *Asymptotic analysis of deterministic and stochastic equations with rapidly varying components*, Comm. Math. Phys. **45** (1975), 217–232.

[55] G. Papanicolaou, L. Ryzhik, and K. Sølna, *The parabolic wave approximation and time reversal*, Matem. Contemp. **23** (2002), 139–159.

[56] ______, *Statistical stability in time reversal*, SIAM J. Appl. Math. **64** (2004), 1133–1155.

[57] G. Papanicolaou and S. Weinryb, *A functional limit theorem for waves reflected by a random medium*, Appl. Math. Optim. **30** (1994), 307–334.

[58] A. Pazy, *Semigroups of linear operators and applications to partial differential equations*, Applied mathematical Sciences, vol. 44, Springer-Verlag, New York, 1983.

[59] M. B. Priestley, *Spectral analysis and time series*, vol. 1 & 2, Academic Press, New York, 1981.

[60] B.L. Rozovskii, *On the Itô-Venttsel' formula*, Vestnik Moskov. Univ. **28** (1973), no. 1, 26–32, transl. Moscow Univ. Math. Bull., **28**:1(1973).

[61] L. Ryzhik, G. Papanicolaou, and J. Keller, *Transport equations for elastic and other waves in random media*, Wave Motion **24** (1996), 327–370.

[62] D.H. Sattinger and O.L. Weaver, *Lie groups and algebras with applications to physics, geometry and mechanics*, Applied mathematical sciences, vol. 61, Springer-Verlag, New York, 1986.

[63] P. Sheng (ed.), *Scattering and localization of classical waves in random media*, World Scientific, Singapore, 1989.

[64] P. Sheng, B. White, Z.Q. Zhang, and G. Papanicolaou, *Minimum wave-localization length in a one-dimensional random medium*, Phys. Rev. B **34** (1986), no. 7, 4757–4761.

[65] P. Sheng, Z.Q. Zhang, B. White, and G. Papanicolaou, *Multiple-scattering noise in one dimension: Universality through localization-length scaling*, Phys. Rev. Lett. **57** (1986), no. 8, 1000–1003.

[66] K. Sølna, *Focusing of time-reversed reflections*, Waves Random Media **12** (2002), 365–385.

[67] K. Sølna and G. Papanicolaou, *Ray theory for locally layered random medium*, Waves Random Media **10** (2000), 151–198.

[68] G. Strang, *On the construction and comparison of difference schemes*, SIAM J. Numer. Anal. **5** (1968), 506–517.

[69] R.L. Stratonovich, *Topics in the theory of random noise*, vol. vols. I & II, Gordon and Breach, New York, 1963.

[70] J.L. Thomas and M. Fink, *Ultrasonic beam focusing through tissue inhomogeneities with a time reversal mirror: Applications to transkull therapy*, IEEE Trans. Ultrason. Ferroelectr. Freq. Control **43** (1996), 1122–1129.

[71] A. Tourin, A. Derode, and M. Fink, *Sensitivity to perturbations of a time-reversed acoustic wave in a multiple scattering medium*, Phys. Rev. Lett. **87** (2001), 274301.

[72] B. White, P. Sheng, and Z.Q. Zhang, *Wave localization characteristics in the time domain*, Phys. Rev. Lett. **59** (1987), no. 17, 1018–1021.

[73] G.B. Whitham, *Linear and nonlinear waves*, John Wiley, New York, 1974.

[74] A. M. Yaglom, *Correlation theory of stationary and related random functions*, Springer series in Statistics, vol. I & II, Springer-Verlag, New York, 1987.